POLITECNICO DI TORINO

Collegio di Ingegneria Chimica e dei Materiali

Corso di Laurea Magistrale

in Ingegneria Chimica e dei Processi Sostenibili

Tesi di Laurea Magistrale

Model curation and validation for a tubular photobioreactor in mixotrophy

Relatori

Prof. Stefania Specchia

Dr. Ir. Marcel Janssen

Candidato

Luca Buscaglia

Marzo 2023

Prefazione alla Tesi

Introduzione

Le microalghe come risorsa promettente per le sfide del futuro

Considerato l'aumento di popolazione mondiale previsto per il prossimo futuro, è fondamentale trovare nuove strategie per risolvere problematiche relative a maggiore richiesta di cibo, acqua ed energia in un contesto di sostenibilità. Una sfida significativa riguarda la sicurezza alimentare e la produzione sostenibile di fonti proteiche alternative a quelle tradizionali. Alcune specie di microalghe, come *Galdieria sulphuraria,* possono accumulare alte quantità di proteine con composizione amminoacidica in linea con le linee guida dell'Organizzazione Mondiale della Sanità. Inoltre, si possono estrarre delle molecole ad alto valore aggiunto, come ad esempio le ficocianine. Considerando queste potenzialità, *G. sulphuraria* è la microalga modello studiata nella presente Tesi.

Attualmente, nonostante le richieste di mercato di prodotti derivati dalle microalghe, la produzione industriale di biomassa e i processi di downstream necessitano di ulteriore ottimizzazione. Analisi tecnico-economiche e di sostenibilità mostrano che le principali problematiche da affrontare siano relative alla bassa produttività di biomassa, bassa concentrazione nella di raccolta, alle alte spese energetiche, rischio di frequente contaminazione e perdite di anidride carbonica in atmosfera.

La coltivazione di *G. sulphuraria* potrebbe essere adatta per affrontare le sfide sopramenzionate e, contemporaneamente, produrre composti di interesse industriale.

Introduzione alla biologia delle microalghe e ai fattori che ne influenzano la crescita

Le microalghe sono microrganismi unicellulari eucariotici che svolgono la fotosintesi (fotoautotrofi, o per semplicità, abbreviato ad autotrofi). Questa via metabolica permette l'utilizzo di luce come fonte di energia e di anidride carbonica come fonte di carbonio per la crescita della biomassa. L'ossigeno è un sottoprodotto delle reazioni (Figure 1.2 A).

Alcune microalghe possono crescere utilizzando solamente un substrato organico, con un metabolismo chemo-organotrofo (per semplicità, indicato in seguito con eterotrofo). Queste colture possono avere luogo in fermentatori tradizionali, con una produttività maggiore delle colture autotrofe (Figura 1.2 B). D'altra parte, il grado di pigmentazione delle microalghe che seguono questo metabolismo è inferiore a quello delle microalghe autotrofe.

Infine, è possibile che, in alcuni ceppi, i due metabolismi possano essere combinati in una coltivazione mixotrofa (Figura 1.2 C). In questo tipo di coltura, si raggiungono produttività maggiori rispetto alle colture autotrofe e non vengono persi i pigmenti, poiché la crescita avviene in condizioni di presenza di luce. Visto che è necessario utilizzare un substrato organico, questo tipo di coltura è più soggetta a contaminazione rispetto alla coltura autotrofa.

Per quanto riguarda le variabili che influenzano colture autotrofe e mixotrofe, la luce ha un ruolo di priorità. La dipendenza tra la velocità di crescita della biomassa e la radiazione luminosa dipende da numerosi fattori, quali l'intensità luminosa, le lunghezze d'onda ma anche dal fotobioreattore specifico impiegato e dalle condizioni di coltura.

Durante una giornata, la radiazione luminosa che raggiunge il suolo è funzione dalla radiazione in arrivo dallo spazio e da come questa è attenuata dagli strati superiori

dell'atmosfera. Inoltre, solo una frazione di circa il 45% della radiazione totale, definita *photosynthetically active radiation* (PAR) è utilizzata per la crescita della biomassa. In Figura 1.3, è riportata la PAR durante il 15/08/2019 a Bennekom, Paesi Bassi, ottenuta dal *National Solar Radiation Database* (NSRDB). Il database contiene misure satellitari di irraggiamento luminoso, e fornisce sia l'irraggiamento in condizioni *clear sky*, ossia quello che sarebbe misurato al suolo durante la giornata se non ci fossero nuvole, sia l'irraggiamento in condizioni reali. Le misure di irraggiamento alla superficie dei fotobioreattori sono generalmente indicate sottoforma di *photon flux density* (PFD, $\mu mol_{ph}\ m^{-2}\ s^{-1}$).

La relazione tra PFD e produzione di ossigeno è rappresentata in Figura 1.4, con la cosiddetta curva P/I. A basse intensità luminose, la produzione di ossigeno netta aumenta linearmente con la PFD. A intensità maggiori, viene raggiunta una condizione di saturazione o inibizione poiché la fotosintesi ha efficienza minore, e parte dell'energia luminosa viene dispersa sottoforma di calore. Poiché queste condizioni sono normalmente raggiunte quando la coltura è esposta alla luce solare, è necessario "diluire" la luce che raggiunge la coltura in modo da mantenere alta l'efficienza di fotosintesi. In pratica, ogni singola cellula della coltura dovrebbe ricevere un'intensità luminosa ottimale per la crescita.

Inoltre, la radiazione luminosa è attenuata nella coltura per via del fatto che le cellule si fanno ombra mutualmente. In pratica, con un'alta concentrazione di biomassa, è presente un volume della coltura in condizioni di buio, non raggiunto dalla luce esterna, che rappresenta un costo energetico senza contribuire alla produttività di biomassa. Questa problematica può essere superata con una coltura mixotrofa, poiché la biomassa può crescere anche in condizioni di buio. Infine, è degno di nota che anche la miscelazione e l'esposizione delle singole cellule a cicli di luce/buio dovuti alla turbolenza abbia effetti positivi sulla produttività.

Un'ulteriore variabile importante per la coltura è la concentrazione di ossigeno disciolto in fase liquida. Alte concentrazioni, possono risultare in reazioni che sono volte al consumo di questo composto, come la fotorespirazione. Queste, convertono ossigeno senza un reale guadagno metabolico, e quindi ostacolano la crescita di biomassa. Anche basse concentrazioni di ossigeno sono dannose per alcune microalghe. In *Galdieria*, l'apparato fotosintetico è danneggiato in condizioni anossiche.

La strategia di coltivazione Oxygen Balanced Mixotrophy (OBM)

Una strategia di coltivazione per microalghe mixotrofe che ha dimostrato risultati promettenti in un fotobioreattore miscelato in scala di laboratorio, è *Oxygen Balanced Mixotrophy* (OBM). Tramite un sistema di controllo, la portata di substrato in ingresso al fotobioreattore è manipolata in modo che l'ossigeno disciolto nel brodo di coltura sia costante (Figura 1.5). In questo modo, è possibile bilanciare l'ossigeno prodotto dalla fotosintesi, con quello consumato dal metabolismo del substrato. Il risultato di questa strategia è la possibilità di risparmiare l'alimentazione di gas al fotobioreattore, ottenendo anche una produttività che è il doppio di quella di una coltivazione autotrofa.

Il sistema di controllo adottato in questo processo è di tipo Proporzionale-Integrale-Derivativo (PID), e il substrato è immesso continuativamente nel reattore. Poiché l'agitazione è piuttosto vigorosa, questo è disperso e consumato immediatamente. La sua concentrazione si può considerare molto bassa e prossima a zero.

Anche *Galdieria sulphuraria* può essere coltivata in OBM. Rispetto ad altre microalghe, essendo acidofila (pH di lavoro 1.8), il rischio di contaminazione è molto basso. Considerando inoltre la possibilità di estrarre proteine e altri composti di interesse, questa microalga coltivata in OBM sembra promettente per scale-up industriale.

Fotobioreattori per la coltivazione di Galdieria sulphuraria

Tra i sistemi in cui possono essere coltivate microalghe, spicca il fotobioreattore tubolare. Nell'apparecchiatura più comunemente utilizzata per colture autotrofe, è diviso in due sezioni: un tubo di vetro o materiale trasparente per assorbire la radiazione solare, e un miscelatore. Nel miscelatore avviene principalmente il trasferimento di materia (arricchimento di anidride carbonica e strippaggio di ossigeno), mentre nella parte tubolare scorre la fase liquida e avviene la crescita di biomassa. La velocità della fase liquida è stabilita da una pompa, in modo da permettere concentrazioni ottimali di ossigeno e anidride carbonica lungo il tubo.

Le problematiche principali di questo reattore sono legate ai consumi energetici dovuti all'alimentazione gassosa (fino al 30% del costo di produzione) e alle perdite di anidride carbonica (fino al 25%, anche in sistemi ottimizzati). La possibilità di coltivare microalghe mixotrofe in OBM in questi bioreattori risolverebbe entrambe queste problematiche, poiché l'alimentazione gassosa non sarebbe presente. In aggiunta, si otterrebbe una maggiore produttività di biomassa.

Alternativamente ai fotobioreattori tubolari monofase, l'azienda Lgem propone un fotobioreattore bifase (Figura 1.6 e Figura 1.7), in cui la fase gas è ricircolata grazie a un compressore e la fase liquida può essere ulteriormente movimentata con una pompa. In questo modo, lo scambio di materia tra la fase liquida e la fase gas può avvenire anche nella sezione tubolare del reattore. Per via dell'assenza di alimentazione gassosa al processo, questo fotobioreattore può essere favorevole alla strategia OBM.

D'altra parte, la strategia di controllo deve essere adattata a questa differente configurazione reattoristica. Sono infatti previsti gradienti di substrato e ossigeno lungo la sezione tubolare del reattore, e bisogna evitare condizioni anossiche in fase liquida, pur garantendo mixotrofia nel reattore. Per questo motivo, considerando che il substrato può essere introdotto solamente all'inizio del tubo, non è possibile aspirare un bilancio di ossigeno in ogni punto, ma solamente a un bilancio nell'intero reattore. Un sistema di controllo di tipo PID può essere implementato anche in questo caso, e la variabile controllata può essere la concentrazione di ossigeno disciolta nel brodo di coltura, oppure la concentrazione di ossigeno in fase gas, all'inizio o alla fine della sezione tubolare.

Infine, si evidenziano alcuni modelli per un reattore tubolare secondo uno studio della distribuzione dei tempi di permanenza (RTD) con le equazioni (1.4) e (1.5), mentre la loro rappresentazione è fornita in Figura 1.9.

Obbiettivi e contenuti

L'obbiettivo di questa tesi è quello di studiare nel dettaglio gli effetti dei gradienti di substrato e ossigeno nel fotobioreattore in scala pilota di Lgem per la coltivazione mixotrofica di *Galdieria sulphuraria*. In particolare, è utile possedere un modello matematico del processo al fine di studiare differenti strategie di controllo. In aggiunta, è stato effettuato un esperimento con un approccio di *down-scale*, al fine di validare la strategia di controllo e i risultati del modello. Gli obbiettivi della Tesi sono:

- Migliorare un modello per il fotobioreattore tubolare di Lgem in condizioni OBM
- Simulare e comparare diversi sistemi di controllo per il fotobioreattore
- Simulare il sistema in condizioni di luce costanti, *clear sky* e reali

- Validare una strategia di controllo in un fotobioreattore in scala di laboratorio in condizioni di luce costante

Modello matematico

Descrizione del modello e assunzioni principali

Il modello matematico si basa sull'assunzione che il fotobioreattore tubolare possa essere descritto come una serie di reattori miscelati in co-corrente (Figura 2.1). La configurazione simulata è quella accelerata, quindi sia il compressore per la fase gas che la pompa per la fase liquida sono accesi. In seguito, sono elencate le principali ipotesi:

- Il reattore tubolare è composto da una serie di 100 stadi perfettamente miscelati.
- La dinamica del reattore nella sezione in cui è presente il miscelatore è trascurata.
- Si trascurano incrementi di pressione e perdite di carico.
- Liquido e gas sono perfettamente miscelati in posizione radiale.
- La fase gas si comporta come un gas ideale.
- La frazione di gas in ogni stadio è la stessa ed è costante nel tempo.
- I coefficienti di trasporto di materia sono costanti per tutto il reattore e non cambiano nel tempo.
- La temperatura è costante e pari a 37°C.
- La stechiometria mixotrofa è la somma delle stechiometrie autotrofa ed eterotrofa. La composizione della biomassa è $CH_{1.62}O_{0.41}N_{0.14}P_{0.011}$.
- Il mantenimento delle cellule è trascurato.
- La produttività volumica di biomassa è assunta costante. Concentrazione di biomassa e velocità di generazione di ossigeno per metabolismo autotrofo sono costanti.

Parametri di input

I coefficienti di partizione alla temperatura di lavoro sono calcolati secondo l'equazione (2.1), considerando come la solubilità di ossigeno e anidride carbonica varia dalla temperatura ambiente a 37°C (Tabella 2.1). L'influenza della temperatura sui coefficienti di trasporto è stata valutata tramite la teoria di penetrazione di Higbie in equazione (2.2), esprimendo la diffusività tramite la relazione di Wilke e Chang in equazione (2.3). Sono trascurati gli effetti della temperatura su area di scambio di materia e tempo di contatto tra le fasi.

I parametri cinetici del microrganismo, che comprendono la resa di biomassa sul substrato in condizioni eterotrofe, la resa di biomassa su fotoni in condizioni autotrofe e le costanti di Monod, sono state ottenute da lavori precedenti (Tabella 2.2).

Equazioni del modello

Le equazioni del modello sono legate alla stechiometria del processo e ai bilanci di materia. Le equazioni (2.5) e (2.6) rappresentano la stechiometria autotrofa ed eterotrofa, supponendo

che la produzione netta di ossigeno sia nulla. L'equazione (2.7) è la somma delle due precedenti, e rappresenta la stechiometria del processo mixotrofo. Quest'ultima assunzione potrebbe non essere rigorosamente valida, in quanto alcuni studi registrano un'interazione negativa tra i due metabolismi, ma rappresenta una buona semplificazione. La portata stechiometrica di substrato è definita in equazione (2.8), e rappresenta la portata di substrato necessaria per ottenere il bilancio di ossigeno (Tabella 2.3).

I bilanci di materia comprendono un termine di generazione per la parte di metabolismo eterotrofo, che include le limitazioni per substrato e ossigeno, e uno per il metabolismo autotrofo, che include limitazione per l'anidride carbonica. Per il trasporto gas-liquido, è utilizzato un coefficiente di scambio globale per ossigeno e uno per anidride carbonica. Le equazioni del modello sono presentate estensivamente nel Capitolo 2.

Sistema di controllo

Un sistema di controllo è fondamentale per ottenere OBM e mantenere costante la concentrazione di ossigeno nel liquido, evitando anossia nel sistema. In questa Tesi, sono state sviluppate due strategie di controllo discontinue con controllore PID. Con il termine discontinuo, si intende che l'azione di controllo avviene ogni tempo di residenza della fase gas nel reattore. Le variabili controllate sono l'ossigeno disciolto nella fase liquida (DO) e la concentrazione di ossigeno in fase gas (COG). Queste due strategie sono evidenziate schematicamente in Figura 2.3.

Un'ulteriore strategia continua è stata implementata e studiata. In questa strategia l'errore in input al sistema di controllo è calcolato a partire da COG, comparandola con il valore di questa variabile di processo al tempo di residenza precedente. In questo modo, non si può definire un set-point costante nel tempo, ma il sistema di controllo dovrebbe essere più efficace nell'affrontare disturbi nel processo.

Materiali e metodi

Metodi numerici e simulazione

Il modello matematico è implementato in MATLAB R2020a. Il risolutore per la soluzione del sistema di equazioni differenziali è ode45, che è in grado di definire un passo temporale in modo che sia raggiunta convergenza (in Figura 3.1 è presentata la funzione in input al risolutore). Per una maggiore flessibilità, è possibile fornire in input alla funzione intervalli temporali sottomultipli del tempo totale da simulare. Per le simulazioni con portata di substrato costante, le equazioni sono state risolte ogni 10 s. Per le simulazioni con sistema di controllo discontinuo, le equazioni sono state risolte ogni tempo di permanenza della fase gas nel reattore. Per le simulazioni con sistema di controllo continuo, le equazioni sono state risolte ogni secondo.

Il valore di N, numero di unità perfettamente miscelate del modello influenza la convergenza del metodo numerico. All'aumentare di N, il passo temporale richiesto per la convergenza è inferiore e il costo computazionale aumenta. In aggiunta, il valore di N ha anche un significato fisico nella fluidodinamica del reattore, in quanto più questo valore è grande, più il modello è adatto a descrivere un reattore a flusso a pistone.

Per questo motivo, sono analizzati i risultati di esperimenti di RTD condotti introducendo un impulso di acido nel miscelatore del reattore tubolare e registrando il cambiamento di pH nel

tempo alla fine del tubo. Inoltre, uno studio dei risultati della simulazione al variare del parametro N è stato svolto, con valori di 100, 500 e 1000.

Approccio di scale-down adottato per la validazione del modello

La validazione del modello è stata svolta in un fotobioreattore miscelato in scala di laboratorio, e il modello è stato adattato a queste condizioni. Questo esperimento è possibile in quanto esiste una similitudine tra le equazioni di un reattore discontinuo e un reattore tubolare con flusso a pistone, sostituendo il tempo di permanenza del reattore tubolare con il tempo trascorso del reattore batch. In pratica, nel reattore batch si può simulare un elemento di fluido che si sposta con flusso a pistone attraverso il tubo del reattore tubolare.

Considerando che nel reattore tubolare il substrato viene immesso nell'elemento di fluido ogni volta che questo raggiunge l'inizio del tubo, anche nel reattore batch il substrato sarà inviato ogni tempo di residenza, per la durata del tempo di residenza di uno stadio. In questo modo, il sistema di controllo discontinuo progettato in precedenza può essere adattato per l'esperimento di laboratorio. La variabile controllata è la concentrazione di ossigeno in fase gas COG.

Poiché non è possibile scambio di gas tra l'esterno e l'interno del tubo nel reattore tubolare, questo deve essere impedito, o limitato per il più possibile, anche nel reattore di laboratorio. Per questo motivo, è stato realizzato un *waterlock*, per produrre una sovrapressione di 10 mbar. Inoltre, è necessario un ricircolo di gas con una portata massica ben definita al fine di ottenere lo stesso coefficiente di scambio di materia del fotobioreattore tubolare.

Configurazione reattoristica

È stato impiegato un reattore miscelato in vetro di volume totale 3 L, con illuminazione omogenea sui lati grazie a dei pannelli con LED (Figura 3.3). La temperatura della fase liquida è mantenuta costante a 37°C grazie a uno scambiatore di calore inserito nel reattore. All'uscita della fase gas è presente un condensatore, per prevenire perdite d'acqua dal reattore e condensazione nella linea di riciclo del gas. L'agitatore è impostato a 500 RPM, il pH è regolato manualmente con l'aggiunta di NaOH per rimanere nell'intorno di 1.8. All'interno del reattore è presente un sensore di concentrazione di ossigeno disciolto in fase liquida (DO). Quest'ultimo è calibrato con aria e azoto, per ottenere rispettivamente valori del 100% e dello 0%. La calibrazione è effettuata con una pressione di 1.12 bar, a causa della presenza di una resistenza addizionale in linea. Nella linea di ricircolo è presente un altro sensore di ossigeno, per misurare la concentrazione di quest'ultimo in fase gas (COG), che è calibrato analogamente al precedente con una concentrazione di 20.95% con aria e 0% con azoto a una pressione di 1.12 bar.

Durante gli esperimenti di validazione, la pressione è di 10 mbar superiore alla pressione atmosferica, grazie al *waterlock* posizionato dopo al condensatore. Il gas è ricircolato grazie a una pompa a diaframma, con portata costante, ed entra dal fondo del reattore grazie a un distributore. Il processo può essere monitorato e controllato grazie al *software* LabView.

Microalga impiegata e metodi sperimentali

La microalga impiegata per gli esperimenti è *Galdieria sulphuraria* ACUF 064, che è incubata in una beuta da 250 mL prima dell'inoculazione nel reattore. Le condizioni di

crescita e la composizione del brodo di coltura utilizzato sono descritti in dettaglio nella Sezione 3.2.3.

Successivamente all'inoculo, si è proceduto con una crescita discontinua in condizioni autotrofe finché la concentrazione di biomassa ha raggiunto 3 g_x/L. Successivamente, dopo una fase di adattamento alle condizioni mixotrofe, è stata effettuata una crescita dicontinua in OBM fino a una concentrazione di 8 g_x/L. A questo punto, è stato avviato un chemostat in condizioni OBM, con una diluizione di 0.2 day^{-1}. L'esperimento di validazione è sempre iniziato dopo almeno tre giorni di chemostat.

Un esperimento di validazione è un periodo di sedici ore in cui il substrato è inviato in impulsi al reattore. Un nuovo sistema di controllo PID è stato integrato nel *software* LabView, e i parametri sono stati progettati dalle simulazioni sul modello. Prima di iniziare la validazione, il reattore è aerato per almeno due ore, in modo da raggiungere condizioni di equilibrio. A questo punto, si è spenta la diluizione e il bioreattore passa in modalità discontinua con il nuovo sistema di controllo attivo. Quest'ultimo, controlla COG manipolando la velocità di rotazione del motore della pompa di substrato, che è attiva solo per 7 s ogni 700 s (tempo di residenza nel reattore tubolare). Il valore di set-point indicato è sul programma è di 17% v/v.

Metodi analitici e calcoli

Durante tutto lo svolgimento degli esperimenti, campioni sono prelevati dal reattore e stati utilizzati per ottenere misurazioni di densità ottica, *absorption cross-section*, *quantum yield* e peso secco di biomassa.

In aggiunta, dei campioni sono stati prelevati dal reattore prima dell'inizio dell'esperimento, dopo 2.5 h, 5 h, 7 h e alla fine dell'esperimento. Questi, sono utilizzati per misurare concentrazione di glucosio, densità ottica e concentrazione di anidride carbonica nel liquido, necessarie per la validazione. Informazioni più approfondite sui metodi analitici e la procedura di campionamento sono disponibili in Sezione 3.2.5.

Per quanto riguarda i calcoli effettuati, è stato necessario convertire le misurazioni di DO e COG, tenendo conto del fatto che la pressione operativa è diversa dalla pressione di calibrazione. A questo scopo, possono essere impiegate le equazioni (3.2) e (3.3), poichè le misurazioni dei sensori di ossigeno dipendono linearmente dal rapporto tra la pressione di calibrazione e quella operativa.

La produttività di biomassa può essere calcolata con le equazioni (3.4) e (3.5), considerando la diluizione del reattore ad ogni campionamento e la biomassa estratta per le misurazioni.

Risultati e discussione

Distribuzione dei tempi di permanenza e numero di stadi

Le distribuzioni dei tempi di permanenza possono essere ricavate dagli esperimenti svolti con il fotobioreattore tubolare. Purtroppo, non è possibile stabilire un valore del numero di stadi seguendo questa analisi. I motivi sono molteplici, ad esempio l'incertezza nella replica di un impulso ideale o il tempo di campionamento del sensore di pH, che non permettono una buona risoluzione delle distribuzioni (Figura 4.1).

L'analisi sui risultati del modello al variare del numero di stadi, invece, dimostra come i risultati siano poco influenzati dal parametro N (Figura 4.2 e Figura 4.3). In conclusione, un numero di stadi pari a 100 è stato scelto in modo da ridurre il tempo impiegato in ogni simulazione.

Risultati del modello: portata stechiometrica costante di substrato e sensitività

Uno studio preliminare della dinamica del sistema con portata di substrato costante e condizioni di luce costante è fondamentale per poter implementare strategie di controllo del processo. In questo caso, i risultati della simulazione sono presentati in Figura 4.4. Dopo un transitorio iniziale, mentre la concentrazione di substrato è stabile nel tempo, sia la concentrazione di ossigeno in fase liquida che quella in fase gas diminuiscono. Il sistema è instabile in queste condizioni. La concentrazione di anidride carbonica in fase liquida e in fase gas cresce nel tempo, a causa della stechiometria del processo. Per studiare il bilancio di ossigeno nel reattore può essere utile considerare le velocità medie volumiche di produzione e consumo di ossigeno nel reattore. Come si vede in Figura 4.5, nel processo prevale il consumo di ossigeno per assimilazione del substrato, tranne verso la fine del processo, dove il bilancio è quasi raggiunto. Il decremento della concentrazione di ossigeno nelle fasi liquida e gas è legato alla preponderanza del consumo di ossigeno, sommato alla perdita di ossigeno nello spurgo gassoso del reattore (Figura 4.6).

Successivamente è studiata la risposta del sistema a differenti portate costanti di substrato. Con riferimento alla portata stechiometrica F_{FEED}, si analizzano le caratteristiche più rilevanti degli scenari 20% F_{FEED} (A), 80% F_{FEED} (B), 96.8% F_{FEED} (C) e 120% F_{FEED}.

- Scenario A (Figura 4.8): il substrato non si accumula nel reattore poiché la sua concentrazione è molto bassa. In media, il metabolismo autotrofo prevale nel reattore poiché la concentrazione di ossigeno in fase liquida e gas aumenta nel tempo. L'incremento, però, non è molto grande, in quanto la fotosintesi è limitata dalla disponibilità di anidride carbonica. La produttività è molto bassa, poiché il metabolismo eterotrofo è minimo.
- Scenario B (Figura 4.9): simile allo scenario A, ma la fotosintesi non è limitata e, perciò, la concentrazione di ossigeno in fase liquida e gas raggiunge livelli più alti. L'anidride carbonica si accumula in fase liquida nel tempo.
- Scenario C (Figura 4.10): l'ossigeno disciolto in fase liquida e la concentrazione di ossigeno in fase gas sono costanti nel tempo. Questa è la situazione che sarà raggiunta con i sistemi di controllo, quindi merita particolare attenzione. Considerando la produzione netta di ossigeno, il metabolismo autotrofo prevale leggermente su quello eterotrofo. Per mantenere costante la concentrazione di ossigeno in fase gas, infatti, è necessario che sia prodotto l'ossigeno per compensare le perdite dallo spurgo.
- Scenario D (Figura 4.11): il substrato si accumula nel reattore e vengono raggiunte le condizioni anossiche. La situazione è da evitare perché danneggia la biomassa, anche se è quella con produttività maggiore tra tutti gli scenari (1.49 g_X/(L d)). Questa produttività supera il limite superiore dei valori raggiungibili mantenendo condizioni sicure nel processo.

Le simulazioni evidenziano che COG, DO e portata di substrato sono variabili dipendenti. La concentrazione di ossigeno può essere aumentata o diminuita agendo sulla portata di substrato. Variazioni troppo grandi di portata possono risultare in anossia nel sistema (scenario D), o produttività molto bassa (scenario A).

Risultati del modello: progetto dei sistemi di controllo

I controllori sono progettati con il criterio di Ziegler-Nichols. Con un controllore proporzionale, si ottiene la risposta del sistema con un'oscillazione sostenuta (Figura 4.12) e, dalle caratteristiche di questa, si definiscono i parametri seguendo regole empiriche (Tabella 4.3).

Controllando COG con il sistema di controllo discontinuo, che agisce ogni tempo di permanenza, un controllore PID risulta essere quello con una risposta più favorevole, meno oscillante e più rapida (Figure 4.13). Controllando DO, il controllore più semplice che permette una risposta soddisfacente è il PI (Figure 4.14). Il confronto tra queste due strategie di controllo in Figura 4.15 permette di trarre delle considerazioni generali: il controllo di DO sembra più efficace del controllo di COG. La ragione potrebbe essere legata al fatto che controllando DO, si controlla in modo più diretto il sistema, poiché si controlla una variabile nella fase in cui stanno avvenendo le reazioni. Un'ulteriore analisi svolta e dettagliata in Sezione 4.2.3 e in Figura 4.16, mostra che DO è anche più sensibile a variazioni di substrato rispetto a COG.

Ulteriori questioni tecniche possono essere prese in considerazione nella scelta della strategia di controllo migliore per un reattore in scala industriale. La gestione di un sensore in fase gas potrebbe essere più semplice, anche se bisogna prestare attenzione alla possibile condensazione sull'elemento sensibile, che potrebbe distorcere la misurazione. Un sensore in fase liquida potrebbe essere più soggetto a rumore di misura, influenzando la misurazione a causa delle condizioni fluidodinamiche e delle reazioni.

L'ultima strategia di controllo studiata in condizioni di luce costante prevede il controllo continuo di COG con un controllore PI. Come precedentemente anticipato, non si tratta di un sistema di controllo con set-point costante, ma l'errore è calcolato sulla base della misura di COG al tempo di permanenza precedente. In questo modo, risulterebbe più efficace nell'affrontare i disturbi. Anche questo sistema di controllo, con i parametri definiti, riesce a raggiungere condizioni stabili, seppur più lentamente dei due precedenti (Figura 4.17).

Considerando le produttività di biomassa ottenute con questi tre sistemi di controllo, si evince che la produttività è maggiore quando il set-point è raggiunto rapidamente (Tabella 4.4).

Risultati del modello: simulazione in condizioni luminose reali

Al fine di valutare i risultati del modello in condizioni luminose reali, è necessario definire una relazione tra irraggiamento al reattore e produzione di ossigeno per fotosintesi. Per confrontare i risultati della simulazione di *clear sky* con quelli a luce costante, si assume che la velocità di produzione autotrofica media sia la stessa in entrambe le situazioni. Per le simulazioni in condizioni luminose reali, si assume che la produzione di ossigeno sia inferiore al caso sinusoidale, e in proporzione nello stesso modo in cui l'irraggiamento *clear sky* sta all'irraggiamento del caso reale (Figura 4.18).

In condizioni di *clear sky*, una simulazione con portata di substrato stechiometrica è mostrata in Figura 4.19. L'ossigeno netto prodotto durante la giornata non è bilanciato: predomina il metabolismo autotrofo metà giornata e quello eterotrofo a inizio e a fine del giorno (Figura 4.20). Inoltre, la concentrazione di ossigeno in fase liquida raggiunge valori critici due volte durante il giorno, dando origine ad anossia. Per evitare la situazione dannosa, può essere usata una portata minore (10% F_{FEED}). In questa situazione, però, la fotosintesi è limitata dall'anidride carbonica in fase liquida e la produttività non raggiunge livelli comparabili a quanto ottenuto in condizioni luminose costanti (Figura 4.21, Tabella 4.5).

Da queste simulazioni, appare che sia indispensabile l'utilizzo di un sistema controllo. La strategia di controllo discontinuo di COG è in grado di controllare efficacemente il processo, con una produttività leggermente inferiore allo scenario di luce costante (Figura 4.22). La strategia continua risulta in prestazioni migliori del processo con meno oscillazioni di DO, COG e produttività maggiore sia del caso precedente, che di quanto ottenuto in luce costante con lo stesso sistema di controllo (Figura 4.24).

Considerando le condizioni luminose reali, entrambi i sistemi di controllo sono in grado di gestire il processo in modo ottimale (Figure 4.23 e 4.25). Anche in questo caso, il sistema di controllo continuo ha prestazioni migliori. Si evidenzia la minore produttività del processo in questa situazione, comunque attesa considerato l'inferiore irraggiamento durante il giorno (Tabella 4.5). Inoltre, la produttività ottenuta in queste simulazioni (media in condizioni *clear sky* e reale, 0.73 ± 0.30 $g_x/(L\ d)$).) è paragonabile al valore ottenuto in scala pilota, di 0.71 ± 0.43 $g_x/(L\ d)$.

Risultati sperimentali: concentrazione di ossigeno in fase liquida e gas

Tutte e tre le validazioni sperimentali hanno permesso di ottenere valori stabili di COG tra le due e le quattro ore dall'inizio dell'esperimento. Inoltre, DO non è mai sceso sotto al 10%, il che significa che non si sono mai verificate condizioni anossiche nel sistema, e che il sistema di controllo progettato dal modello funziona. Nelle figure da 4.26 a 4.28, le risposte del sistema sono confrontate con il modello con le stesse condizioni di partenza. Inoltre, sia nel secondo che nel terzo esperimento, è presente la stessa risposta inversa prevista dal modello. In tutti gli esperimenti, è raggiunto uno stato stabile più velocemente di quanto previsto dal modello, mentre DO rimane sempre inferiore a quanto atteso. Tutte e tre le risposte sono confrontate con il modello in Figura 4.29.

Risultati sperimentali: concentrazione di substrato

La misurazione di glucosio nel brodo di coltura permette di ottenere dei valori sotto i limiti di misurazione dell'apparecchiatura analitica. Questo significa che sono presenti solo tracce di substrato nel reattore, e questo non si sta accumulando nel tempo. Anche dal modello, sono previste basse concentrazioni di substrato (Figura 4.30).

Considerando la portata di substrato immessa nel reattore, questa è simile in tutti e tre gli esperimenti, una volta che stabilità è raggiunta (Figura 4.31, le linee hanno coefficiente angolare simile dopo 6 ore). La massa di glucosio inviata al reattore durante gli esperimenti è di 3.4 ± 0.5 g_{glu}, un valore in accordo con le previsioni del modello (3.7 g_{glu}).

Risultati sperimentali: pigmenti, quantum yield, anidride carbonica in fase liquida, produttività di biomassa

Il *quantum yield* è un parametro utilizzato per valutare l'efficienza del fotosistema II, in condizioni di adattamento al buio. Durante gli esperimenti di validazione, sono stati registrati alti valori QY, addirittura crescenti durante l'esperimento (Tabella 4.6). Questo andamento può essere spiegato dall'incremento di concentrazione di biomassa durante gli esperimenti, ed è segno che non sono mai state raggiunte condizioni dannose all'apparato fotosintetico della microalga.

L' *absorption cross-section* è correlata alla pigmentazione del microrganismo. Anche questa misurazione mostra che i pigmenti incrementano durante gli esperimenti e che il profilo spettrale non cambia (Figura 4.32).

Non è stato possibile validare la concentrazione di anidride carbonica in fase liquida prevista dal modello, in quanto la tendenza crescente attesa non è stata registrata (Figura 4.33). Possibili motivazioni possono essere correlate a bassa risoluzione dell'apparecchiatura analitica utilizzata oppure alla procedura di campionamento eseguita. Inoltre, nel modello non è incluso il termine di produzione di anidride carbonica per il mantenimento della biomassa, che potrebbe influenzare i risultati.

La produttività di biomassa ottenuta sperimentalmente, pari a 1.24 ± 0.15 $g_x/(L\ d)$, è in buon accordo con la previsione del modello di 1.22 $g_x/(L\ d)$. In lavori precedenti vengono misurate produttività maggiori, ma può essere semplicemente dovuto a un progressivo adattamento nel tempo delle microalghe a condizioni mixotrofe (Tabella 4.7).

Conclusioni

In questa Tesi è stato migliorato un modello per prevedere i gradienti di substrato e ossigeno in un fotobioreattore tubolare, per poi essere applicato con successo ad una coltivazione mixotrofica di *Galdieria sulphuraria* in condizioni di luce reali.

Il modello è stato migliorato nei metodi numerici e nei parametri, in modo da ottenere buoni risultati per la coltura di interesse. Uno studio di distribuzione di tempi di permanenza e una sensitività sul modello hanno permesso di definire un numero di stadi pari a 100.

In condizioni luminose costanti, il bilancio di ossigeno avviene solamente quando DO e COG diminuiscono nel tempo. Si può ottenere un DO costante con una portata di substrato costante, ma questo risulta in una sovraproduzione di ossigeno per metabolismo autotrofo.

Sono state studiate e testate tre diverse strategie di controllo del processo, che hanno dimostrato buone prestazioni e risposta stabile del sistema. Il controllo di DO risulta in una risposta più veloce, poiché è un approccio più diretto per mantenere valori stabili di DO.

In condizioni di luce reale, la strategia di controllo continuo di COG ha permesso di ottenere risultati migliori, con una produttività leggermente maggiore della strategia di controllo discontinua, con le stesse condizioni luminose. La produttività ottenuta nello scenario *clear sky* è comparabile con quella ottenuta in luce costante. Quando l'intensità luminosa è inferiore, una produzione di ossigeno più bassa ha come conseguenza una portata inferiore di substrato in ingresso al sistema, e quindi, a una minore produttività del reattore.

È stato utilizzato un nuovo approccio sperimentale di *down-scale* per simulare i gradienti di un fotobioreattore tubolare in un fotobioreattore miscelato di laboratorio, operato in modalità discontinua. Il sistema di controllo discontinuo, progettato con l'aiuto del modello, permette di raggiungere valori stabili di COG in alcune ore. L'ossigeno disciolto nel brodo di coltura non raggiunge mai valori inferiori al 10%. Non sono mai state registrate condizioni anossiche durante gli esperimenti.

La concentrazione di glucosio in ogni campione è risultata nell'intorno del limite di misurazione. Di conseguenza, il substrato non si è mai accumulato nel reattore. In aggiunta, la massa di glucosio inviata al reattore durante gli esperimenti è di 3.4 ± 0.5 g_{glu} è simile al valore di 3.7 g_{glu} previsto dal modello. L'analisi dei pigmenti e dello stato del fotosistema II non mostra segni dovuti a condizioni sfavorevoli raggiunte durante il processo. La produttività di

biomassa ottenuta è 1.24 ± 0.15 $g_x/(L\ d)$, in accordo con la previsione del modello di 1.22 $g_x/(L\ d)$.

I risultati ottenuti con il modello e gli esperimenti mostrano che questo processo può essere implementato in scala pilota e industriale. L'ottimizzazione del sistema di controllo è la chiave per raggiungere alti valori di produttività di biomassa, e prevenire anossia in condizioni di luce reale.

Raccomandazioni

Possono essere condotti ulteriori studi per migliorare il modello, le simulazioni e l'esperimento di validazione.

Per quanto riguarda il modello, potrebbe essere migliorato includendo il termine di mantenimento. Questo, infatti, appare importante da quanto rilevato sperimentalmente con le misurazioni di concentrazione di anidride carbonica in fase liquida.

Possono essere condotte simulazioni aggiuntive per studiare differenti strategie di controllo. Ad esempio, possono essere analizzate strategie di controllo continue con set-point. In aggiunta, i sistemi di controllo per DO possono essere studiati in condizioni luminose reali, in modo da verificare che i risultati ottenuti in condizioni di luce costante siano estendibili in termini generali.

Per la validazione sperimentale, può essere utile ricercare un nuovo metodo di prelevare i campioni per l'analisi di anidride carbonica in fase liquida. In aggiunta, la concentrazione di anidride carbonica in fase gas potrebbe essere misurata con un sensore apposito. Infine, altre strategie di controllo potrebbero essere testate secondo l'approccio seguito in questa Tesi.

Il modello potrebbe anche essere adattato per studi ulteriori. Ad esempio, per la simulazione di una coltura autotrofa. In generale, l'alimentazione di anidride carbonica a queste colture in fotobioreattori tubolari è sotto controllo di pH, che dovrebbe essere implementato tra le equazioni del modello. In aggiunta, il modello potrebbe essere utilizzato per comprendere meglio se la configurazione bifasica tipica del reattore Lgem sia effettivamente più conveniente e performate che le configurazioni monofasiche tradizionali. Infine, potrebbero essere simulate altre colture mixotrofe, confrontando i risultati con quelli ottenuti con *Galdieria* in questa tesi. Se si utilizzasse *Chlorella sorokiniana*, tutte le velocità di reazione sarebbero doppie rispetto ai valori utilizzati in questa Tesi. Di conseguenza, un quantitativo differente di substrato dovrà essere inviato al reattore. Le strategie di controllo sviluppate con *Galdieria* potrebbero funzionare con successo anche con *Chlorella*, anche se i sistemi di controllo dovranno essere progettati per il processo specifico.

Summary

Abstract

Effective scale-up of microalgae cultures in photobioreactors is often limited by low biomass productivity. Even though mixotrophic cultivation may be an effective solution, oxygen balance, and concentration gradients are crucial aspects for optimization which have scarcely been investigated. Thus, this Thesis describes the improvement of a model that predicts substrate, oxygen, carbon dioxide, and inert gases concentration profiles in a biphasic tubular photobioreactor for *Galdieria sulphuraria*. In this photobioreactor, gas and liquid phase flow in cocurrent, leading to mass transfer between phases through the tube. The model can effectively simulate the reactor with constant light input or real daylight irradiance data.

Three different control strategies have been integrated into the model for comparisons. All the Proportional-Integral-Derivative (PID) control logics, designed and tested in silico, resulted in a favorable response of the system in both constant and real light regimes, also preventing anoxic conditions in the reactor. These results suggest the process is appropriate for further optimization in pilot-scale and large-scale reactors.

A scale-down experiment to simulate the substrate and oxygen gradients in the tubular photobioreactor has been successfully conducted in a lab-scale stirred tank reactor under constant light conditions. The experiment demonstrated that oxygen concentration in the gas phase could be an effective control variable to reach stability and prevent anoxia. The control strategy was designed beforehand with the aid of the model, and it resulted in a stable and robust control system. Oxygen concentration in the gas phase, dissolved oxygen, substrate concentration, and biomass productivity have been compared with the model results, and they reasonably match the model's predictions. Furthermore, it has been proven that the dissolved oxygen gradients achieved with the employed cultivation strategy did not affect the pigment profile of the microalga nor the dark-adapted efficiency of photosystem II.

The model that has been improved and the findings presented in this Thesis demonstrate the feasibility of pilot-scale cultivation of *G. sulphuraria*, and they will also be important for future developments and optimization of mixotrophic cultivation of other microalgal strains in tubular photobioreactors.

1. Introduction

1.1. Microalgae are a promising resource to face world challenges

As world population is projected to grow as high as 9.6 billion by 2050 (United Nations, 2022), issues regarding the increase in food, water, and energy demand need to be addressed. To tackle the environmental and socio-economical global challenges, the United Nations proposed the Sustainable Development Goals (SDGs). Cultivating microalgae and using them as an industrial feedstock can be effective in contributing to fulfilling more than one-third of SDGs (Peter et al., 2022). For instance, focusing on food security (SDG2), they can be considered one of the most promising alternative and sustainable sources of food and food ingredients. Microalgae can accumulate proteins and bio-active compounds for human nutrition (Caporgno & Mathys, 2018; Nethravathy et al., 2019) while growing in wastewaters and with a lower land usage than traditional protein sources (Caporgno & Mathys, 2018; Rodrigues-Sousa et al., 2021).

Some microalgae species, like *A. platensis* and *C. vulgaris,* can accumulate a considerable amount of proteins (up to 60% dry weight), comparable or even higher than the average protein content in plant sources. The aminoacidic profile, and hence the nutritional quality of the protein extract, depends on the microalga species and the growth conditions. However, there are several microalgae with an aminoacidic profile that is considered in line with WHO and FAO recommendations for a healthy diet (Kumar et al., 2022). Moreover, several high-value bioactive compounds and pigments can be found in microalgae, including essential lipids, chlorophylls, carotenoids, or phycobilins. Phycocyanin is a good example of a phycobiliprotein used in the food, nutraceutical, and cosmetics industries. Its market is expected to expand in the following years (Future Market Insights, February 2021 report). Up to this date, this compound is mainly produced from *Arthrospira* species (*Spirulina*), but it can also be obtained from other microalgae species, for instance *Galdieria sp.* (Abiusi et al., 2022). Considering its high protein content with favorable aminoacidic composition, *Galdieria* is the model species employed in this Thesis.

Even though there is a considerable demand for microalgae-based products such as proteins and phycocyanin, industrial biomass production and downstream processing still need to be improved. The economics of the process depends on the specific characteristics of the microalga, the cultivation strategy, and the biomass processing. Only a few Life Cycle Assessments (LCAs) that compare protein production from microalgae with traditional protein sources are available in the literature, and the sustainability of the process is still under debate (Zhang et al., 2022). However, both in economic and sustainability analysis, the main bottlenecks of the process can be pointed out, such as the ones related to low biomass productivity, low harvesting biomass concentration, high energy requirements, contamination risk, and carbon dioxide losses to the atmosphere (Bhatt et al., 2022).

Addressing all these issues requires further process optimization and the development of new strategies for microalgae cultivation. This Thesis is about the optimization of a cultivation strategy for the growth of *Galdieria sulphuraria* in a pilot-scale photobioreactor in order to provide a possible solution to the abovementioned challenges and the production of interesting compounds such as proteins and phycocyanin.

1.2. Microalgae and variables affecting their growth

Before going through the description of the contents and the approach followed in this Thesis, a short introduction to microalgae biology is provided. In addition, some of the variables that influence their growth are briefly discussed.

1.2.1 Introduction to microalgae biology: photosynthesis and carbon metabolism

The interest in growing microalgae cultures is mainly related to the fact that they are photoautotrophic eukaryotic unicellular microorganisms with higher areal productivity and lower land usage than terrestrial crops (Wijffels and Barbosa, 2010). Microalgae can perform photosynthesis, using light as a source of energy and carbon dioxide as a source of carbon for their growth, producing oxygen as a main byproduct (Figure 1.1).

The oxygenic photosynthesis reaction can be described as reported in Equation (1.1) (Masojídek et al., 2021).

$$CO_2 + 2H_2O + (8 \div 10)\ photons \rightarrow CH_2O + H_2O + O_2 + heat \quad (1.1)$$

Light absorption occurs in the internal membrane of chloroplasts (the thylakoid), where light-capturing pigments and enzymes for carbon fixation are located. These pigments are chlorophylls, carotenoids, and phycobilins. They are organized in enzymatic complexes called photosystem I and photosystem II, connected by a chain of electron carriers, all located on the so-called thylakoid membranes.

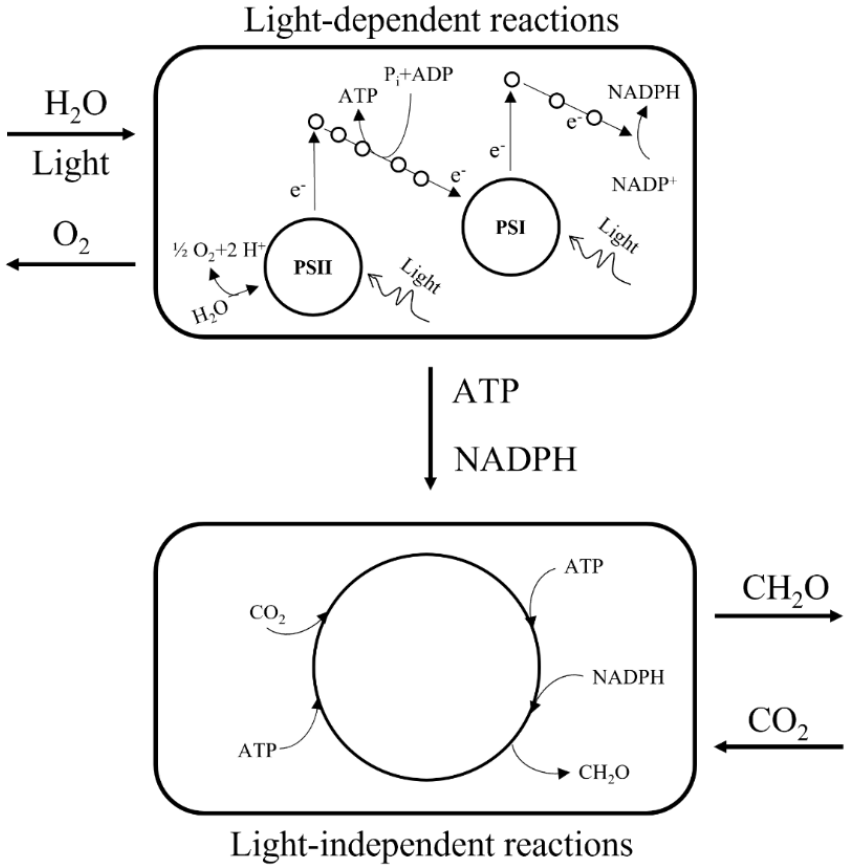

Figure 1.1: Schematic representation of the oxygenic photosynthesis reaction. Modified from Masojídek et al. (Masojídek et al., 2013).

In the light-dependent reactions of photosynthesis, photons are the reducing agents that extract a total of four electrons by the photolysis of two molecules of water (in order to produce one oxygen molecule). The electrons are transported through the series of electron carriers to produce NADPH. Simultaneously, protons are transferred into the intra-thylakoid space, leading to a pH gradient that drives ATP synthesis. During the light-independent reactions, one carbon dioxide molecule is fixed, and ATP and NADPH are consumed to produce carbohydrates and water.

As an alternative to photoautotrophic cultures (henceforth referred as autotrophic) (Figure 1.2, A), some microalgae can grow using an organic substrate and oxygen in chemo-organotrophic cultures (henceforth referred as heterotrophic). In these cultures, there is no need for light, and even though higher biomass productivities than autotrophic cultures can be reached, pigmentation may be affected by darkness (Figure 1.2, B). Microalgae cultures in dark conditions can be conducted in fermenters with intensive aeration, in a process that is similar to bacterial fermentation.

In some microalgal strains, both autotrophic and heterotrophic metabolisms can be active simultaneously so that the microalgae can grow using light and an organic substrate (mixotrophic cultivation). Therefore, oxygen and carbon dioxide can be internally recirculated inside the cell to the extent that depends on autotrophic and heterotrophic specific rates (Figure 1.2 C). Mixotrophic cultivation can lead to high biomass productivity and concentration without affecting pigmentation as much as heterotrophic cultivation. However, mixotrophic cultivation is more challenging than heterotrophic cultivation because light plays an important role, thus, a traditional fermenter is unsuitable. Compared to autotrophic cultivation, there is a higher risk of contamination due to the presence of the organic substrate. It is more difficult to control the culture because of a more complex metabolism.

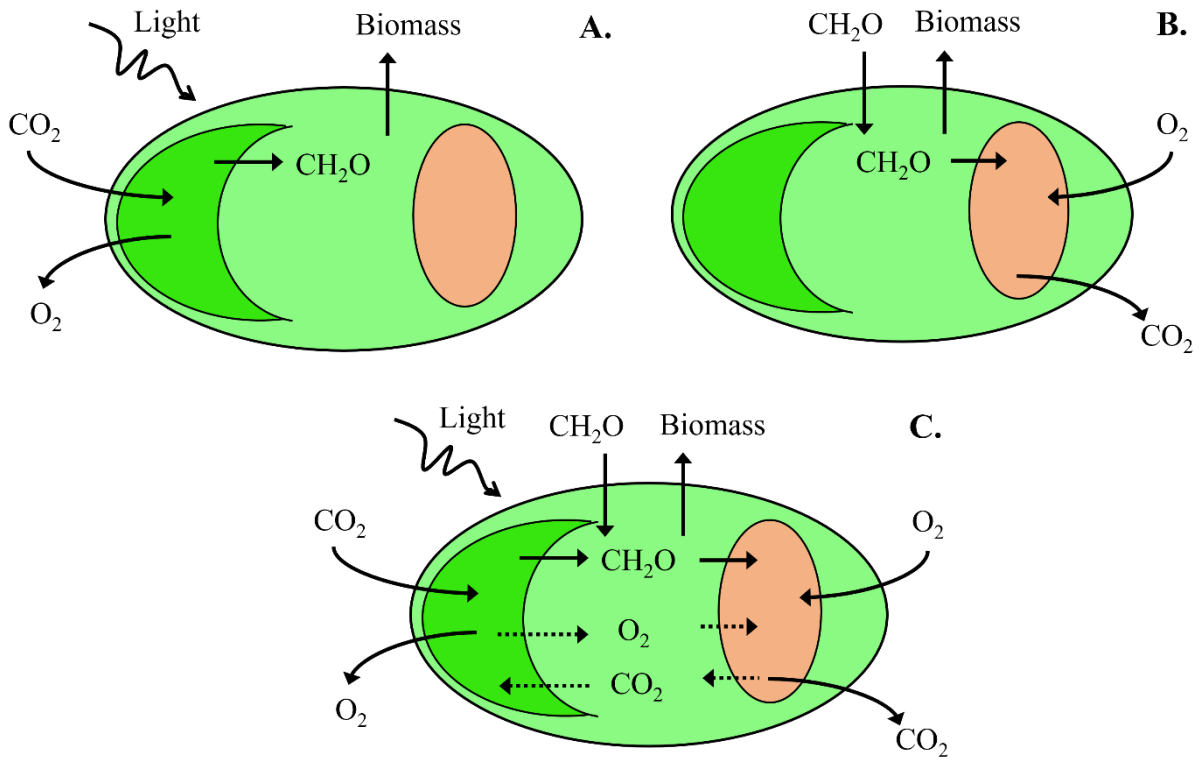

Figure 1.2: Different carbon metabolisms in autotrophic cultures (A), heterotrophic cultures (B), and mixotrophic cultures (C). Modified from Abiusi et al. (Abiusi et al., 2020a).

1.2.2 Light and light penetration effect

Light is one of the most critical factors for autotrophic and mixotrophic outdoor cultures. Light intensity and quality are crucial for biomass growth, as photosynthetic reactions that require light depend on both. However, the description of the influence of light on the culture is not straightforward, because the photobioreactor specific design and the culture conditions influence the average amount of photons received by an individual cell.

For a specific geographic location on a particular day of the year, the daily global solar radiation at ground level (on a horizontal surface) depends on the extraterrestrial solar radiation and its attenuation at higher atmospheric levels. However, only the incident photosynthetically active radiation (PAR, wavelengths between 400-700 nm) contributes to biomass growth. It is only a fraction of around 45% of the global incident radiation (Masojídek et al., 2013), depending on the pigments composition of the light-harvesting antenna of the microalgae cells (Fernández et al., 1998).

The irradiance during the day can be measured at ground level or from satellites. The National Solar Radiation Database (NSRDB, https://nsrdb.nrel.gov/) is a publicly accessible physics-based database containing irradiance data from satellites in various locations and years. The global irradiance at the clear sky scenario is obtained from raw datasets, employing a cloud mask and specific algorithms. The real irradiance is computed by different algorithms, when the cloud mask identifies the cloudy sky. Further information about the database, its validation, and the algorithms can be found on the NSRDB website (https://nsrdb.nrel.gov/) or in Sengupta and colleagues' work (Sengupta et al., 2015).

In Figure 1.3, as an example, it is reported a plot of the photosynthetic active radiation in time considering both the clear-sky global horizontal irradiance and the real one taking into account the current atmospheric conditions during the day 15/08/2019 in Bennekom, The Netherlands. As clearly shown in the Figure, a sinusoidal function can model the clear sky conditions.

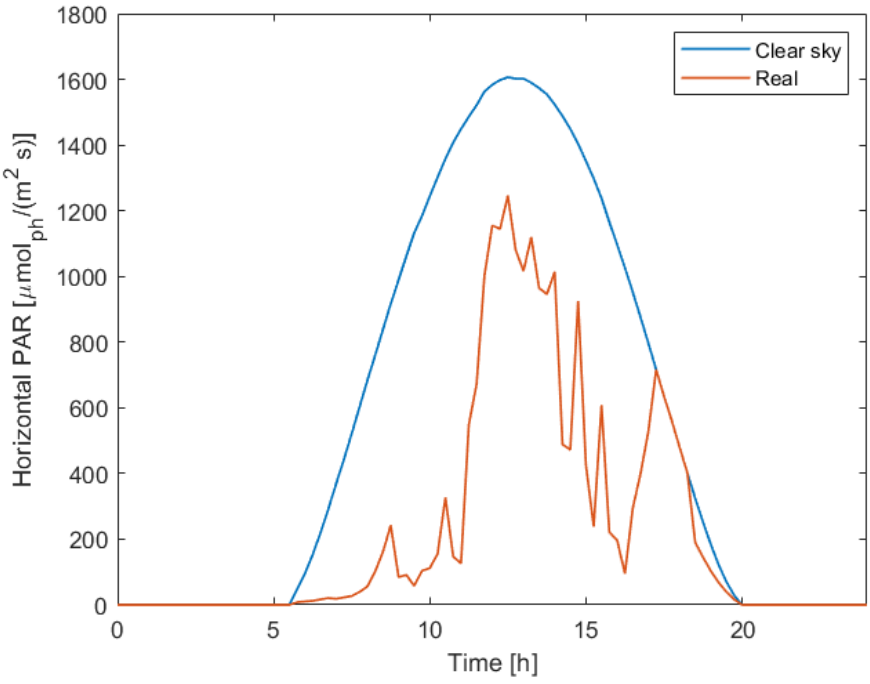

Figure 1.3: clear sky and real horizontal photosynthetically active radiation, 15/08/2019 in Bennekom, The Netherlands. The plots are obtained from data belonging to the NSRDB database.

The geometry of the cultivation unit and its orientation to light during the day play a role in the available radiation for the culture. The irradiance at the surface of the reactor is usually given as a photon flux density (PFD, $\mu mol_{ph}\ m^{-2}\ s^{-1}$), it can be measured or estimated with models and is crucial for the growth rate of the culture.

Figure 1.4 shows the relationship between the rate of oxygen production and irradiance of an autotrophic culture (Masojídek et al., 2013). In dark conditions or with extremely low light, oxygen production is negative as the oxygen consumption for maintenance (dark respiration) is higher than oxygen production by photosynthesis. At low light intensities, the gross oxygen production (the sum of the net photosynthesis and respiration) increases linearly with irradiance. For higher light intensities, photosynthesis becomes less efficient, and oxygen production reaches saturation, or it decreases as the culture could be photoinhibited. Photosynthesis is generally saturated at irradiances much lower than the maximum sunlight irradiance during the day. In order to achieve high efficiency of photosynthesis and growth rates, light must be "diluted" into the culture so that every individual cell receives an optimal irradiance for its growth.

A final point to mention is the effect of light attenuation inside the culture, mainly due to the mutual shading of the cells. In dense cultures, light irradiance decreases rapidly from the surface of the reactor, meaning that the cells deeper in the culture would receive a low light intensity, or no light at all (Wang et al., 2015). This means that, with increasing biomass concentration, a larger volume fraction of the culture does not contribute to biomass productivity but only to energy costs. In a mixotrophic culture, biomass can grow in the dark volume so that biomass productivity is higher when compared with an autotrophic reference culture in the same conditions.

Lastly, mixing and turbulence are other important aspects because they are linked to exposure to short-timescale dark/light cycles, which strongly enhance growth (Masojídek et al., 2011). In this way, light is diluted, available in small amounts for a higher number of cells, and used more efficiently.

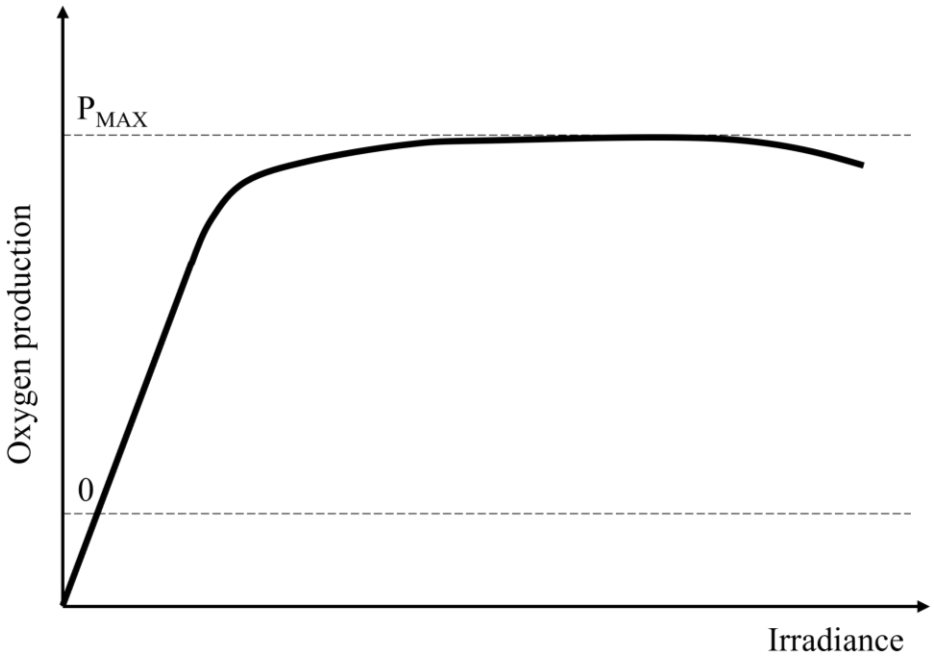

Figure 1.4: the oxygen production as a function of irradiance in an autotrophic culture (P/I curve). Modified from Masojídek et al. (Masojídek et al., 2013).

1.2.3 Dissolved oxygen effect

Oxygen is a product of photosynthesis, and its concentration in the liquid medium may affect the performance of the process. Photosynthetic activity and growth can be affected by high dissolved oxygen levels typical of dense microalgal cultures. When oxygen concentration increases, oxygen-consuming reactions, like photorespiration, gain more importance at the expenses of the photosynthesis reaction (Sforza et al., 2020). Photorespiration is the photo-oxidation of one of the intermediates in the carbon dioxide reduction cycle, without a metabolic gain and lowering the overall yield of biomass. The reaction is favored when the ratio between oxygen and carbon dioxide concentrations is high. Thus, a good gas exchange in the system is needed to avoid this reaction.

In a mixotrophic culture, oxygen consumption due to substrate oxidation can decrease dissolved oxygen levels. Low dissolved oxygen concentration leads to anoxia, which may affect substrate assimilation (Rhie et al., 2022) and biomass productivity. In *Galdieria sulphuraria,* low dissolved oxygen limits pigment synthesis, meaning that phycocyanin concentration is also affected by anoxic conditions (Sarian et al., 2016). If the culture is run without gas inputs, heterotrophic oxygen consumption and autotrophic oxygen production should be balanced to avoid dissolved oxygen concentration becoming too low.

1.3. Oxygen balanced mixotrophy

Recently, a new cultivation method for mixotrophic cultures, called "Oxygen Balanced Mixotrophy" (OBM), has been developed for the model microalga *Chlorella sorokiniana* (Abiusi et al., 2020a). In this method, the substrate supply rate is manipulated so that the dissolved oxygen in the reactor remains constant. Keeping dissolved oxygen constant in an ideal stirred tank reactor means that the autotrophic oxygen production rate balances the heterotrophic oxygen consumption rate. Thus, oxygen is entirely recycled inside the cells, and only a small amount of CO_2 is produced (Figure 1.5). In this way, the photobioreactor is run without gas input.

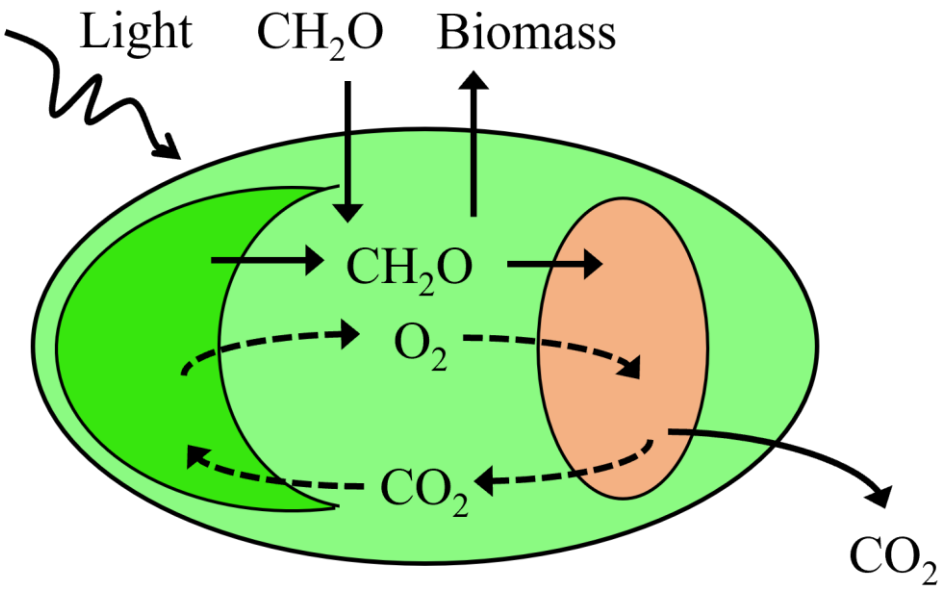

Figure 1.5: In a mixotrophic cultivation with oxygen balance (OBM), oxygen is internally recirculated inside the cell. Modified from Abiusi et al. (Abiusi et al., 2020a).

This type of cultivation can be implemented in the stirred tank photobioreactor with a PID control system. Glucose, which is the organic substrate, is continuously added from the top of the reactor, and it is mixed inside the vessel due to its intensive stirring. In OBM conditions, glucose does not accumulate in the reactor: its consumption is linked to oxygen consumption that balances autotrophic production.

As a result of the cultivation strategy, biomass productivity is doubled with respect to the autotrophic reference culture. However, due to the presence of the organic substrate, mixotrophic cultures are usually more sensitive to contamination than autotrophic ones. One way to circumvent this problem could be using an extremophilic mixotrophic microalga, like *Galdieria sulphuraria* (Abiusi et al., 2021).

G. sulphuraria belongs to the class of *Cyanidiaceae* (phylum *Rhodophyta*) (Merola et al., 1981), composed of thermoacidophilic microalgae that grow in volcanic and hot environments in acidic conditions. *G. sulphuraria* can grow at temperatures up to 57°C, pH levels below 3, and high osmotic pressure (up to 400 g/L of sugar and 2-3 M of salt) (Čížková et al., 2020; Schmidt et al., 2005; Sloth et al., 2006) on a large variety of substrates or wastewater for nitrogen recovery (Gross & Schnarrenberger, 1995; Zhu et al., 2022). It can accumulate a high quantity of phycocyanin (10% w/w) and up to 60% w/w total protein content with a favorable amino acid profile when grown in OBM. Furthermore, phycocyanin extracted from *Galdieria* has been proven to be more thermo-stable and acid-stable than the one produced from *Spirulina* (Abiusi et al., 2022). Considering the high biomass productivity achieved with the OBM cultivation strategy, and the very low contamination risk due to the culture conditions, this process is being further studied for an industrial scale-up.

1.4. Outdoor photobioreactors for microalgae cultivation

Microalgae are currently autotrophically grown in various large-scale cultivating systems (Apel & Weuster-Botz, 2015; Touloupakis et al., 2022). Open systems such as open or raceway ponds are usually the cheapest choice. Still, they require high areas, are likely to have an increased risk of contamination, and are much affected by outdoor weather conditions. For better control and optimization of culture conditions, closed photobioreactors are generally preferred to open systems. These cultivation units are vessels made of glass or transparent polymeric material, closed but transparent reactors that can be exposed to sunlight or artificial light. Several photobioreactor designs are available, with different geometry, fluid dynamics, and optical path. As a result, biomass concentration and productivity in the systems are strongly related to the specific design.

The performances of a photobioreactor can be characterized by parameters such as photosynthetic efficiency (PE) and biomass areal productivity. Photosynthetic efficiency is a measure of the fraction of solar energy converted into chemical energy. Its maximum theoretical value has been estimated at around 10% in full sunlight, but that is not reached with the current state of art cultivation systems (Masojídek et al., 2021). It is also essential to consider the energy expenditure during the cultivation, which significantly impacts the overall cost of the process. Vertical photobioreactors with a large surface area usually have a higher PE than horizontal ones because of the higher capture of sunlight, which is also diluted in a large reactor area. In this way, the lower average irradiance received by the individual cells leads to higher efficiency in photosynthesis. However, they are also generally more expensive for investment and energy expenses because of the higher pressure in the system.

One of the most appropriate photobioreactors for large-scale dense cultures is the tubular photobioreactor (Sirohi et al., 2022). It usually comprises two main sections: the tubular solar

collector and a mixing tank. The tubular part is made of a transparent material to let photosynthesis and biomass growth occur in the liquid phase (dispersed flow). The diameter of the tube is usually small (4-10 cm) to provide a large surface area, and the length can go up to hundreds of meters. The mixing tank is needed for gas exchange (stripping of oxygen and enrichment of carbon dioxide) and to adjust other culture variables (pH and temperature, for instance). The volume of this tank should be minimal compared to the volume of the tubular section, considering that it is usually a dark volume in the overall tubular reactor. As previously stated, microalgae will produce oxygen during autotrophic metabolism, which will inevitably accumulate in the tubular section of the reactor. The velocity of the liquid phase is set by a pump or an airlift device, and it has to be defined so that the oxygen concentration remains in a safe range for the culture in the reactor. Furthermore, turbulence in the reactor is needed for mass transfer and acceptable light/dark cycles. Considering the carbon dioxide needed for the culture, transfer in the liquid phase, and uptake kinetics, a high flowrate of pure carbon dioxide or enriched air is needed in the mixing tank (Apel & Weuster-Botz, 2015).

In summary, the main expenses for this kind of photobioreactor configuration are related to the energy cost for liquid recirculation, gas input in the system, and using carbon dioxide to enrich the liquid phase. The supply of carbon dioxide has been estimated to be up to the 30% of the overall microalgae production cost. Furthermore, carbon dioxide losses of around 25% have been detected even in optimized systems (Acién et al., 2012).

An alternative to face the high costs of autotrophic cultures in tubular photobioreactors is the mixotrophic cultivation of microalgae. An economic evaluation of the mixotrophic cultivation of *G. sulphuraria,* compared with the autotrophic reference, shows that the higher biomass productivity and concentration do not lead to much higher energy expenses for recirculation. However, mixotrophic cultivation could lower the energetic requirements because the culture does not require aeration. It is estimated that OBM cultivation of *G. sulphuraria* is three-fold cheaper than the autotrophic one (Abiusi, 2021). Considering environmental impacts, the main bottleneck for the sustainability of the process also seems to be related to the energy demand in the cultivation stage (Smetana et al., 2017; Somers et al., 2021). Another option to reduce costs and increase the sustainability of the process might be using a low-cost industrial byproduct or waste as substrate feed for the mixotrophic photobioreactor (D'Imporzano et al., 2018; Gross & Schnarrenberger, 1995).

1.5. Scale-up of oxygen balanced mixotrophy for Galdieria sulphuraria

Scaling up OBM in a tubular photobioreactor, aiming for the same performances obtained in the lab-scale reactor, is not a trivial task. Diurnal variations in light and temperature affect biomass productivity and mixotrophic metabolism. Furthermore, the liquid phase is not ideally mixed, and it resembles more of a plug flow. As substrate enters the system only at the beginning of the tubes, the substrate concentration is expected to decrease along the reactor. In addition, the oxygen concentration is not uniform, and it must be evaluated whether its value allow a safe operation avoiding anoxic conditions. A control system different from the one used in the lab-scale reactor, described in Section 1.3, must be designed to obtain mixotrophic conditions through the tubes and avoid anoxia.

1.5.1 Lgem two-phase tubular photobioreactor

The tubular photobioreactor selected for the scale-up of this process is a GemTube MK1 – 1500s (Lgem, The Netherlands), situated in AlgaePARC (Bennekom, The Netherlands) (Figure 1.6).

The main difference with the single-phase tubular photobioreactors described in section 1.4 is that the gassing of the system is not performed in a separate mixing unit but in the tubular section. Therefore, the fluid dynamic regime in the tubes can be described as an elongated bubble regime. This different configuration might improve mass transfer across the reactor so that oxygen stripping and carbon dioxide enrichment in the liquid phase can happen along the tube. Therefore, this design aims to achieve higher productivity in autotrophic cultures, as this photobioreactor should lower the chances of carbon limitation and oxygen inhibition in the solar collector.

Improved mass transfer across the tubes is also beneficial when running the reactor with a mixotrophic culture when external gas input is not provided. The gas phase can be recycled in the system, supplying oxygen when heterotrophic metabolism prevails (so that anoxic conditions are avoided) and stripping it when oxygen production is dominant. A liquid pump can also be used to increase the velocity of the liquid phase (accelerated mode). This increase goes along with a slight increase in the mass transfer coefficient.

A drawing of the Lgem photobioreactor is provided in Figure 1.7, alongside with its dimensions. It comprises two distinct tubular sections (two helices, 280 m each with an internal diameter of 6.2 cm) connected to a mixing tank where temperature and pH may controlled. The reactor has two air circulation pumps, two substrate pumps (a gas pump and a substrate pump for each helix), and a liquid pump. Some additional fluid dynamic parameters of this photobioreactor are presented in Table 1.1 (Zetrialdi, 2020).

1.5.2 Control strategy for large-scale mixotrophic cultivation

The control strategy that is implemented in the stirred tank photobioreactor must be adapted to the tubular photobioreactor, to achieve oxygen-balance. It is impossible to keep a constant substrate concentration level in the whole reactor as was happening in the stirred tank reactor. In the tubular reactor, the substrate flowrate can be controlled only at the beginning of the tube, and it is consumed over its length. This means that the net oxygen production will be a function of the position in the tube, and it is impossible to achieve a balance in every position. With a control system, stable substrate, and dissolved oxygen profiles can be obtained so that the average oxygen production in the whole reactor approaches zero. The PID controller acts on the error signal, calculated from an input set-point value and a measurement of a process variable. The process variable can be dissolved oxygen or oxygen concentration in the gas phase. Considering the design of the reactor, it is useful to place the oxygen probe at the end or the beginning of the tube.

Table 1.1: fluid-dynamic characterization of the Lgem reactor (Zetrialdi, 2020).

Configuration	$\mathbf{F_G}$ **[m³/s]**	$\mathbf{F_L}$ **[m³/s]**	$\boldsymbol{\varepsilon_G}$ **[-]**	$\boldsymbol{\tau_G}$ **[min]**	$\boldsymbol{\tau_L}$ **[min]**	$\boldsymbol{v_G}$ **[m/s]**	$\boldsymbol{v_L}$ **[m/s]**
Accelerated	20	52.7	0.28	11.98	11.92	0.39	0.39
Normal	20	18.3	0.27	11.51	34.76	0.41	0.13

Figure 1.6: Photo of the Lgem photobioreactor discussed in this Thesis in operation.

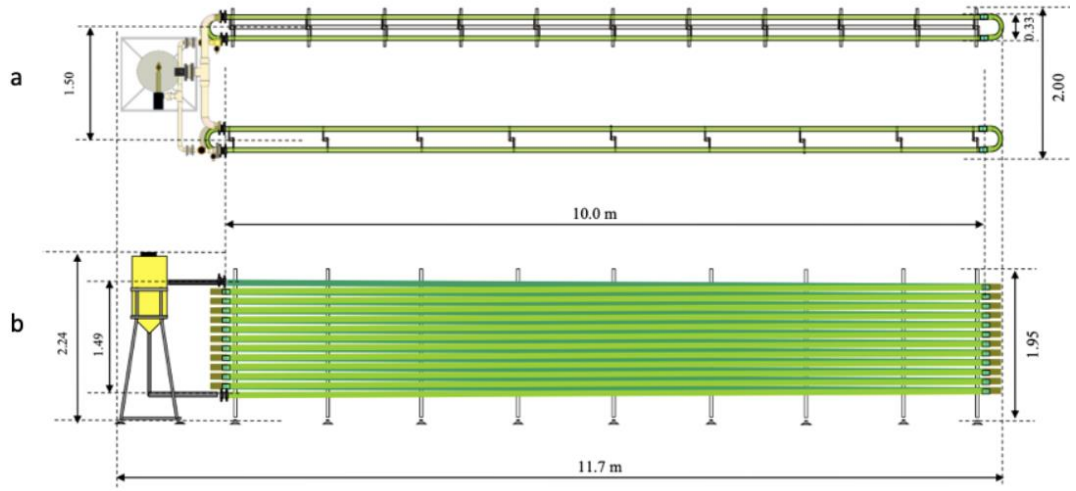

Figure 1.7: Drawing of the Lgem photobioreactor discussed in this thesis (GemTube MK-1 1500s product spec., 2015). Top view (a) and side view of the reactor (b). Length measurements in meters.

1.5.3 Residence time distributions

The study of residence time distributions in a reactor helps to understand the dynamics of the fluid phases and may be helpful as a starting point for developing a model.

The residence time of a small element of fluid that enters inside a reactor is the time it requires to reach its outlet. Considering a set of different fluid elements, their residence time in the vessel depends on the fluid dynamics of the system. Therefore, fluid elements of different ages may be found in the outlet of the reactor. The residence time distribution (RTD or *E(t)*) is a normalized statistical function that aims to describe the distribution of residence

time of the flowing fluid. It is particularly useful in detecting non-ideal flow behavior in the reactor. This type of description is usually done for a single vessel in a steady state without reactions or density change (Levenspiel, 1999).

A cumulative normalized function for residence time distribution is defined in equation (1.2). Calculating *E(t)* and *F(t)* functions for a real system may be the first step to estimating how its behavior differs from ideal conditions.

$$F(t) = \frac{\int_0^t E(t)dt}{\int_0^\infty E(t)dt} \tag{1.2}$$

E(t) function for model systems can be obtained by simulating a simple experiment (Figure 1.8). An inert tracer ideal pulse is fed in the inlet of the system at time zero, and its concentration is measured at the outlet of the system as a function of time. The *E(t)* function for this experiment can be calculated as reported in equation (1.3).

$$E(t) = \frac{C(t)}{\int_0^\infty C(t)dt} \tag{1.3}$$

If the reactor is an ideal one, or it can be modelled by various ideal components (e.g. tank in series), the tracer concentration in time in the outlet stream can be calculated knowing the properties of the ideal reactor or solving unsteady-state material balances. As an example, all fluid elements in the outlet of an ideal plug flow reactor at a certain time have the same residence time, so the equation to describe the residence time distribution is straightforward [equation (1.4)].

$$E(t) = \delta\,(t - \tau) \tag{1.4}$$

Where δ is the Dirac delta function and τ_L the liquid residence time in the reactor. A solution is also available for the tank in series model [equation (1.5)] (Toson et al., 2019).

$$E(t) = \frac{t^{N-1}}{(N-1)!}\left(\frac{N}{\tau_L}\right)^N \exp\left(-\frac{N}{\tau}\,t\right), \quad N \geq 1 \tag{1.5}$$

When the number of tanks N tends to infinity, equation (1.4) can be obtained from equation (1.4). However, it is not possible to use equation (1.5) with values of N much higher than 100 because it will result in overflow during the calculation of $E(t)$. These models are graphically reported in Figure 1.9 as an example for comparisons.

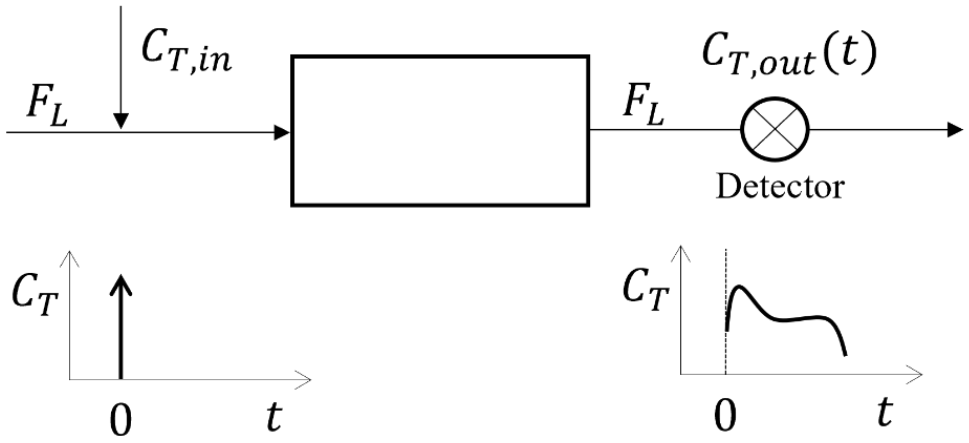

Figure 1.8: Sschematic representation of the experiment to calculate the residence time distribution.

1.6. Aim and contents

This Thesis focuses on understanding the effects of substrate and oxygen gradients in the pilot-scale Lgem tubular photobioreactor when growing *G. sulphuraria*. A model is helpful to have qualitative and quantitative information on the concentration profiles across the tubular section of the reactor to upscale the process. Different strategies have to be compared and evaluated. The control system for substrate feeding in the reactor is a crucial aspect of this mixotrophic cultivation. Lastly, a downscale experiment in the lab-scale setting is conducted to validate the model's results.

The aims of this Thesis are:

- Improving a model for the Lgem photobioreactor in OBM conditions
- Simulating different control systems
- Simulating the system under constant, sinusoidal, and real light conditions in a cloudy day
- Validating the control strategy in a lab-scale reactor in constant light conditions

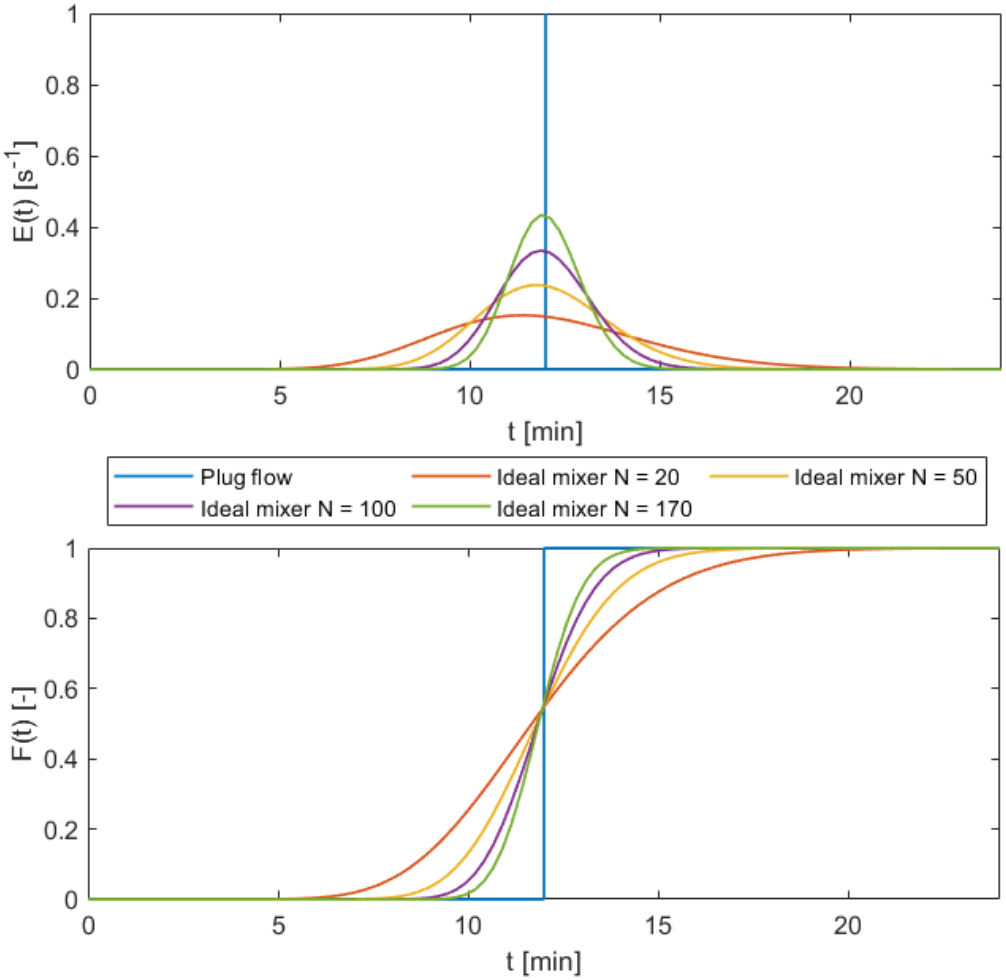

Figure 1.9: Theoretical residence time distribution functions for the plug flow and tanks in series models [equations (1.3) and (1.4)]. In this example, the residence time of the fluid is 12 min.

2. Mathematical model

Scaling up a photobioreactor is not a trivial task, because its performance generally depends on its dimensions. Up-scaling a lab-scale stirred tank reactor process in an already existing tubular photobioreactor is challenging due to the non-homogeneous conditions across the length of the tubes and the different fluid-dynamics of the system. Furthermore, microalgal cultures are influenced by several variables, and the effect of scale and the different reactor configurations on them is not intuitive. Lastly, tubular photobioreactors are not designed for mixotrophic cultures. A model that describes the interaction between process variables, organism parameters, and environmental conditions in a pilot-scale photobioreactor can be extremely useful in studying and scaling the system. In addition, the metabolic rates depend on the position in the reactor because substrate, carbon dioxide, and oxygen concentrations in the liquid phase change through the tube. For this reason, for oxygen-balanced mixotrophic cultivation in a tubular reactor, a different control system is needed than in a lab-scale reactor.

2.1 Model description and assumptions

The mathematical model for the process is developed with a common assumption for tubular photobioreactor modeling (Fernández et al., 2012): the light collector can be described as a series of co-current ideal stirred tanks (or mixers). A block diagram for the system is represented in Figure 2.1. For this simplified process, dynamic material balance equations accounting for both kinetic and mass transfer in each tank are solved (Jordaan, 2022). The reference condition for the simulations is the accelerated mode, with the liquid pump switched on and the gas flowrate at the lowest value (Table 1.1). Only one helix of the reactor will be simulated, assuming that the second one will behave similarly.

The model has been developed with the following assumptions and limitations:

- The tubular section of the reactor is approximated as a series of 100 identical ideal tanks. This assumption will be further addressed in chapter 4, comparing experimental residence time distributions to theoretical ones, and performing a sensitivity on the final model.
- Mass transfer, autotrophic and heterotrophic productivities in the central degasser are neglected, as the residence time there is much lower than the residence time in the tubes. This vessel is almost dark, with low substrate concentration in normal conditions.

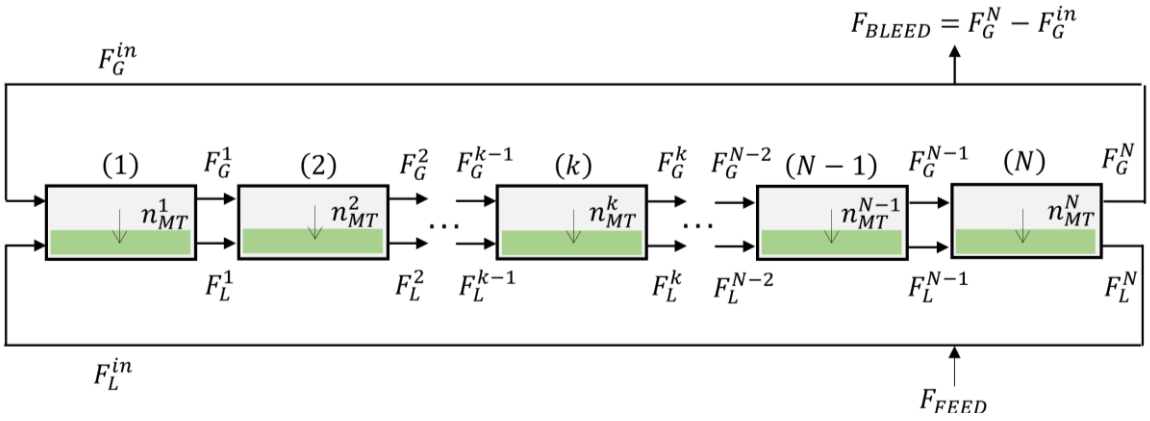

Figure 2.1: Schematic representation of the system as a series of co-current ideal stirred tanks.

- Pressure increase due to the pumping system and pressure losses in the tubes are assumed negligible.
- Liquid and gas are well mixed in the radial direction.
- The gas phase behaves like an ideal gas.
- The gas holdup for each tank is the same and does not change in time. This parameter has been measured for the tubes of the photobioreactor in different flow configurations (Table 1.1 in section 1.5).
- The gas-liquid transfer coefficient is assumed to be constant in time and length. It is the average value of the transfer coefficient in the reactor for a specific flow configuration at ambient temperature (Zetrialdi, 2020).
- Temperature is constant, and it is set to 37°C. However, the temperature fluctuates during the day (de Winter, 2022), and kinetic parameters, transport coefficients, gas holdup, and thermodynamic parameters are influenced by it. Even though the temperature in the greenhouse where the photobioreactor is located is generally around 30-40°C during Summer, the transport coefficients are calculated at ambient temperature (Zetrialdi, 2020). In section 2.2, an estimation of these parameters at 37°C is provided.
- The mixotrophic stoichiometry is the sum of heterotrophic and autotrophic stoichiometries (Section 2.3), and the reference biomass composition is $CH_{1.62}O_{0.41}N_{0.14}P_{0.011}$ (Kliphuis et al., 2012).
- The maintenance of cells is neglected.
- The volumetric productivity is assumed to be constant. In the model, a constant biomass concentration and a constant specific photoautotrophic oxygen production rate are assumed. The biomass concentration increases during the day, together with a decrease in specific photoautotrophic rate, because of increased light limitation. However, the product of concentration and specific rate (volumetric productivity) is constant over a day and even multiple days in a row. Previous lab-scale experiments showed that OBM cultivations of *G. sulphuraria* can reach biomass productivity as high as 1.72 g_X/(L d) (Abiusi et al., 2021) and that productivity is constant from a biomass concentration of 2 g_x/L up to a concentration of 10 g_x/L. Furthermore, if the incoming light intensity on the photobioreactor is constant, specific autotrophic oxygen production is constant. In a following section, some real daylight conditions will be tested to understand the effects of a variable light intensity external supply on the dynamics of the system.

2.2 Input parameters estimation

Considering that temperature has an important role in the system, all the parameters are calculated accordingly.

The partition coefficients m_{O2} and m_{CO2} are obtained from the reference parameters for oxygen and carbon dioxide given in Sander's work (Sander, 2015) using equation (2.1),

$$m(T) = \left(H_{cp}(T_{ref})\, exp\left(-\frac{\Delta_{sol}H}{R}\left(\frac{1}{T} - \frac{1}{T_{ref}}\right)\right)(R\,T)\right)^{-1} \tag{2.1}$$

Where $H_{cp}(T_{ref})$ is the Henry solubility for the gas component in water at reference temperature (298.15 K) and $\Delta_{sol}H$ is its enthalpy of dissolution. Using the parameters in table 2.1, the calculated values of m_{O2} and m_{CO2} at 37°C are 44.4 and 1.84. In this estimation it is assumed a gas-water system, neglecting the influences of chemical equilibria, composition of the system or pH.

Temperature influences the physical parameters and transport properties in the system by increasing the liquid diffusivity, but also decreasing viscosity and surface tension of the liquid. The lower viscosity and surface tension also favors the formation of smaller bubbles in the system and so, an increase of the interfacial area, gas holdup and bubble velocity (Lau et al., 2004).

Considering Higbie's penetration theory for the liquid film that affects the mass transfer rates, the liquid transport coefficient k_L is proportional to the square root of diffusivity D_{GL} divided by the average contact time between phases τ_C [equation (2.2)].

$$k_L \propto \sqrt{\frac{D_{GL}}{\tau_C}} \tag{2.2}$$

Liquid diffusivity can be expressed with the Wilke and Chang relationship, that shows the direct effect of temperature and the indirect effect of temperature on viscosity [Equation (2.3)].

$$D_{GL} \propto \frac{T}{\mu} \tag{2.3}$$

With a temperature increase from 20°C to 37°C, viscosity decreases from 1.002 mPa s to around 0.65 mPa s, leading to an increase in D_{GL} of a factor around 1.65. However, the average contact time between phases, that can be defined as a ratio of bubble Sauter-mean diameter to the bubble velocity, indirectly increases with temperature (because of the effects of surface tension and viscosity). Furthermore, the gas-liquid transport area increases with temperature because gas holdup increases and bubble diameter decreases [equation (2.4)] (Nedeltchev, 2022).

$$a \propto \frac{\varepsilon_G}{d_{Bubble}} \tag{2.4}$$

Neglecting both the increase in the gas liquid transport area and in the contact time, the transport coefficient increases of a factor around 1.3. Thus, considering the effect of temperature, $k_{O2,L}a$ and $k_{CO2,L}a$ are assumed 2.6E-3 1/s and 2.21E-3 1/s.

Table 2.1: Parameters used to calculate the partition coefficients.

Parameter	Value for O_2	Value for CO_2
$H_{cp}(T_{ref})$ [mol/(m^3 Pa)]	1.2E-5	3.3E-4
$\frac{\Delta_{sol}H}{R}$ [K]	1700	2400
T [K]	310.15	310.15

Finally, the organism parameters used in the simulations and reported in Table 2.2 are measured at 37°C, so no correction is needed. The heterotrophic yield on substrate has been measured in a heterotrophic culture of *G. sulphuraria* (Abiusi et al., 2021). The value chosen for the autotrophic yield on photons is an average value of the yields obtained in the autotrophic chemostat in another work (Abiusi et al., 2022). The half-saturation constants for oxygen and substrate have been measured in heterotrophic experiments with a mixotrophic acclimated culture (Jordaan, 2022). The value of the maximum specific substrate consumption rate has been derived by the heterotrophic specific oxygen consumption rate, using the oxygen yield on substrate derived with the stoichiometric equations (Section 2.3). The value of the half-saturation constant for carbon dioxide is a typical value for other algae strains. A sensitivity analysis of this parameter shows that the results of the simulations do not depend much on this value, as $C_{CO2} >> K_{CO2}$ (carbon dioxide accumulates in the reactor as a consequence of OBM stoichiometry).

2.3 Model equations

Autotrophic and heterotrophic stoichiometry can be written for *G. sulphuraria*, assuming that the elemental composition per C-mol of biomass is $CH_{1.62}O_{0.41}N_{0.14}P_{0.011}$ (Kliphuis et al., 2012). The stoichiometric coefficients are expressed as volumetric rates in mol/(m^3 d).

For the autotrophic growth, the stoichiometry can be solved knowing the light intensity, and the autotrophic biomass yield on photons. Considering a light input of 1.5 mol_{ph}/(L d), and a yield of 22 C-$mmol_X$/mol_{ph}, the elemental and charge balances can be solved and the stoichiometric equation (2.5) can be written.

$$33\ CO_2 + 4.6\ NH_4^+ + 0.4\ H_2PO_4^- + 19.3\ H_2O + 1.5\ 10^3\ \text{photons} \rightarrow$$
$$33\ CH_{1.62}O_{0.41}N_{0.14}P_{0.011} + 36.6\ O_2 + 4.3\ H^+ \qquad (2.5)$$

Because of the OBM cultivation strategy, the heterotrophic oxygen consumption rate is equal to the autotrophic oxygen production rate, and the heterotrophic biomass yield on substate ($Y_{X/S}$) is 0.59 C-mol_x/C-mol_s. The heterotrophic stoichiometry can be solved [equation (2.6)].

Table 2.2: Organism parameters (Abiusi et al., 2021; Jordaan, 2022).

Description	Parameter	Value
Heterotrophic biomass yield on substrate	$Y_{X/S}$	0.59 C-mol_X/C-mol_S
Autotrophic biomass yield on photons	$Y_{X/ph}$	22 C-$mmol_X$/mol_{ph}
Half saturation constant for substrate	K_S	0.304 C-mol_S/m^3
Half saturation constant for oxygen	K_{O2}	1.3E-3 mol_{O2}/m^3
Half saturation constant for carbon dioxide	K_{CO2}	1E-2 mol_{CO2}/m^3
Maximum specific substrate consumption rate	$q_{S,max}$	9.63E-6 C-mol_S/(C-mol_X s)

$$105.9\ CH_2O + 36.6\ O_2 + 8.7\ NH_4^+ + 0.7\ H_2PO_4^- \rightarrow$$
$$62.5\ CH_{1.62}O_{0.41}N_{0.14}P_{0.01} + 43.4\ CO_2 + 69.4\ H_2O + 8.1\ H^+ \quad (2.6)$$

Assuming that mixotrophic metabolism is the sum of the two abovementioned ones, equation (2.7) can be obtained.

$$105.9\ CH_2O + 13.4\ NH_4^+ + 1.1\ H_2PO_4^- + 1.5\ 10^3\ photons \rightarrow$$
$$95.5\ CH_{1.62}O_{0.41}N_{0.14}P_{0.01} + 10.4\ CO_2 + 50.1\ H_2O + 12.3\ H^+ \quad (2.7)$$

However, it is important to state that this last assumption is not valid in reality: experimental results (Abiusi et al., 2021) show that there is a negative interaction between autotrophic and heterotrophic metabolisms in *G. sulphuraria* so that the mixotrophic biomass productivity is not the sum of the autotrophic and heterotrophic one. However, further studies on the mixotrophic metabolism of this strain of *G. sulphuraria* are needed before this feature may be implemented into the mathematical model of the process.

From the stoichiometric equations, the parameters needed for the simulation can be obtained (Table 2.3). The value of glucose concentration is based on the glucose concentration in the solution used for this process at the pilot scale (around 100-200 g/L). The value of biomass concentration and specific oxygen production rate are obtained in an autotrophic chemostat in the lab-scale reactor. However, they are reasonable for the pilot-scale tubular photobioreactor. It is assumed that this is the oxygen production of the light-limited system in constant incident light condition at 500 $\mu mol_{ph}\, m^{-2}\, s^{-1}$ and biomass concentration 200 Cmol/m^3. The stoichiometric feed flowrate is calculated with equation (2.8), assuming that all the autotrophic oxygen production is balanced by heterotrophic oxygen consumption. This equation is based on stoichiometry, so no limiting conditions other than light are considered (carbon dioxide, substrate, and oxygen limitation).

$$F_{FEED} = \frac{q_{O2,auto}\ C_X\ V_L}{Y_{O/S}\ C_{S,FEED}} \quad (2.8)$$

The balances for the mixers refer to Figure 2.2, and they are written for substrate, oxygen, carbon dioxide, inert gas, total liquid, and total gas (equations (2.9) - (2.24)).

Table 2.3: Parameters calculated from stoichiometric relationships.

Description	Parameter	Value
Heterotrophic carbon dioxide yield on substrate	$Y_{C/S}$	0.41 C-mol$_{CO2}$/C-mol$_S$
Autotrophic oxygen yield on carbon dioxide	$Y_{O/C}$	1.11 mol$_{O2}$/mol$_{CO2}$
Heterotrophic oxygen yield on substrate	$Y_{O/S}$	0.346 mol$_{O2}$/C-mol$_S$
Specific autotrophic oxygen production rate (biomass concentration 200 C-mol/m^3)	$q_{O2,auto}$	1.96E-6 mol$_{O2}$/(C-mol$_S$ s)
Stoichiometric substrate feed flowrate (glucose solution 6700 C-mol/m^3)	F_{FEED}	0.371 L/h

The molar balances account for a heterotrophic generation term that is calculated with Monod kinetics for substrate and oxygen limitation, and an autotrophic generation term accounting for carbon dioxide limitation. The former expression prevents heterotrophic activity when oxygen or substate concentration reach zero, the latter prevents autotrophic metabolism when carbon dioxide concentration approaches zero. The gas-liquid exchange terms are expressed with an overall transport coefficient, gas and liquid total moles are assumed in steady state, so that the holdup is constant in each mixer and in time.

For the first mixer, the differential equations for the relevant components are (2.9 - 2.14).

$$\frac{dC_S^1}{dt} = \frac{F_L^{in}}{V_L/N}\, C_S^N + \frac{F_{FEED}}{V_L/N} C_{S,FEED} - \frac{F_L^1}{V_L/N}\, C_S^1 - q_{S,max} \frac{C_S^1}{C_S^1 + K_S} \frac{C_{O2,L}^1}{C_{O2,L}^1 + K_{O2}} C_X \qquad \text{(S in Liq, 2.9)}$$

$$\frac{dC_{O2,L}^1}{dt} = \frac{F_L^{in}}{V_L/N}\, C_{O2,L}^N - \frac{F_L^1}{V_L/N}\, C_{O2,L}^1 + k_{O2,L}a \left(\frac{C_{O2,G}^1}{m_{O2}} - C_{O2,L}^1\right) + q_{O2,auto} \frac{C_{CO2,L}^1}{C_{CO2,L}^1 + K_{CO2}} C_X - q_{S,max}\, Y_{O/S} \frac{C_S^1}{C_S^1 + K_S} \frac{C_{O2,L}^1}{C_{O2,L}^1 + K_{O2}} C_X \qquad (O_2 \text{ in Liq, 2.10})$$

$$\frac{dC_{O2,G}^1}{dt} = \frac{F_G^{in}}{V_G/N}\, C_{O2,G}^N - \frac{F_G^1}{V_G/N}\, C_{O2,G}^1 - k_{O2,L}a \left(\frac{C_{O2,G}^1}{m_{O2}} - C_{O2,L}^1\right) \frac{V_L}{V_G} \qquad (O_2 \text{ in Gas, 2.11})$$

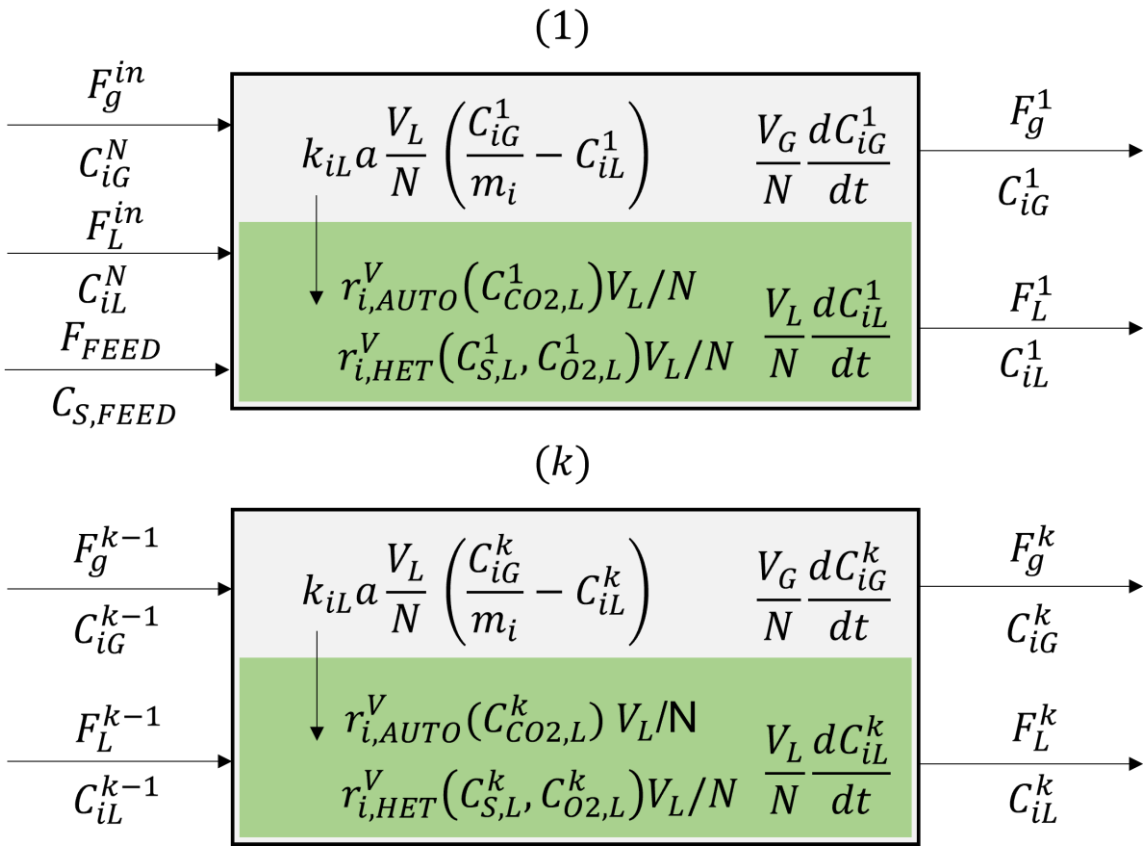

Figure 2.2: Mass balance at the first and the k[th] mixers.

$$\frac{dC_{CO2,L}^1}{dt} = \frac{F_L^{in}}{V_L/N}\, C_{CO2,L}^N - \frac{F_L^1}{V_L/N}\, C_{CO2,L}^1 + k_{CO2,L}a \left(\frac{C_{CO2,G}^1}{m_{CO2}} - C_{CO2,L}^1\right) - q_{O2,auto}\frac{1}{Y_{OC}}\,\frac{C_{CO2,L}^1}{C_{CO2,L}^1 + K_{CO2}}\,C_X + q_{S,max}\,Y_{C/S}\,\frac{C_S^1}{C_S^1 + K_S}\,\frac{C_{O2,L}^1}{C_{O2,L}^1 + K_{O2}}\,C_X \qquad (\mathrm{CO_2}\text{ in Liq, 2.12})$$

$$\frac{dC_{CO2,G}^1}{dt} = \frac{F_G^{in}}{V_G/N}\, C_{CO2,G}^N - \frac{F_G^1}{V_G/N}\, C_{CO2,G}^1 - k_{CO2,L}a \left(\frac{C_{CO2,G}^1}{m_{CO2}} - C_{CO2,L}^1\right)\frac{V_L}{V_G} \qquad (\mathrm{CO_2}\text{ in Gas, 2.13})$$

$$\frac{dC_I^1}{dt} = \frac{F_G^{in}}{V_G/N}\, C_I^N - \frac{F_G^1}{V_G/N}\, C_I^1 \qquad (\text{I in Gas, 2.14})$$

For the other mixers, the equations are (2.15- 2.20).

$$\frac{dC_S^k}{dt} = \frac{F_L^{k-1}}{V_L/N}\, C_S^{k-1} - \frac{F_L^k}{V_L/N}\, C_S^k - q_{S,max}\frac{C_S^k}{C_S^k + K_S}\,\frac{C_{O2,L}^k}{C_{O2,L}^k + K_{O2}}\,C_X \qquad (\text{S in Liq, 2.15})$$

$$\frac{dC_{O2,L}^k}{dt} = \frac{F_L^{k-1}}{V_L/N}\, C_{O2,L}^{k-1} - \frac{F_L^k}{V_L/N}\, C_{O2,L}^k + k_{O2,L}a \left(\frac{C_{O2,G}^k}{m_{O2}} - C_{O2,L}^k\right) + q_{O2,auto}\frac{C_{CO2,L}^k}{C_{CO2,L}^k + K_{CO2}}\,C_X - q_{S,max}\,Y_{O/S}\,\frac{C_S^k}{C_S^k + K_S}\,\frac{C_{O2,L}^k}{C_{O2,L}^k + K_{O2}} \qquad (\mathrm{O_2}\text{ in Liq, 2.16})$$

$$\frac{dC_{O2,G}^k}{dt} = \frac{F_G^{k-1}}{V_G/N}\, C_{O2,G}^{k-1} - \frac{F_G^k}{V_G/N}\, C_{O2,G}^k - k_{O2,L}a \left(\frac{C_{O2,G}^k}{m_{O2}} - C_{O2,L}^k\right)\frac{V_L}{V_G} \qquad (\mathrm{O_2}\text{ in Gas, 2.17})$$

$$\frac{dC_{CO2,L}^k}{dt} = \frac{F_L^{k-1}}{V_L/N}\, C_{CO2,L}^{k-1} - \frac{F_L^k}{V_L/N}\, C_{CO2,L}^k + k_{CO2,L}a \left(\frac{C_{CO2,G}^k}{m_{CO2}} - C_{CO2,L}^k\right) - q_{O2,auto}\frac{1}{Y_{O/C}}\,\frac{C_{CO2,L}^k}{C_{CO2,L}^k + K_{CO2}}\,C_X + q_{S,max}\,Y_{C/S}\,\frac{C_S^k}{C_S^k + K_S}\,\frac{C_{O2,L}^k}{C_{O2,L}^k + K_{O2}}\,C_X \qquad (\mathrm{CO_2}\text{ in Liq, 2.18})$$

$$\frac{dC_{CO2,G}^k}{dt} = \frac{F_G^{k-1}}{V_G/N}\, C_{CO2,G}^{k-1} - \frac{F_G^k}{V_G/N}\, C_{CO2,G}^k - k_{CO2,L}a \left(\frac{C_{CO2,G}^k}{m_{CO2}} - C_{CO2,L}^k\right)\frac{V_L}{V_G} \qquad (\mathrm{CO_2}\text{ in Gas, 2.19})$$

$$\frac{dC_I^k}{dt} = \frac{F_G^{k-1}}{V_G/N}\, C_I^{k-1} - \frac{F_G^k}{V_G/N}\, C_I^k \qquad (\text{I in Gas, 2.20})$$

However, these equations can be solved only if liquid and gas flowrates along the reactor are known.

From the total gas concentration in each mixer (C_{TG}), the gas flowrate can be obtained by a total material balance of the gas components [equation (2.21) for the first mixer, equation (2.22) for the others] assuming steady state conditions in each tank.

$$F_G^1 = \frac{F_G^{in} C_{TG}^N - k_{O2,L}a \left(\frac{C_{O2,G}^1}{m_{O2}} - C_{O2,L}^1\right)\frac{V_L}{N} - k_{O2,L}a \left(\frac{C_{O2,G}^1}{m_{O2}} - C_{O2,L}^1\right)\frac{V_L}{N}}{C_{TG}^1} \quad (2.21)$$

$$F_G^k = \frac{F_G^{k-1} C_{TG}^{k-1} - k_{O2,L}a \left(\frac{C_{O2,G}^k}{m_{O2}} - C_{O2,L}^k\right)\frac{V_L}{N} - k_{O2,L}a \left(\frac{C_{O2,G}^k}{m_{O2}} - C_{O2,L}^k\right)\frac{V_L}{N}}{C_{TG}^k} \quad (2.22)$$

On the other side, liquid flowrate is assumed constant in the reactor [equation (2.23)]. In principle, it should depend on position and time because of the liquid products of the mixotrophic metabolism and the mass transfer between the two phases. However, considering the high density of the water phase in relation to the gas phase, this volumetric flowrate change is extremely small.

$$F_L^{in} = F_L^1 = \cdots = F_L^k = \cdots = F_L^N = F_L \quad (2.23)$$

The bleed gas flowrate is calculated as reported in equation (2.24).

$$F_{BLEED} = F_G^N - F_G^{in} \quad (2.24)$$

To solve the model equations some initial conditions are required. At time zero, the reactor is in operation with air and without substrate input, so carbon dioxide and oxygen concentrations in the liquid are the ones at air saturation. At the beginning, liquid and gas flowrate are assumed to be constant in the reactor and equal to F_L and F_G^{in}.

2.4 Control system

To achieve OBM in the reactor, a control system that aims at a constant dissolved oxygen concentration in the reactor must be designed. Considering the oxygen profile across the tube, the control system should be able to keep the dissolved oxygen concentration in an optimal range in the dynamic evolution of the process both to prevent anoxia and too high oxygen concentration.

The dynamics of a system can be modified by the influence of a controller so that it results in the desired response. The most common control system is the feedback PID control system, that aims at keeping a process variable to a certain set-point. Two different feedback control strategies will be integrated in the model and compared. In one, the controlled variable is oxygen concentration in gas phase at the end of the tubular section, and in the other one it is dissolved oxygen at the same point. In both strategies, the manipulated variable is substrate flowrate. In Figure 2.3 the two control system strategies are compared.

In the first two control systems proposed in this Thesis, the control action is performed at each gas residence time. In this way, the control action is based on a single fluid element and is implemented each time this element passes through the outlet of the tube. Therefore, the substrate feed flowrate to the system is changed each gas residence time. With this type of control strategy (which will be addressed as discontinuous control strategy in the Thesis), it is possible to simulate this cultivation in a lab-scale stirred tank reactor in batch mode. In fact, in a batch stirred tank reactor, only the evolution of an element of fluid that flows through the reactor can be represented (Section 3.2.1).

The controlled variable *y* (for example, the oxygen concentration in the gas phase) is measured each gas residence time (Figure 2.4) using an ideal measuring device that does not

introduce further disturbances to the signal. The value of y is compared to the set-point value $y_{sp,}$ and the error signal e is calculated as a "feedback" deviation [equation (2.25)].

$$e = C^N_{O2,G} - C^N_{O2,G,sp} \tag{2.25}$$

The value of the error is supplied to the controller, and by means of equation (2.26) the change in the input parameter in the process u is calculated.

$$u(t) = K_p\left(e(t) + \frac{1}{\tau_I}\int_0^t e(t)dt + \tau_D\frac{de(t)}{dt}\right) \tag{2.26}$$

The control action is implemented by an ideal final control element (acting on the pump's rotational speed). As shown in equation (2.26), the output signal from the controller is made by three different contributions: the proportional one, the integral one, and the derivative one. The relative importance of the latter two parts can be adjusted by setting appropriate values for the parameters τ_I and τ_D. Tuning the control system means finding the three parameters that result in the desired response of the system.

The control action for each gas residence time (i.e., control time, $t_{control}$) is calculated with the steps reported in equations (2.27) to (2.32). First, the bias term is calculated using the input and output values at time zero [equation (2.27)].

$$Bias = F_{FEED}(t=0) - K_P\, e(t=0) \tag{2.27}$$

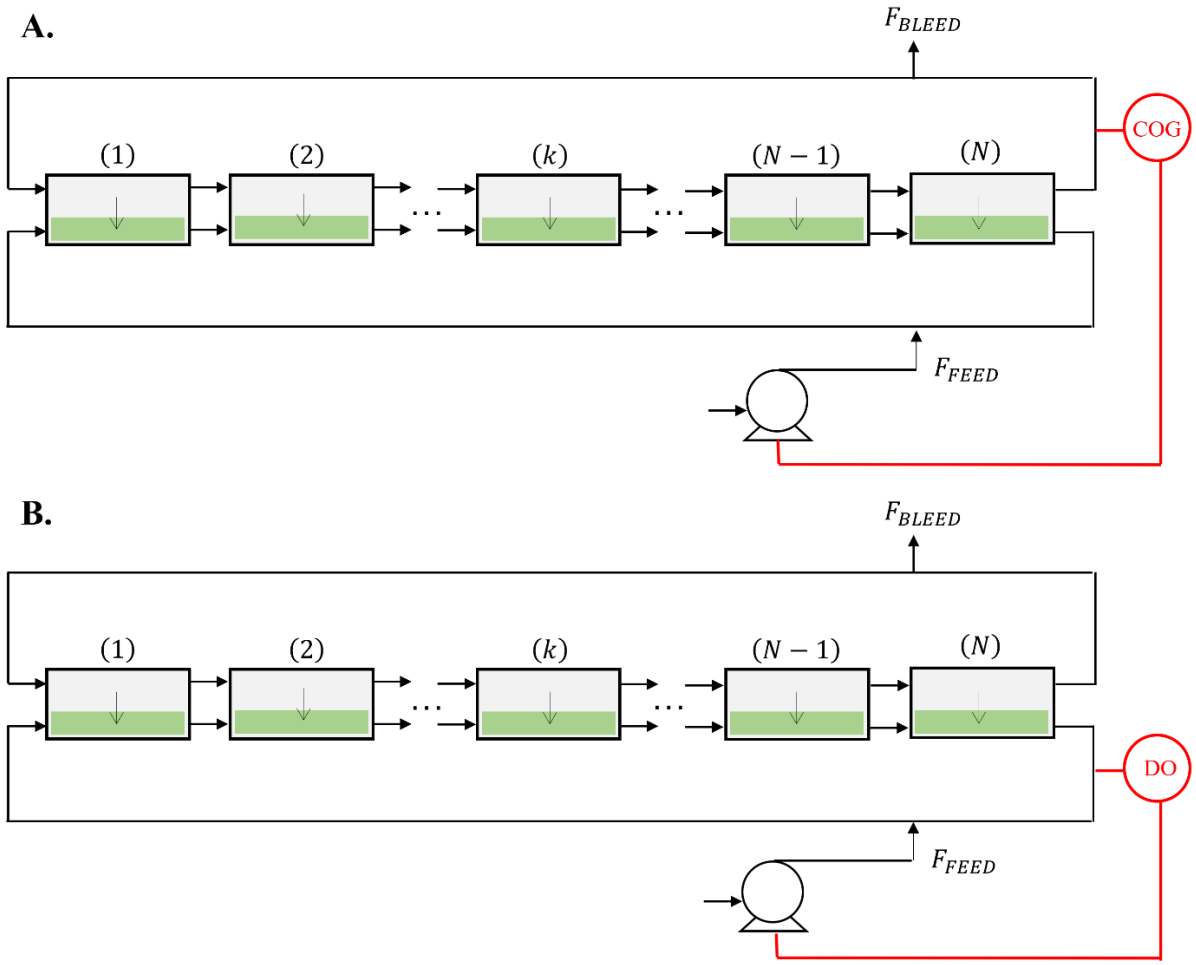

Figure 2.3: Schematic representation of the control system. A: the controlled variable is oxygen concentration in gas phase, B: the controlled variable is dissolved oxygen.

Then, each control time, the error is computed, and the integral error is calculated. This parameter is the integral of the error function from time zero to the actual time and it is calculated with a trapezoidal integration as shown in equation (2.28).

$$e_{I,i} = e_{I,i-1} + (e_i + e_{i-1}) * \frac{t_{control}}{2} \qquad i = 0, \dots, t_{end}/t_{control} \tag{2.28}$$

The control action is calculated by computing the proportional action (2.29), the integral action (2,30), and the derivative action (2.31).

$$u_{P,i} = K_p\, e_i \qquad i = 1, \dots, t_{end}/t_{control} \tag{2.29}$$

$$u_{I,i} = K_p \left(\frac{1}{\tau_I}\, e_{I,i}\right) \qquad i = 1, \dots, t_{end}/t_{control} \tag{2.30}$$

$$u_{D,i} = K_p \left(\tau_D \frac{e_i - e_{i-1}}{t_{control}}\right) \qquad i = 1, \dots, t_{end}/t_{control} \tag{2.31}$$

Finally, the process variable (substrate pump flowrate) is calculated with equation (2.32).

$$F_{FEED,i} = Bias + (u_{P,i} + u_{I,i} + u_{D,i}) \qquad i = 1, \dots, t_{end}/t_{control} \tag{2.32}$$

Additionally, a last continuous control strategy is studied. In this one, the oxygen concentration in the gas phase is the controlled variable. Each second, the value of the controlled variable is compared with its value at the previous residence time in order to compute the error [equation (2.33)]. Thus, the setpoint of this control system is not a user-defined value but is related to the value of the control variable, the previous residence time.

$$e(t) = C^N_{O2G}(t) - C^N_{O2G}(t - t_{control}) \qquad t > t_{control} \tag{2.33}$$

The same PID algorithm previously explained is adapted to this different error definition.

The main requirements for the control systems are that the dissolved oxygen in the liquid through the reactor is in a suitable range and the response is stable in time after a first transient period.

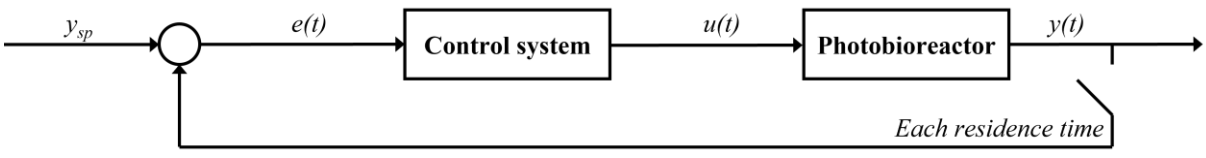

Figure 2.4: Schematic representation of a PID control system that acts each residence time.

3. Materials and methods

3.1 Model simulations and residence time distribution

3.1.1 Numerical methods

The mathematical model is implemented and solved in MATLAB R2020a. The number of ordinary differential equations to solve depends on the number of mixers N. Considering all the balances, there are 6N equations to solve simultaneously, and 5N are nonlinear. Furthermore, the timestep size must be defined considering the Courant–Friedrichs–Lewy (CFL) condition to obtain an accurate solution. This condition is typically evaluated in transient simulations and is related to the stability of the solver: the distance that any information travels during the timestep must be lower than the distance between mesh elements (i.e., perfectly mixed length in the photobioreactor). Considering 100 mixers and the gas-phase velocity in accelerated mode as a reference, the CFL conditions can be calculated as shown in equation (3.1).

$$CFL = \frac{v_G\,\Delta t}{\Delta L} < CFL_{MAX} \tag{3.1}$$

Considering a value of CFL_{MAX} of 1 (value suggested for explicit solvers), it means that the timestep size should be lower than 7.2 s. However, most times CFL condition is not sufficient for convergence because of the nonlinearities in the equations. The chosen solver is the MATLAB function ode45. It defines the timestep size in an adaptive way for a high accuracy of the results (setting low tolerances on the target solution function). First, it evaluates the timestep required for each equation to converge, then it selects the lowest value of the set, making sure that all the equations reach convergence.

The equations are written in a matrix form, as shown in Figure 3.1 so that it can be the input function to the solver. Furthermore, the function ode45 requires a time interval to perform the integration. This parameter may be set equal to a fraction of the total simulated time to subdivide the total simulated time in input to the solver. After each integration, the outlet flowrates of each mixer are corrected by using the results of the solver at the final time of the interval, following the steady-state equations (2.21) and (2.22) in Section 2.3. Eventually, the control system action is computed. For the simulation with a constant flowrate, the time interval to the solver is set to ten seconds. For the simulations with the discontinuous control system, it is set to the gas residence time in the reactor. For the simulations with the continuous control system, it is set to one second. The algorithm is shown in Figure 3.2.

The number of stages is important for the model and the computational method. Increasing N, the timestep to satisfy the CFL condition is lower. It means that the computational cost of the solver increases and, thus, the simulation time. The more the model approaches a plug flow reactor, the higher the computational cost.

$$\boldsymbol{C} = [\boldsymbol{C_S}, \boldsymbol{C_{O2L}}, \boldsymbol{C_{O2G}}, \boldsymbol{C_{CO2L}}, \boldsymbol{C_{CO2G}}, \boldsymbol{C_I}]$$

$$\begin{aligned}
\boldsymbol{C_S} &= [C_S(1), \dots, C_S(N)] \\
\boldsymbol{C_{OL}} &= [C_{O2L}(1), \dots, C_{O2L}(N)] \\
\boldsymbol{C_{OG}} &= [C_{O2G}(1), \dots, C_{O2G}(N)] \\
\boldsymbol{C_{CL}} &= [C_{CO2L}(1), \dots, C_{CO2L}(N)] \\
\boldsymbol{C_{CG}} &= [C_{CO2G}(1), \dots, C_{CO2G}(N)] \\
\boldsymbol{C_I} &= [C_I(1), \dots, C_I(N)]
\end{aligned} \quad \longrightarrow \quad \frac{d\boldsymbol{C}}{dt} = f(t, [\boldsymbol{C_S}, \boldsymbol{C_{O2L}}, \boldsymbol{C_{O2G}}, \boldsymbol{C_{CO2L}}, \boldsymbol{C_{CO2G}}, \boldsymbol{C_I}]')$$

Figure 3.1: Mathematical process model in matrix form

3.1.2 Number of stages: residence time distributions and sensitivity on the model

The number of stages should be defined based on residence time distribution results. The residence time distribution experiment has been conducted in one helix of the Lgem photobioreactor, with the injection of a pulse of a concentrated acid solution at the beginning of the tubular section (Rinzema, n.d.). The response in time is recorded at the end of the tube employing a pH probe. Data is imported in MATLAB R2020a, and the first passage residence time distribution is studied by calculating *E(t)* and *F(t)* functions. In order to calculate the number of stages in the model, the moments of the distribution are also computed.

The study of the effect of the number of stages on the model results is then performed. For comparisons, a simulation with a stoichiometric constant substrate flowrate of 1.11E-7 m^3/s [equation (2.8)] and constant light conditions is run with 100, 500 and 1000 mixers.

3.2 Validation experiment

The validation experiment is carried out in a lab-scale stirred tank reactor with a gas recycling system using a downscale approach. The concentration gradients in the length of the tube of the pilot scale reactor are simulated as gradients in time with the lab-scale stirred tank reactor. In order to appropriately adapt the model to the constraints of validation in a different type of photobioreactor, some unknown parameters of the system are evaluated (Appendix B).

3.2.1 Scale down approach to simulate concentration gradients

The main principle of the experiment is the similarity in the equations of a plug flow reactor and a batch reactor. The expressions of performance equations for an ideal, isothermal, and homogeneous system at constant density with a single reaction are identical, if substituting the residence time of the plug flow reactor with the elapsed time in the batch reactor (Levenspiel, 1999). Furthermore, this observation has also been exploited in a biological system, for example studying enzyme kinetics (Karanth, 1981) both from a mathematical point of view and in experimental studies. The same concept can be extended to aim to simulate the performances of the pilot-scale tubular photobioreactor with the lab-scale batch photobioreactor, with the idea of following an element of fluid through the length of the tube with a lagrangian approach. With this approach, the result of the experiment will be a path on the tri-dimensional surface plot obtained from the simulations (Section 4).

```
for i = 1:ceil(t_end/res_time)

    dCdt = @(t,C) […];

    [t_out,y_out] = ode45(dCdt,[(i-1)*res_time,i*res_time],Y0);
    Y0 = y_out(end,:);

    %STEADY STATE ASSUMPTION FOR FG
    FG(i,:) = …;
    Fbleed(i) = FG(i,end)-Fgin;
    Fgin = FG(i,:)';

    %CONTROL SYSTEM (if ON)
    …

end
```

Figure 3.2: Algorithm employed to solve the system.

To design the proper reactor configuration, it is crucial to define the pilot-scale reactor configuration to simulate. Referring to Table 1.1, the configuration in accelerated mode is chosen. This decision is because the fluid dynamic regime is similar to the one in pilot scale experiments, and liquid and gas have approximately the same residence time of around 12 minutes. It is not feasible to use this method to represent a process where the gas and liquid have different velocities in the reactor because the lagrangian approach cannot be adopted.

In the lab-scale reactor, the substrate input inside the system occurs each residence time of the plug flow reactor, and it lasts for the residence time of a mixer. In this way, the same feeding strategy of the tubular photobioreactor can be simulated. The fluid element traveling through the tube does not exchange gas with the external environment (excess gas can only escape the system at the mixing tank). To simulate this feature, the lab-scale reactor will work under slight overpressure. In this way, excess gas can be released, simultaneously preventing air from entering the reactor. In addition, the mass transfer in the stirred tank can be increased with a gas recycle stream with a mass flowrate set to 102 NmL/min (normal-mL/min) to provide an oxygen mass transfer coefficient of 2.42E-3 s^{-1} (the same value as the pilot-scale reactor, estimated at 37°C). This flowrate is obtained from linear interpolation of mass transfer coefficients calculated at different gas flowrates in the same reactor (Abiusi et al., 2020b).

3.2.2 Reactor configuration

The photobioreactor employed in this study is a 3 L glass cylindrical stirred tank bioreactor (Applikon, The Netherlands) with a liquid working volume of 2 L described in detail by Abiusi et al. (Abiusi et al., 2020a). The reactor is homogeneously illuminated from all sides via an octagon of vertical light panels composed of warm-white LEDs that provide an average PFD of 459.4$\pm$13.4 $\mu mol_{ph}\, m^{-2}\, s^{-1}$, measured with PAR quantum sensor (LI-250 Light Meter, LI-COR, USA). The reactor is equipped with a heat exchanger to keep the liquid temperature at 37°C. A condenser is installed at the gas outlet to prevent water losses from the reactor and condensation in the gas line. The condenser is fed with cold water of 2°C from a cryostat. Additionally, a new recycle line is installed after the condenser, as shown in the schematic drawing in Figure 3.3.

Continuous stirring at 500 RPM is provided during the experiment. The reactor has a pH probe and a dissolved oxygen (DO) sensor (VisiFerm DO 120, Hamilton, USA). The pH is kept constant at 1.8 $\pm$ 0.2 by manual base addition (NaOH, 2 M). The DO sensor is calibrated inside the reactor with air and nitrogen to obtain levels of respectively 100% and 0% at a pressure of 1.12 bar. Another oxygen sensor is placed right after the condenser, to measure the oxygen concentration in gas phase (COG). Calibration is done in the same conditions as the DO sensor, with a value of 20.95% with air and 0% with nitrogen at a pressure of 1.12 bar. The overpressure during calibration is due to the presence of an additional resistance in the gas recycle line (a one-way valve). This valve was removed after calibration, before the start of the validation experiment.

The pressure in the system is set to 10 mbar above atmospheric pressure via a waterlock placed after the condenser. Possible deviations from the operative pressure are monitored by using a manometer. The gas coming from the reactor is compressed into the recycle line with a diaphragm gas pump (NMP 830 KNE, KNF, Switzerland), and its flowrate is controlled with a mass flow controller (TMF 5800S, Brooks Instruments B.V., The Netherlands) before entering the reactor again via the sparger. The reactor can also be aerated with air, or air enriched by carbon dioxide, at a constant mass flowrate (Smart TMF 5850S, Brooks

Instruments, USA). The glucose solution feed and the liquid outlet from the reactor are pumped via peristaltic liquid pumps whose flowrates can be remotely controlled. The base solution, the glucose solution, and the harvest bottle are placed on balances. The balances, the mass flow controllers, and the pumps are remotely monitored and controlled utilizing a software tool (LabView, National Instruments, USA).

3.2.3 Strain, growth conditions and medium

A stock culture of *G. sulphuraria* ACUF 064 was incubated in a 250 mL flask containing 100 mL of culture at 37°C, 2% v/v CO_2, 120 RPM and 100 $\mu mol_{ph}\, m^{-2}\, s^{-1}$. The culture was used to inoculate the photobioreactor already working at operative conditions. The medium is composed by the following components with a concentration in mol/L: 7.99E-2 $(NH_4)_2SO_4$, 6.49E-03 $MgSO_4 \cdot 7\ H_2O$, 4.68E-04 $CaCl_2 \cdot 2\ H_2O$, 6.32E-04 $FeCl_3 \cdot 6\ H_2O$, 1.22E-02 H_3PO_4, 1.71E-03, NaCl, 8.05E-03 KCl, 8.02E-04 H_3BO_3, 8.08E-05 $MnCl_2 \cdot 4\ H_2O$, 8.22E-05 $ZnCl_2$, 3.20E-05 $CuSO_4 \cdot 5\ H_2O$, 1.65E-05 $Na_2MoO_4 \cdot 2\ H_2O$, 1.68E-05 $CoCl_2 \cdot 6\ H_2O$. The pH of the medium is adjusted to 1.8 with addition of H_2SO_4.

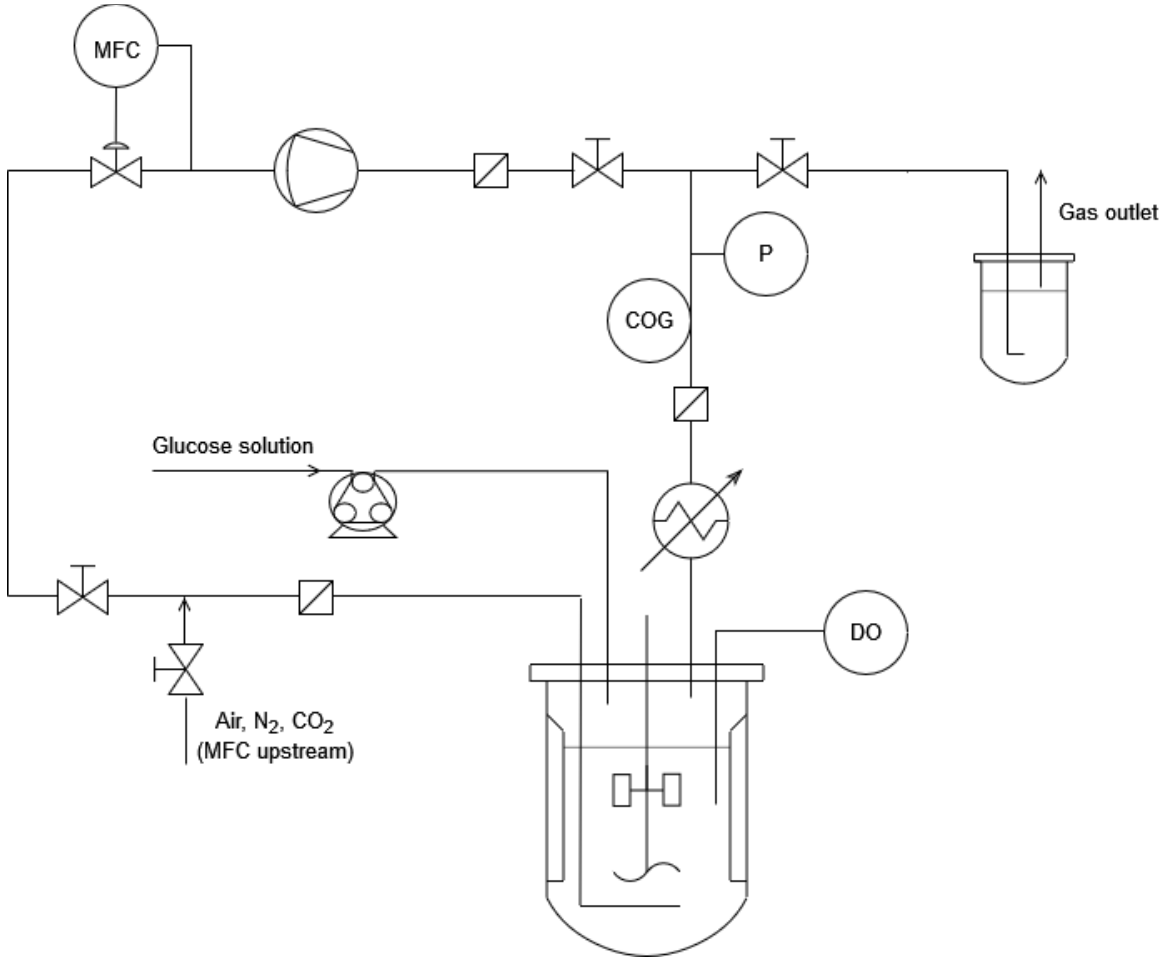

Figure 3.3: Schematic drawing of the reactor and the gas recycle line.

3.2.4 Experimental methods

After inoculation, the culture was grown autotrophically in batch until biomass concentration reached 3 g_x/L. During this phase, light intensity was gradually increased to the maximum value to avoid photodamage to the culture when concentration is still very low. The reactor is aerated with 1 NL/min of air enriched with carbon dioxide (2% v/v). Next, a low flowrate of glucose solution (1.1 g/h, concentration 100 g/L) is fed into the reactor for a mixotrophic adaptation phase that lasted for one day. At the end of this adaptation period, aeration is switched off, and dissolved oxygen is controlled at 105% air saturation by manipulating the substrate supply to the reactor (OBM batch) (Abiusi et al., 2020a). When biomass concentration reached a value of 8 g_x/L, dilution at 0.2 day^{-1} was activated (OBM chemostat), aiming to reach a stable state for the culture. The validation experiments always started after at least three days of chemostat operation.

A validation experiment is sixteen hours of batch growth in which the substrate is fed in pulses into the system. In order to do so, a new control system has been integrated into the software and the PID parameters of the controller are derived from the model, adjusted to the lab scale setting ($K_p = -40$, $\tau_I = 60$ min, $\tau_D = 5$ min). Before the beginning of the validation, the gas recycle pump is switched on and the reactor is aerated with 1 NL/min of air for at least 2 hours until the liquid phase is in equilibrium. The waterlock is connected to the system so that 10 mbar overpressure is achieved. Furthermore, a solution of 150 g/L of glucose is used, pH is adjusted to 1.8, the reactor is operated in batch mode, and the new control system is switched on. This control system aims to control the oxygen concentration in the gas phase with a setpoint strategy by manipulating the rotational speed of the substrate pump (thus, the substrate flowrate), which is only active for 7 s (residence time in the first mixer of the model) every 700 s (residence time in the model tubular reactor). The setpoint value for the oxygen concentration in the gas phase on the software is set to 17% v/v. This value is lower than the oxygen concentration in the gas phase after aerating the reactor. This way, the substrate will be added to the system so that the microalgae can produce carbon dioxide for photosynthesis. In the first experiment, this value was initially set to 21% but lowered to 17% after the first pulse. This change influenced the control system and its output value of pump flowrate.

3.2.5 Analytical methods

Samples of variable volume were taken daily from the reactor for offline measurement. During the validation experiment, a sample was taken before the experiment, three more samples at 2.5 h, 5 h, and 7 h from the beginning of the experiment, and one last sample before switching the system to chemostat. Samples were collected by injecting fresh medium and taking the same amount of liquid from the reactor. Before collecting a sample, a valve placed before the waterlock was closed to prevent gas loss during the medium injection.

Three 1 ml aliquots of each sample were centrifuged at 20000 RCF for 10 minutes, and the supernatants were stored at -20°C until analysis (glucose concentration). A further 13.5 ml aliquot was alkalinized immediately after sampling by adding 1.5 ml of NaOH 2.5M and centrifuged at 4200 RCF for 5 minutes. The base addition is needed to avoid carbon dioxide stripping for the liquid. The supernatant is stored at -20°C until analysis (total inorganic carbon, TIC). Biomass dry weight, optical density, average dry weight-specific optical cross-section, and photosystem II quantum yield were measured at least once daily.

Optical density was measured in triplicate on a spectrophotometer (DR6000, Hach-Lange, USA) at 480 nm, 680 nm, and 750 nm.

Photosystem II quantum yield (QY) was measured in triplicate after 15 minutes of dark adaptation at 37°C with AquaPen-C AP-C 100 (Photon Systems Instruments, Czech Republic). Samples were diluted before the measurement to reach an optical density at 750 nm between 0.3 and 0.7.

The average dry weight-specific optical cross section (a_x m^2/kg) was measured and calculated according to de Mooij's work (de Mooij, 2016) in duplicate using absorbance between 300 to 800 nm with a step size of 1 nm. The absorbance was measured with a UV-VIS/double beam spectrophotometer (Shimadzu UV-2600, Japan) equipped with an integrated sphere (ISR-2600). Cuvettes with an optical path of 2 mm were used, and samples were diluted to a concentration of approximately 1 g_x/L.

Biomass dry weight (DW) was measured in duplicate using pre-weighted Whatman GF/F glass microfiber filters with a diameter of 55 mm and pore size of 0.7 µm (SigmaAldrich, USA). A volume of 1 mL of sample is diluted to 30 mL with deionized water in a volumetric cylinder and filtered in vacuum conditions. The filter is rewashed with 30 mL of deionized water and dried at 100°C for at least three hours before weighing.

After defrosting the previously stored supernatant, glucose concentration was measured with a YSI analyzer (YSI 2700, YSI Life Sciences, USA). For each sample, at least three technical replicates were performed.

The samples were tested for inorganic carbon in the medium. The measurements were executed in a TOC-L analyzer, with inorganic carbon standards at 20 ppm, 10 ppm, 4 ppm, 1 ppm, and a blank. The defrosted samples were diluted with additional deionized water until a total volume of 16 ml was reached, and they were stored again until the analysis.

A last sample from the reactor was taken before biomass disposal. This sample was employed for contamination analysis via microscopy.

3.2.6 Data treatment and calculations

On-line data was recorded every minute by the software LabView, and it includes dissolved oxygen, oxygen concentration in gas phase and the mass on the balances. The file was imported in MATLAB R2020a for further analysis and comparisons with the results of the model.

The values of DO and COG measured by the probes linearly depend on pressure. DO and COG values can be converted to account for the effect of different operative and calibration pressure, by dividing the value of each measurement by the conversion factor defined in equations (3.2) and (3.3).

$$DO_{actual} = DO_{measured} \frac{P_{calibration}}{P_{operative}} \tag{3.2}$$

$$COG_{actual} = COG_{measured} \frac{P_{calibration}}{P_{operative}} \tag{3.3}$$

For clarity, all the values of DO and COG presented in the following sections will be actual values considering the pressure correction.

Biomass volumetric productivity is calculated accounting for the dilution of the culture during each sampling and the amount of biomass sampled. The biomass concentration inside the reactor before sampling was calculated according to equation (3.4), and the productivity is

obtained with equation (3.5), where the sum over the index *i* includes only the first, second, third and end sample.

$$C_{x,before} = C_{x,after}\,\frac{V_{injected} + V_L}{V_L} \tag{3.4}$$

$$r_x = \frac{(C_{x,before}^{end}\,V_L + \sum_i C_{x,i}\,V_i - C_{x,after}^{start}\,V_L)}{V_L\,(t_{start} - t_{end})} \tag{3.5}$$

4. Results and discussion

4.1 Residence time distributions results and number of stages sensitivity

Residence time distributions can be analyzed and compared by computing the moments of the first and second order of $E(t)$, following equation (4.1). The first order moment m_1 is related to the mean residence time, and the distribution's variance σ^2 can be calculated from m_1 and m_2 [equation (4.2)]. The values of these parameters and the residence time for the experiments are shown in Table 4.1.

$$m_k = \int_0^\infty t^k \, E(t) \, dt \tag{4.1}$$

$$\sigma^2 = m_2 - {m_1}^2 \tag{4.2}$$

The experimental distributions are compared with the series of mixers model in equation (1.5) for different values of N (Figure 4.1). The residence time parameter required by the equation equals the values obtained in each experiment and reported in Table 3.1.

The tanks in series model can approximate the residence time distribution of the reactor if the number of tanks is sufficiently high. From the variance and mean residence time of the experimental distribution, the parameter N to best represent the data can be calculated as reported in equation (4.3) (Toson et al., 2019).

$$N = \frac{{m_1}^2}{\sigma^2} \tag{4.3}$$

This equation suggests a different value of the N parameter to be used for each experiment (92 tanks for experiment A and 682 for experiment B, even though flow conditions are the same). A possible explanation for this behavior is related to the accuracy of the distribution, hence to the detection time chosen for the experiments (the time between two pH measurements). Another reason could be that the lower acid concentration in experiment A was not sufficient to simulate a Dirac delta pulse. An additional uncertainty in the analysis is related to the concentration peak chosen for the single passage residence time distribution. As time progresses, peaks become shorter and broader because the tracer is dispersing to reach a steady state. Therefore, they are not the response to a tracer pulse, and the abovementioned methods to calculate $E(t)$ cannot be employed. Each peak can be considered as the response to the previous one, so even if they get shorter and broader, it does not mean that the axial dispersion of the system is increasing.

Table 4.1: Parameters calculated from stoichiometric relationships.

Tracer - Experiment	Replicate	Residence time [min]	Variance [min^2]	Number of stages
HCl, 1M (A)	1	13.1	1.6	94
HCl, 2M (B)	2	12.7 / 12.9	0.28 / 0.17	563 / 955
HCl, 2M (C)	1	37.1	2.1	659

According to the plots shown in figure 4.1, a deviation from the ideal plug flow behavior can be seen, but axial dispersion is overall low. However, further similar experiments should be done to decide a value of N that better represents the residence time distribution for different liquid flowrates. The effect of the sampling frequency and the initial incomplete radial distribution on the curves should be assessed.

Because of the inconclusive results of the residence time distributions in the reactor, the sensitivity analysis is carried out. The simulation with 100 mixers requires 35 s, the one with 500 requires time 160 s, and the last one with 1000 mixers requires 312 seconds. The results are shown in Figure 4.2 and Figure 4.3. Even though concentration profiles are slightly different, the error is overall very low, and thus, aiming for a low simulation time, a number of mixers of 100 is chosen. However, the results will not be much different if a different number is chosen.

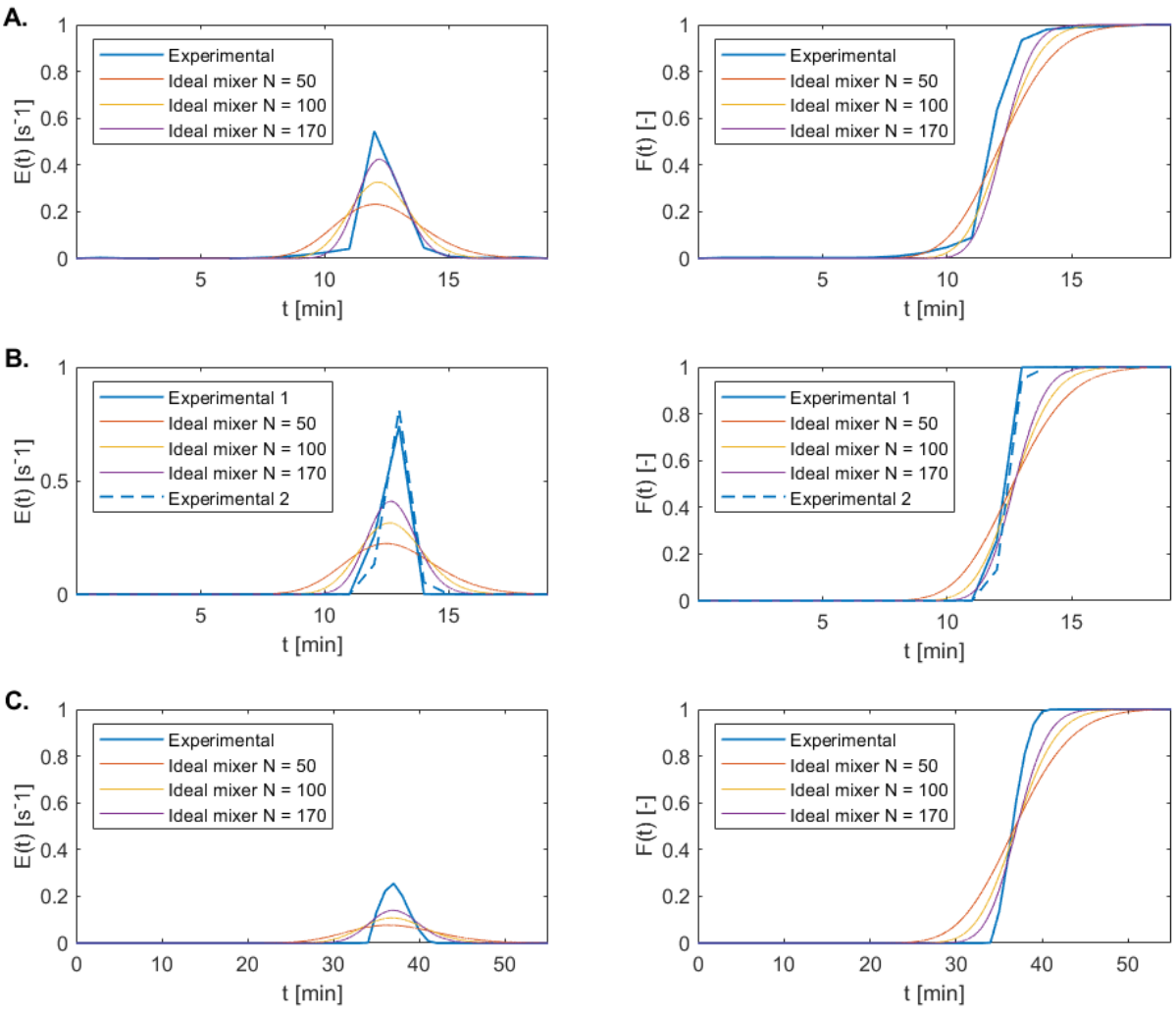

Figure 4.1: Experimental and model [equation (0.4)] residence time distribution functions *E(t)*, *F(t)*.

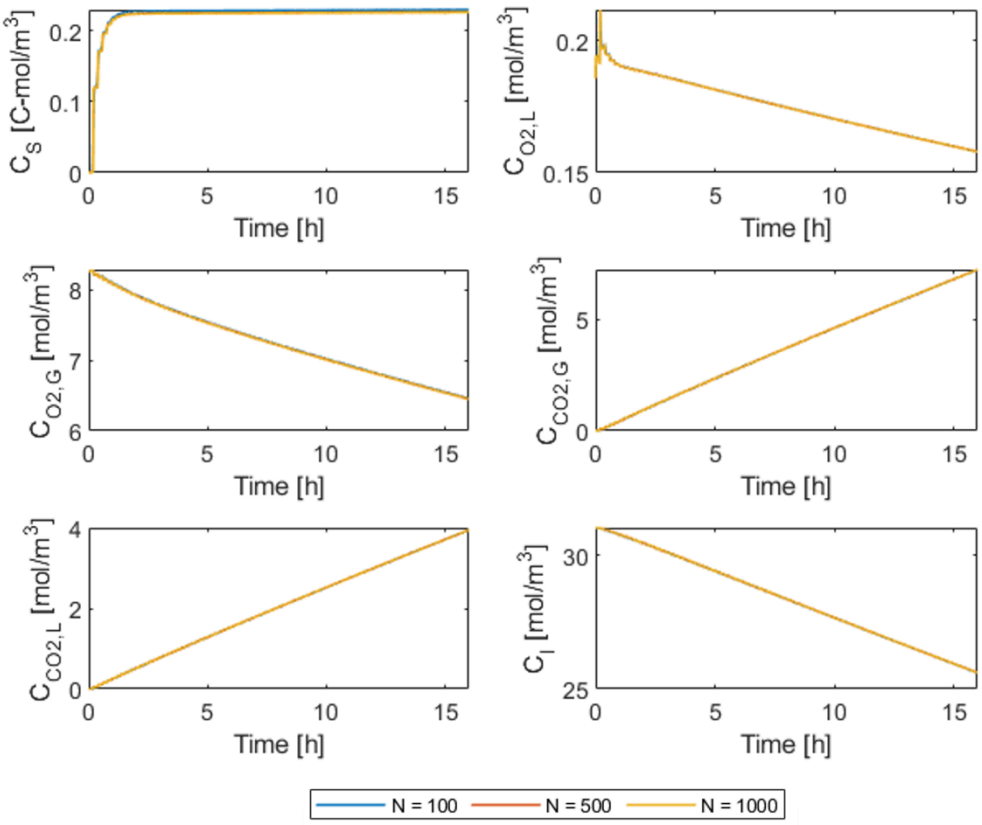

Figure 4.2: Concentration profiles in time at the end of the reactor

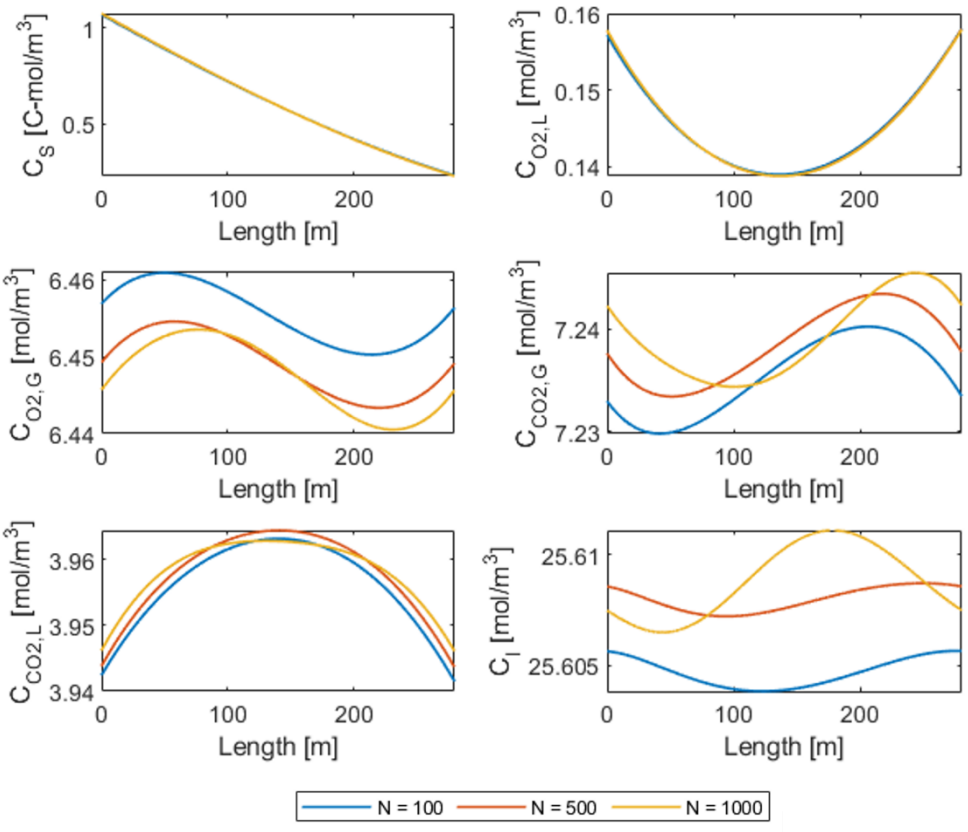

Figure 4.3: Concentration profiles in the reactor at the final time

4.2 Model results and sensitivity analysis

The primary simulation is run with the parameters defined in the previous sections, considering the accelerated operation mode with the lowest gas flowrate (accelerated configuration, Table 1.1). First, the most important features of the system when the substrate input flowrate is constant will be explained. Then, the control systems' designs will be shown, alongside with the results of the control actions on the concentration profiles in the reactor. Lastly, some results of the simulation in sinusoidal light conditions and real light conditions on a cloudy day are presented.

4.2.1 Constant substrate flowrate

Understanding the dynamic behavior of the system when substrate flowrate is constant in time is a necessary operation to define the optimal control strategy. In the first simulated scenario, a constant flowrate defined in equation (2.8) enters the system. This is defined as the flowrate that results in a glucose input in the system equal to the glucose consumed for OBM, considering a maximum fixed photosynthetic capacity and no net oxygen production. Because of microalgal metabolism and reactor design, the liquid and gas phase composition changes over time. In this situation, the system does not reach a stable dissolved oxygen value in the simulated 16 hours (i.e., a day).

The surface plots of the most significant variables in the reactor can be seen in Figure 4.4, as a function of the length of the reactor and time. Looking at the behavior of the dissolved oxygen, after the first period in which it oscillates, it decreases in time. Oxygen concentration in the gas phase is decreasing in time as well. Carbon dioxide concentration in liquid and gas phases (not shown in the figure) is linearly increasing in time, because of the oxygen-balanced mixotrophic stoichiometric equation. After the first transient period, substrate concentration reaches a stable profile in time. This variable is maximum at the beginning of the reactor, where the substrate is fed, and a minimum value is reached at the end of the tube. However, all the reactor is in mixotrophic conditions as glucose concentration is higher than zero in the tubes.

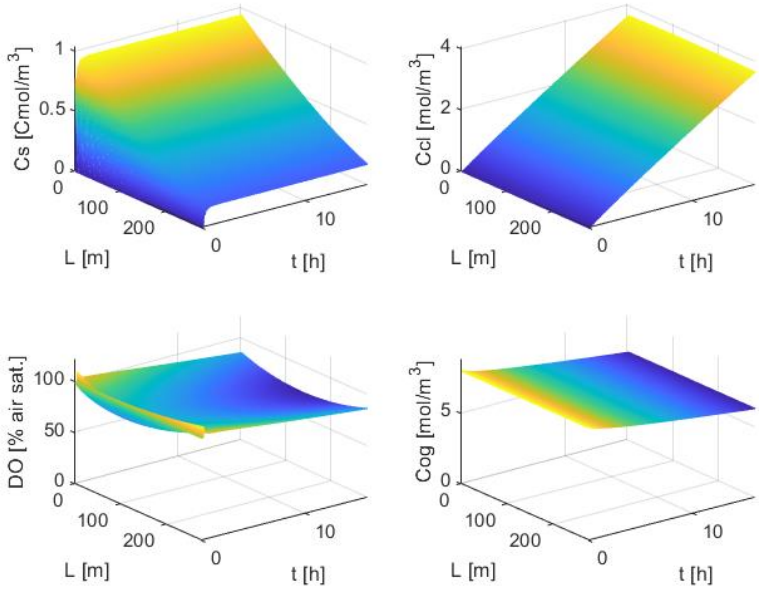

Figure 4.4: Surface plot of substrate concentration (C_S), carbon dioxide concentration in liquid phase ($C_{CO2,L}$), dissolved oxygen in liquid phase (DO), oxygen concentration in gas phase ($C_{O2,G}$).

To better assess the relative importance of heterotrophic and autotrophic metabolisms across the tubes, the average volumetric oxygen production (hereafter, oxygen production) and consumption rates (hereafter, oxygen consumption) in the whole reactor as a function of time can be computed following equations (4.4) and (4.5). The net volumetric oxygen production rate (hereafter, net oxygen production if positive and consumption if negative) defined in equation (4.6) and its average in the reactor [equation (4.7)] can also be calculated.

$$r_{O2,auto}^{V} = \frac{1}{V_L} \sum_{k=1}^{100} \frac{V_L}{N} r_{O2,auto}^{k} \tag{4.4}$$

$$r_{O2,het}^{V} = \frac{1}{V_L} \sum_{k=1}^{100} \frac{V_L}{N} r_{O2,het}^{k} \tag{4.5}$$

$$r_{O2,net} = r_{O2,auto} + r_{O2,het} \tag{4.6}$$

$$r_{O2,net}^{V} = \frac{1}{V_L} \sum_{k=1}^{100} \frac{V_L}{N} (r_{O2,net}^{k}) \tag{4.7}$$

As shown in Figure 4.5 A, there is a net oxygen production only at the beginning of the simulated time, as the substrate is not present inside the reactor. When glucose enters it, there is a net oxygen consumption as heterotrophic oxygen consumption prevails over autotrophic oxygen production. Only towards the end of the simulated period, the oxygen production approaches oxygen consumption (Figure 4.5 B). This mechanism results in the driving force for oxygen transfer from the gas phase. However, the average volumetric oxygen transfer rate [equation 4.8] cannot balance the net oxygen consumption. Therefore, dissolved oxygen decreases over time (Figure 4.5 C).

$$r_{O2,trans}^{V} = \frac{1}{V_L} \sum_{k=1}^{100} \frac{V_L}{N} (r_{O2,trans}^{k}) \tag{4.8}$$

The decrease in oxygen transfer is related to a decrease in driving force over time. As oxygen is transferred to the liquid phase, the concentration in the gas phase also decreases because an additional fresh air input is not provided in the system. In addition, oxygen is also lost in the bleed gas. Its flowrate and composition are plotted to show that oxygen is drained from the system so that the inlet gas flowrate sent to the reactor is constant (Figure 4.6).

The concentration profiles across the reactor can be plotted considering a constant time. The most meaningful one is the parabolic profile of dissolved oxygen, shown for the end of the simulated time in Figure 4.7 A, resulting from the oxygen production and consumption rates across the reactor. Even though there is a small net oxygen consumption at the end of the process, autotrophic oxygen production and heterotrophic oxygen consumption are balanced only at a point in the length of the reactor (at 157 m). Before this point, at around 57% of the length of the reactor, heterotrophic metabolism prevails, leading to average oxygen consumption in the reactor (Figure 4.7 B). Also, the microalgae metabolism affects the transfer rate, and its parabolic profile is the opposite of the one of dissolved oxygen. The sign of the oxygen transfer rate is related to the direction of transport: the liquid phase is enriched with oxygen between 56 m and 218 m and stripped elsewhere (Figure 4.7 C). However, considering that the magnitude of oxygen transfer is much lower than oxygen consumption, the oxygen concentration in the whole reactor is still decreasing over time.

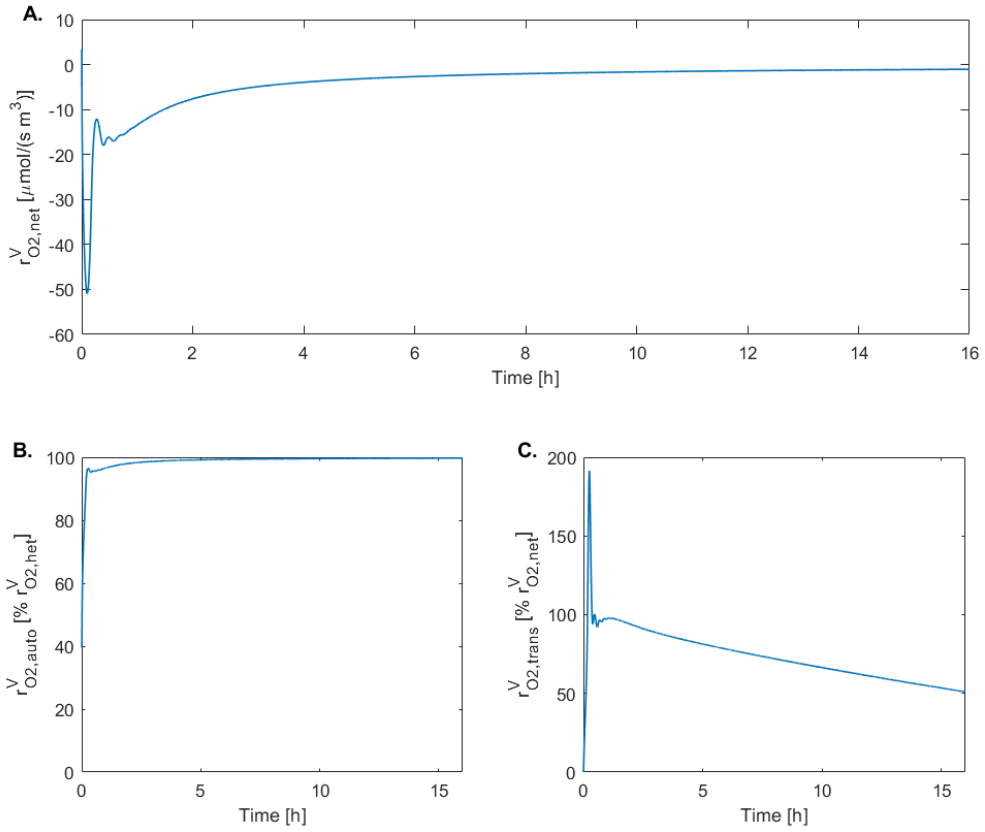

Figure 4.5: Net oxygen production (A), autotrophic oxygen production as a percentage of heterotrophic oxygen consumption (B), oxygen transfer as a percentage of net oxygen production (C).

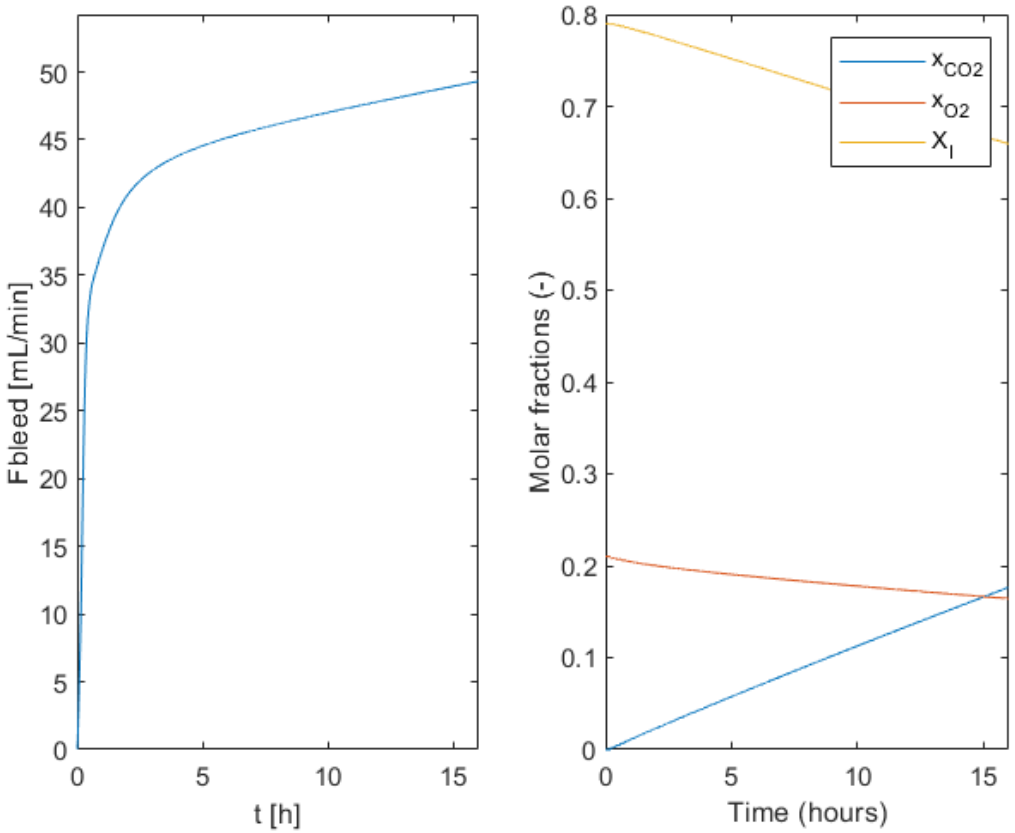

Figure 4.6: Bleed gas flowrate and composition.

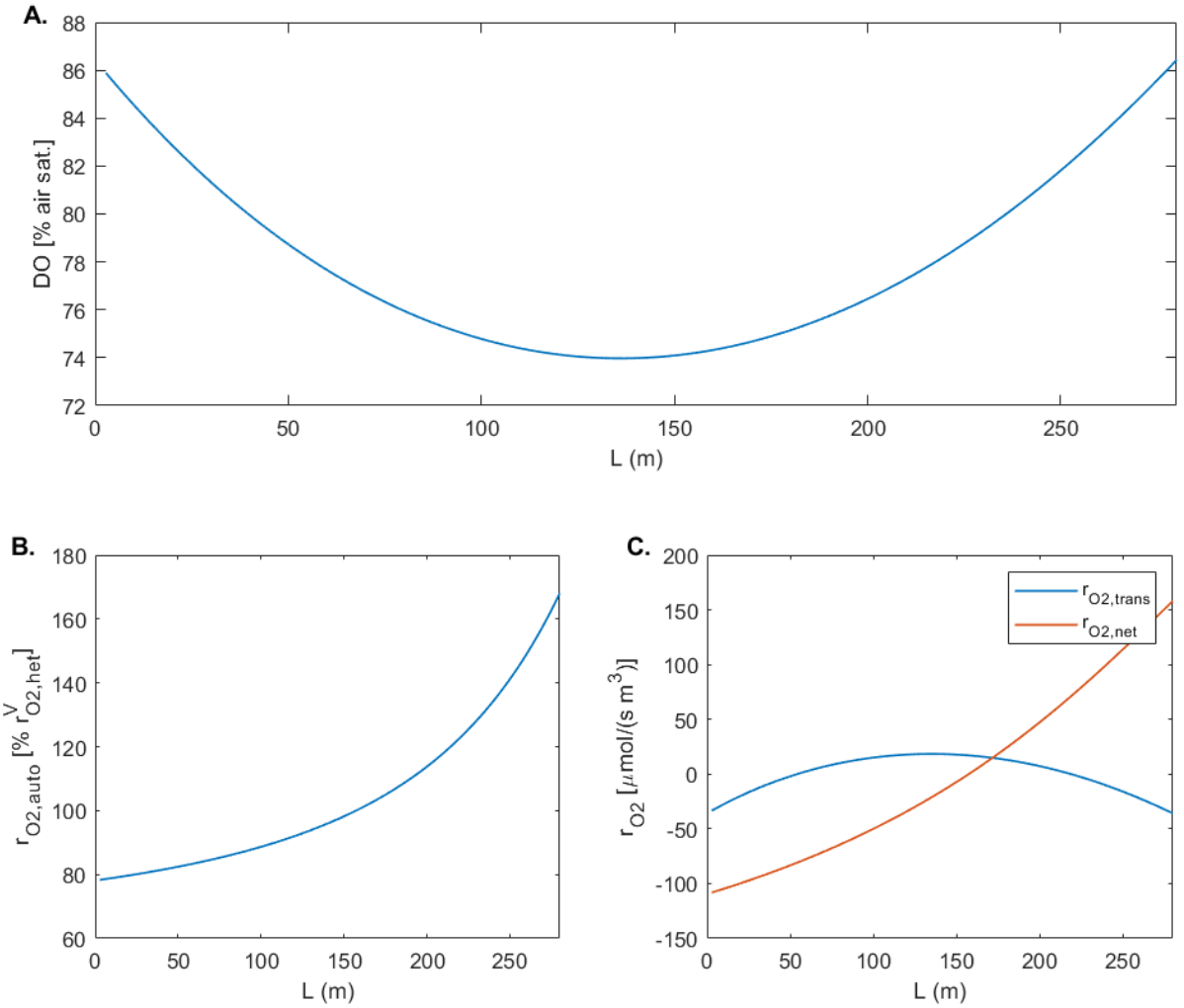

Figure 4.7: Dissolved oxygen profile (A), autotrophic oxygen production as a percentage of heterotrophic oxygen consumption (B), comparison between net oxygen production/consumption and oxygen transfer (C). The profiles are plotted over the length of the reactor at the 16th hour of the simulation.

4.2.2 Substrate flowrate sensitivity

Substrate concentration, dissolved oxygen, oxygen consumption, and production rates in time and position are affected by substrate flowrate. The effect of substrate flowrate on DO and COG is important when comparing the two control strategies. Considering as a reference the value the substrate flowrate value set in the simulation of the previous section (F_{FEED}), a sensitivity analysis is run with 20% F_{FEED} (scenario A), 80% F_{FEED} (scenario B), 96.8% F_{FEED} (scenario C) and 120% F_{FEED} (scenario D) and the results are compared.

In scenario A, a very low constant substrate flowrate leads to the surface plots shown in Figure 4.8. The substrate is not accumulating in the reactor as it is consumed in each tube passage. Carbon dioxide concentration in the liquid phase increases and reaches its maximum value in 55 m, before decreasing to zero. Both these two surface plots suggest that the reactor is unbalanced: heterotrophic metabolism strongly prevails in the first part of the reactor and autotrophic metabolism in the latter. Both DO and COG increase in time, as the system has a high net oxygen production. However, the increase in DO is relatively small (maximum value 140%), as photosynthesis is limited by the small amount of carbon dioxide produced by substrate consumption. The direction of oxygen transfer is from the liquid to the gas phase.

For scenario B, the surface plots are reported in Figure 4.9. Also, in this case, autotrophic oxygen production prevails over heterotrophic oxygen consumption, and DO, and COG increase over time. However, the increase is larger than in the previous case as photosynthesis is not carbon-limited (maximum value 200%). Carbon dioxide in the liquid phase increases over time, and substrate concentration is high enough to ensure mixotrophic conditions in the whole reactor. Also, in this scenario, oxygen transport is directed to the gas phase.

A special mention is needed for scenario C (Figure 4.10): DO is constant after the first transient period, and, therefore, the system is stable. However, oxygen production is not only balanced by oxygen consumption but also by oxygen consumption and losses in bleed gas. When using a control system to keep DO or COG to stable values, autotrophic and heterotrophic rates are indirectly controlled. However, when the system reaches a stable DO or COG, oxygen production is not only balanced with only oxygen consumption, and OBM is not happening in the system, as shown in this simulation. The average autotrophic oxygen production in the reactor is 103% of the average heterotrophic oxygen consumption.

In scenario D, due to the high substrate concentration in the reactor, and thus the high oxygen consumption rate, DO and COG are dropping to unsafe values, reaching 1%. When oxygen is absent in the liquid phase, heterotrophic metabolism is oxygen-limited, and substrate accumulates into the system. Carbon dioxide in the liquid phase also reaches a plateau as the heterotrophic carbon dioxide production rate decreases.

For further comparisons, the amount of substrate fed to the system is obtained from the simulation $m_{S,tot}$, and the productivity is calculated from the results following equation (4.9).

$$r_X = Y_{X/S,mixo}\left(\frac{m_{S,tot}}{MW_S} - \sum_{k=1}^{100}\frac{V_L}{N}(C_S^k)\right) \tag{4.9}$$

In the equation, MW_S is the molar mass of the substrate (30 g/C-mol) and $Y_{X/S,mixo}$ is the mixotrophic stoichiometric yield of biomass on substrate (0.9 C-mol$_X$/ C-mol$_S$). The second term in the equation represents the amount of substrate that is not being consumed in the end of the simulation. The results are shown in Table 4.2 where the day is referred to the 16 hours.

Table 4.2: Simulation results with constant substrate flowrate. Substrate input, productivity and DO.

Scenario - substrate feed flowrate [L/min]	**$m_{S,tot}$ [kg/day]**	**r_X [g_X/(L day)]**	**Minimum DO - Maximum DO**
A – 0.0741	0.238	0.264	98% - 140%
B – 0.297	0.954	1.05	89% - 204%
C – 0.359	1.15	1.27	85% - 107%
Stoich - 0.371	1.19	1.31	74% - 110%
D – 0.445	1.43	1.49	1% - 109%

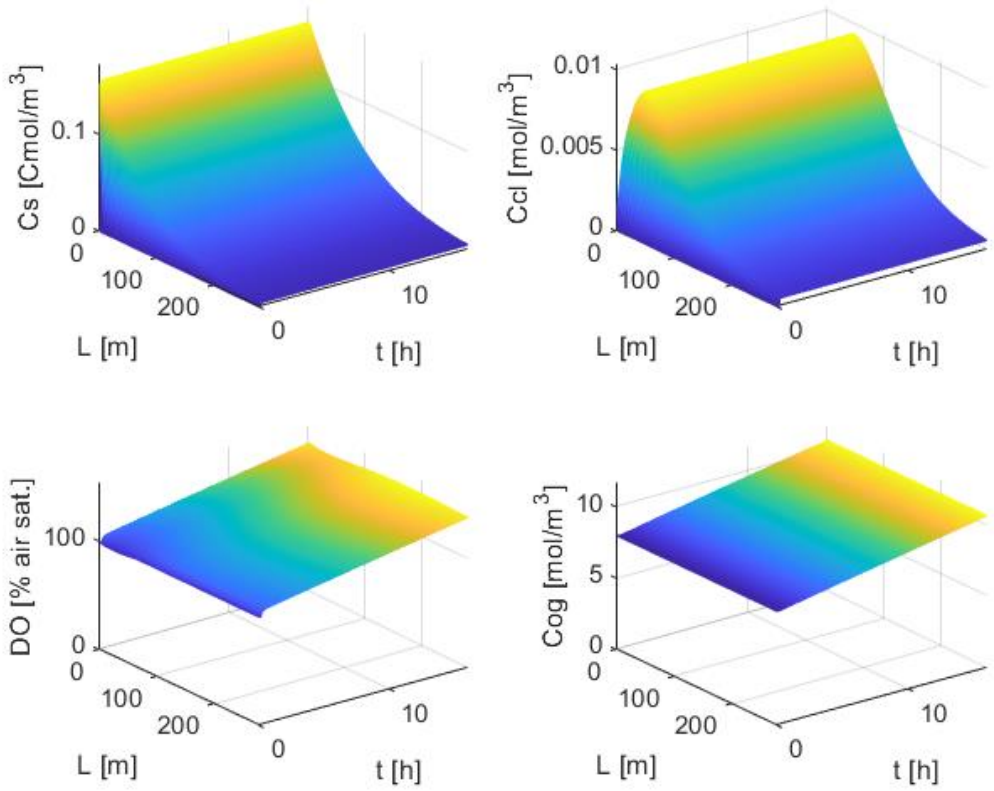

Figure 4.8: Scenario A. Surface plot of substrate concentration (C_S), carbon dioxide concentration in liquid phase ($C_{CO2,L}$), dissolved oxygen in liquid phase (DO), oxygen concentration in gas phase ($C_{O2,G}$).

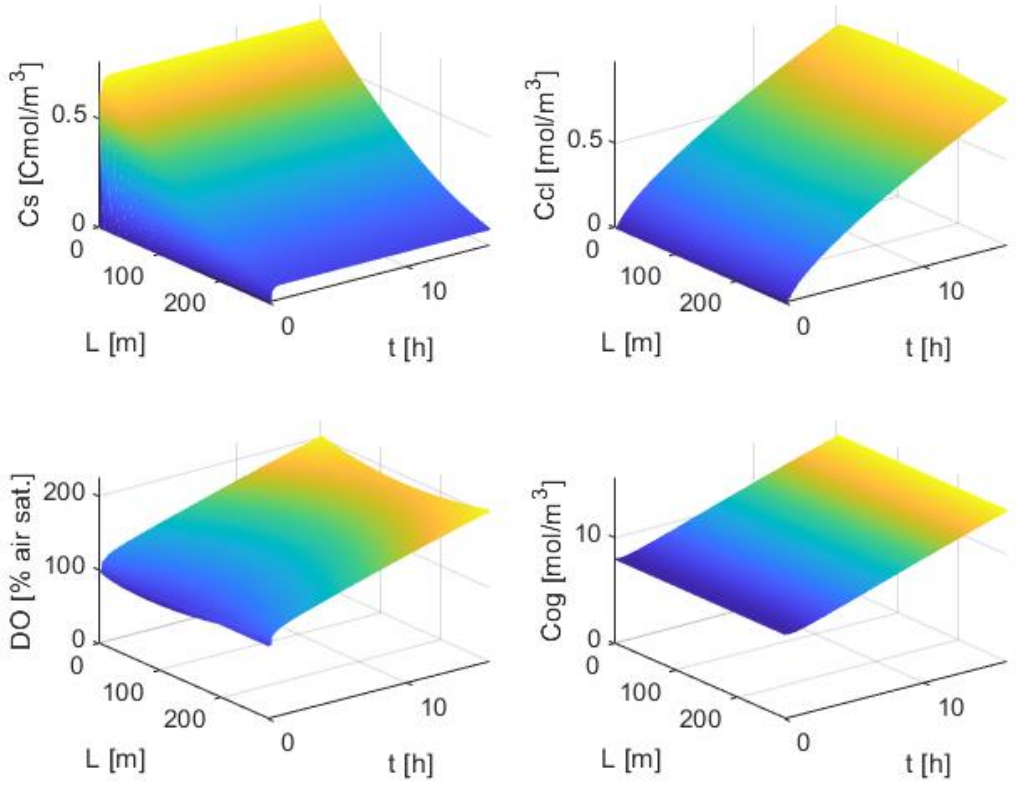

Figure 4.9: Scenario B. Surface plot of substrate concentration (C_S), carbon dioxide concentration in liquid phase ($C_{CO2,L}$), dissolved oxygen in liquid phase (DO), oxygen concentration in gas phase ($C_{O2,G}$).

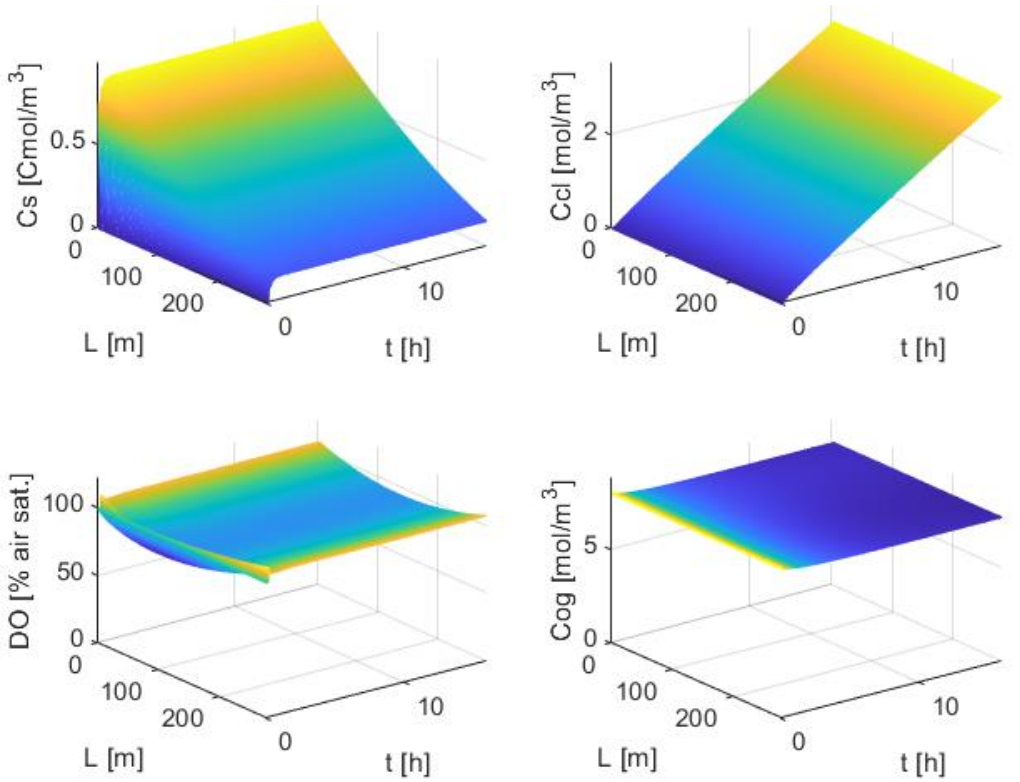

Figure 4.10: Scenario C. Surface plot of substrate concentration (C_S), carbon dioxide concentration in liquid phase ($C_{CO2,L}$), dissolved oxygen in liquid phase (DO), oxygen concentration in gas phase ($C_{O2,G}$).

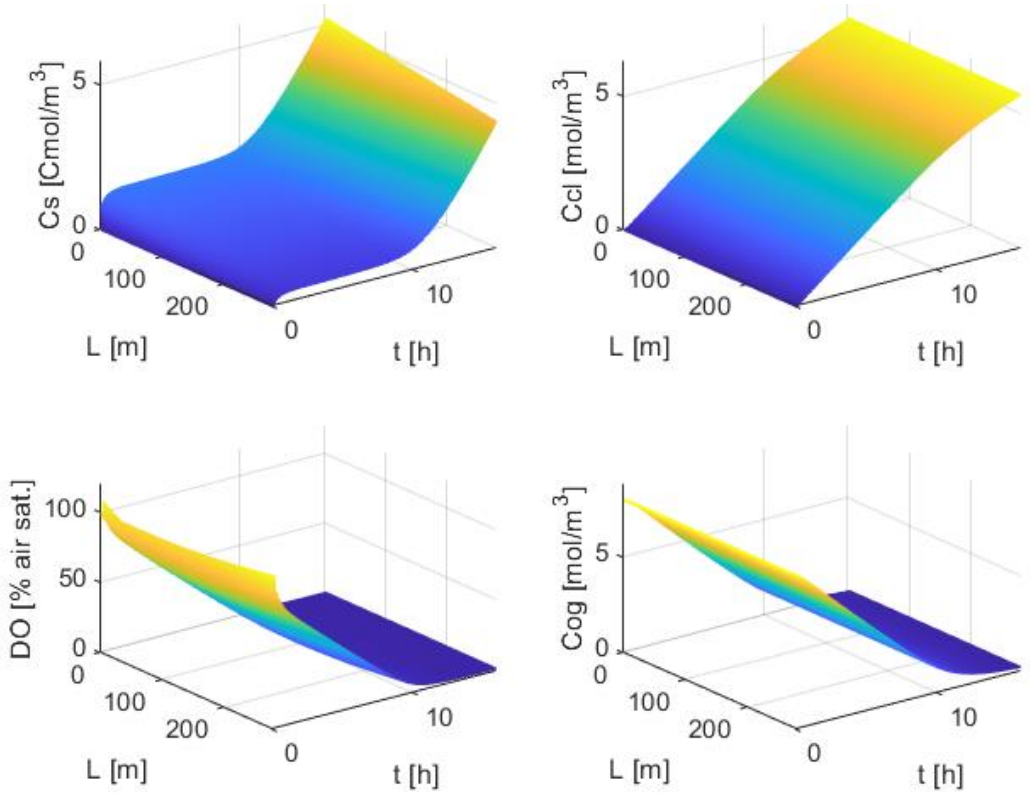

Figure 4.11: Scenario D. Surface plot of substrate concentration (C_S), carbon dioxide concentration in liquid phase ($C_{CO2,L}$), dissolved oxygen in liquid phase (DO), oxygen concentration in gas phase ($C_{O2,G}$).

Biomass volumetric productivity increases with increasing glucose input in the system. In constant light conditions, values higher than 1.44 $g_x/(m^3\ day)$ are not expected, as anoxic conditions should not be approached during the day. The abovementioned productivity is simulated with a substrate flowrate of 110% of the stoichiometric value, and a minimum value of DO of 10% is reached at the end of the day.

As concluding remarks after these simulations, it has been shown that COG, DO, and substrate flowrate are dependent variables. Oxygen concentration can be increased or decreased by acting on substrate flowrate. Small changes in flowrate can effectively act on DO in the system. Too big changes can lead to problematic implications in the culture with anoxia (scenario D) or low productivity (scenario A). A control system that accurately acts on substrate flowrate is indispensable to achieving high productivity and keeping dissolved oxygen at safe levels.

4.2.3 Control system design

The effect of a control system on the process depends on the specific control system design, thus, on the values of its three parameters. The chosen tuning method to find the parameters for the discontinuous control systems is the Ziegler-Nichols stability margins method. The controller design is performed with no initial substrate input in the system, and the setpoint values of COG and DO to reach are 18% and 90%, respectively. This section shows the complete control system design for oxygen concentration in the gas phase. The results of the same procedure for the control system based on dissolved oxygen are then presented.

With a proportional controller, the value of the control parameter $K_{p,u}$ so that the system has stable and consistent oscillations is found. The ultimate period of oscillation P_u is obtained from the simulated response. The parameters for the system are defined according to the relations in Table 4.3.

When the controlled variable is COG, the sustained oscillation is obtained for a $K_{p,u}$ value of 8.5E-6, corresponding to a P_u value of 5760 s (Figure 4.12). The P, PI, and PID controllers are designed with these parameters, and the performances are compared (Figure 4.13). The criteria for the choice of the control system for the process is based on the simulated response: it should reach stability quickly, the oscillations at the beginning of the process should be small, dissolved oxygen should not reach unsafe levels, and offset with the setpoint should be low. With a proportional controller, even though oscillations are negligible, reaching a COG setpoint value lower than the initial conditions is impossible due to offset. In addition, the dynamic evolution of the system is very slow, therefore, biomass productivity would be low.

Table 4.3: Ziegler-Nichols stability margins method to design a P, PI and PID controller.

Controller	K_P	τ_I	τ_D
P	$0.5\ K_{p,u}$	–	–
PI	$0.45\ K_{p,u}$	$P_u/1.2$	–
PID	$0.6\ K_{p,u}$	$P_u/2$	$P_u/8$

Conversely, a PI controller eliminates the offset but introduces oscillations. In addition, the dynamic evolution of the system is still slow, and the response is in between the settling limits, defined as ±2% of the final value, only after 4.6 h. The best dynamic evolution is the one of the system with a PID controller, but the more extensive oscillations may significantly affect values reached by DO over time. The parameters of the control system are K_P = 5.1E-6, τ_I = 2.9E3, τ_D = 7.2E2.

The same procedure has been followed for the control system in which the controlled variable is DO. In this case, a PI controller is chosen as it is the simplest one, with a response that is fast, stable, and satisfactory (Figure 4.14). The parameters of the control system are K_P = 2.0E-9, τ_I = 1.8E3. A comparison between the two control strategies is provided in Figure 4.15, where the setpoint is defined so that the results are comparable.

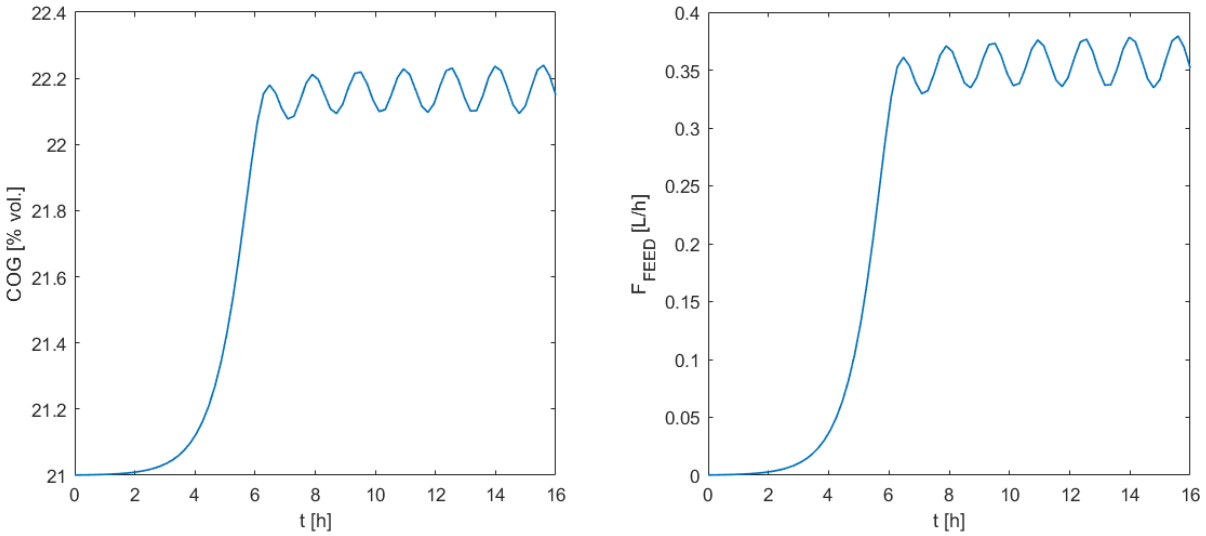

Figure 4.12: Design of the control system for COG. The reactor is controlled with a proportional controller and the response represented is the one with stable and consistent oscillations.

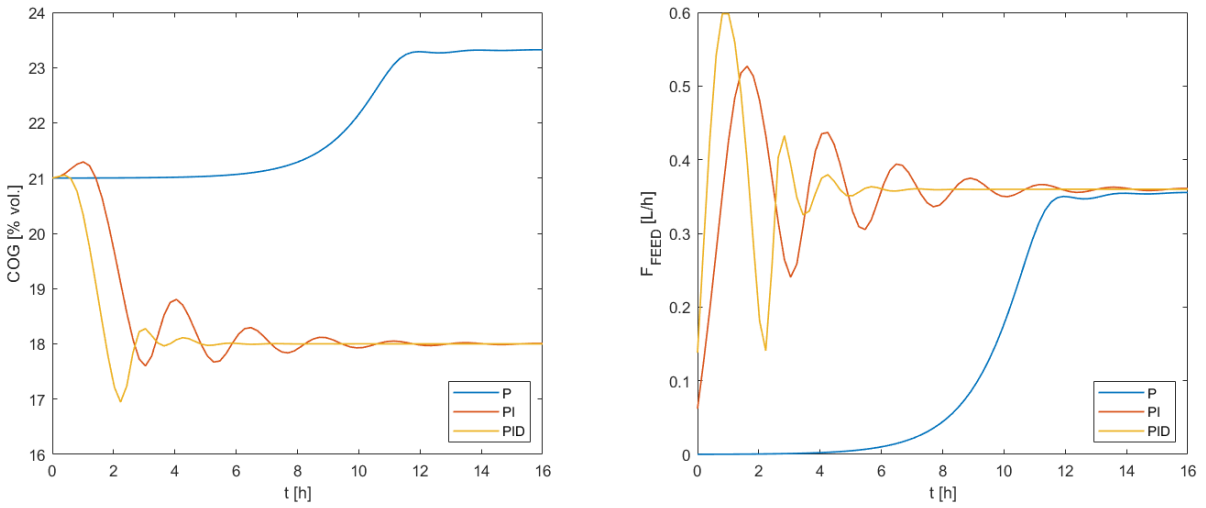

Figure 4.13: Control system for COG tuned with Ziegler-Nichols stability margin method. Response of the P, PI and PID controllers for comparisons.

The performance of the control strategy that uses DO as a controlled variable seems to be more effective in reaching a stable DO value; it is faster and with fewer oscillations than the other control strategy. The reason could be the more direct control approach, as the driving force for oxygen consumption/production is in the liquid phase. In addition, smaller oscillations mean that the control system may be more robust. This is ideal when dealing with other disturbances in the real process that are not included in the model (for example, temperature changes or technical issues with the equipment).

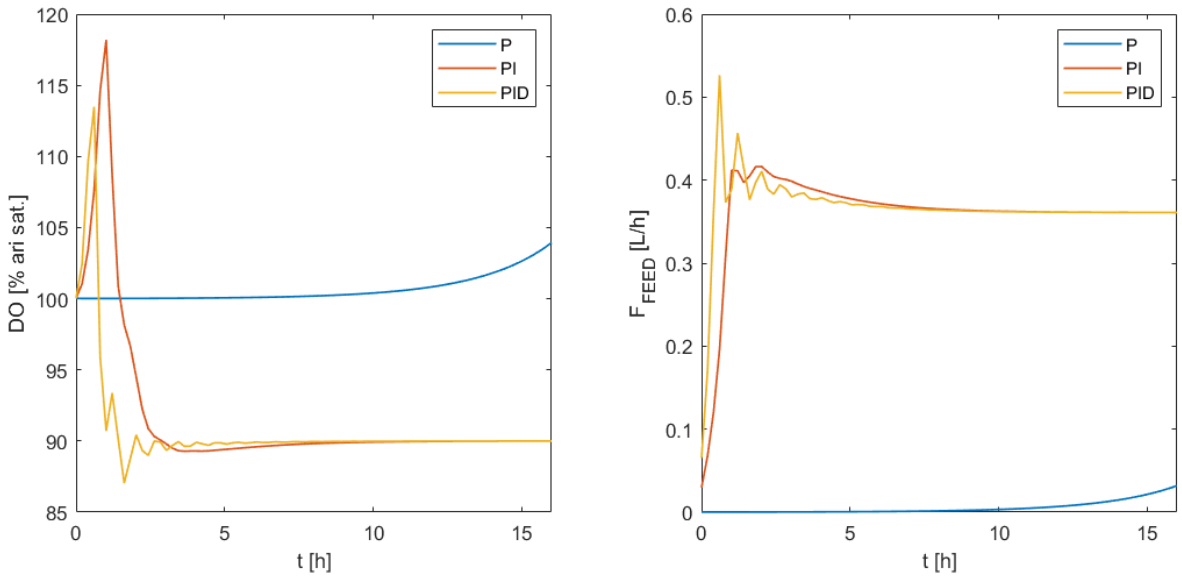

Figure 4.14: Control system for DO, tuned with Ziegler-Nichols stability margin method. Response of the P, PI and PID controllers for comparisons.

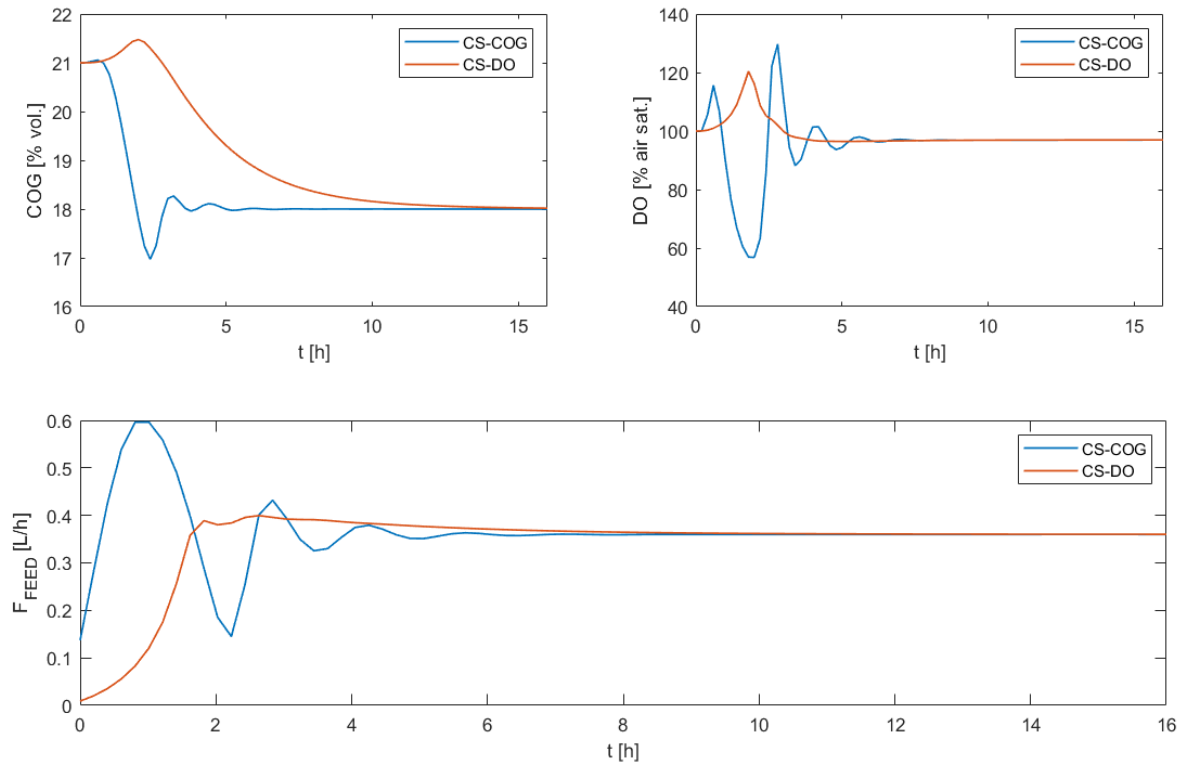

Figure 4.15: Comparison between the two control systems (DO and COG).

To better understand why controlling DO seems better than controlling COG, a sensitivity analysis with constant substrate feed flowrate is conducted. The analysis aims to verify whether a change in substrate flowrate has a more substantial effect on DO or COG. The variables DO and COG at the end of the tube and at the end of the day are stored for each substrate flowrate investigated. Then, the relative change of these variables with respect to the results of the stoichiometric substrate feed flowrate simulation is computed. The sensitivity is presented in Figure 4.16, and it shows that there is a linear tendency around the substrate feed flowrate. The change in substrate flowrate has a faster effect on DO as the magnitude of the slope of the line is higher. Thus, this might be one of the reasons why it seems to work better as a controlled variable.

Further technical issues must also be considered to decide the best control strategy for the process. An oxygen probe in the gas phase might be easier to manage in a large-scale system, as it can be placed in the mixing tank, and thus, maintenance and cleaning could be done in a simple way. However, condensation on the probe affects the oxygen measurements and, thus, the control system performances. To avoid this issue, a gas recycle line with a condenser placed before the oxygen probe could be installed in the mixing tank. When the control system is based on oxygen measurements in the liquid phase, noise due to cell metabolism and mixing phenomena must be considered. It might result in a less stable response than the one that has been modeled.

The last control system explored is the continuous one, which measures COG and calculates the error with a setpoint that changes in time. The setpoint is the value of COG a residence time in the past. The response of this PI control system with K_P = 5E-7 and τ_I = 5E3 is shown in Figure 4.17.

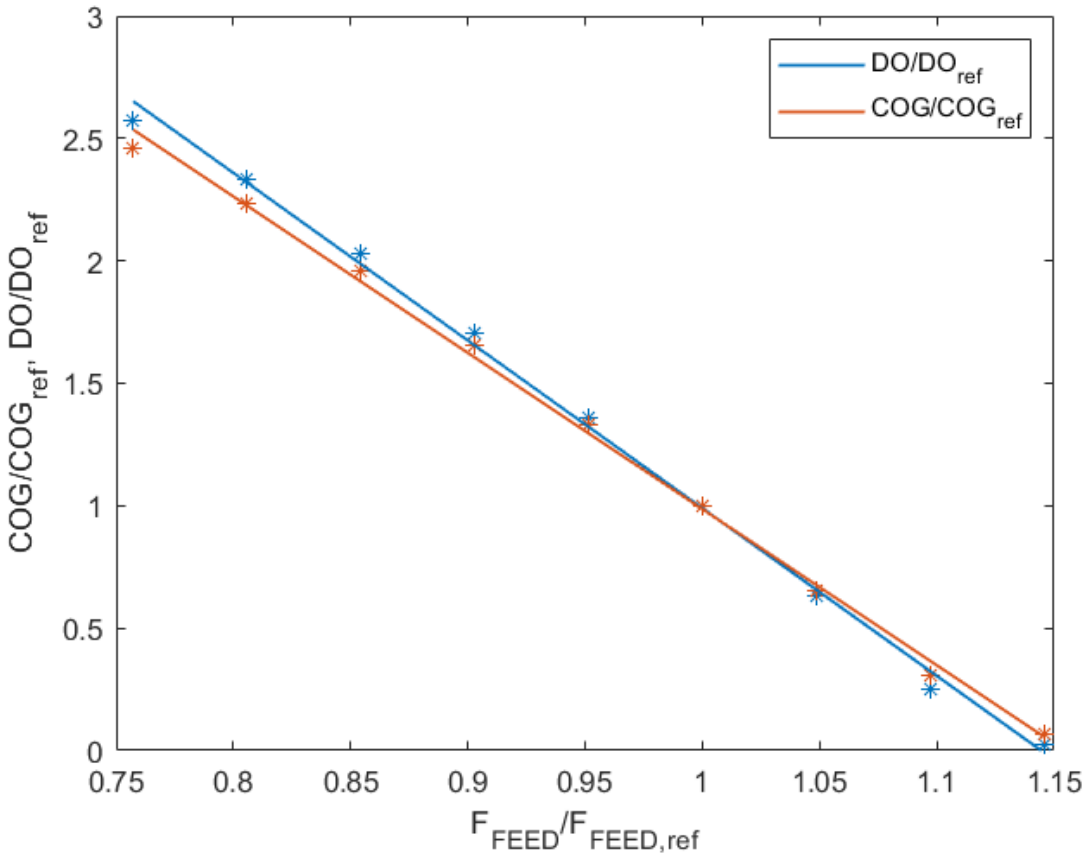

Figure 4.16: Sensitivity analysis on DO and COG at different substrate feed constant flowrates.

This control system successfully reaches stability and keeps dissolved oxygen at safe values. This control logic is more prone to suppress disturbances, but a constant setpoint value cannot be defined. In fact, the error is calculated based on COG at the previous residence time, that can be considered the setpoint of the control strategy. Furthermore, it is essential to state that one of the stable states for the system, where COG is not changing in time, is when COG is zero. A proper and careful controller design is needed to avoid this stable state, as it is harmful to the culture. In addition, at least with the set of design parameters explored, the dynamic evolution of the system is relatively slow, which is relatable to low productivity.

A comparison between biomass productivity obtained with the three different control systems is provided in Table 4.4, where the day is referred to the 16 hours. In general, the fastest the control system reaches a stable state, the highest the productivity. For this reason, the continuous one that controls COG is the control system with the lowest productivity among the ones proposed. The productivity achieved with the set-point control strategies is comparable, even though a more extensive range of DO fluctuations is seen when controlling COG. Furthermore, it is similar to the one obtained with constant stoichiometric substrate feed flowrate (1.31 g_X /(L day), Section 4.2.2) as the flowrate rapidly increases from zero to the stoichiometric value.

A continuous set-point control system with control variable COG or DO could also be studied. However, this control strategy is not included in this Thesis.

Table 4.4: Simulation results with control systems. Substrate input, productivity and DO.

Control variable	**Control action each**	**Setpoint value**	**$m_{S,tot}$ [kg/day]**	**r_X [g_x/(L day)]**	**Minimum DO - Maximum DO**
DO	Residence time	90%	1.19	1.32	77% - 110%
COG	Residence time	18%	1.18	1.30	55% - 126%
COG	1 s	-	0.64	0.70	100% - 131%

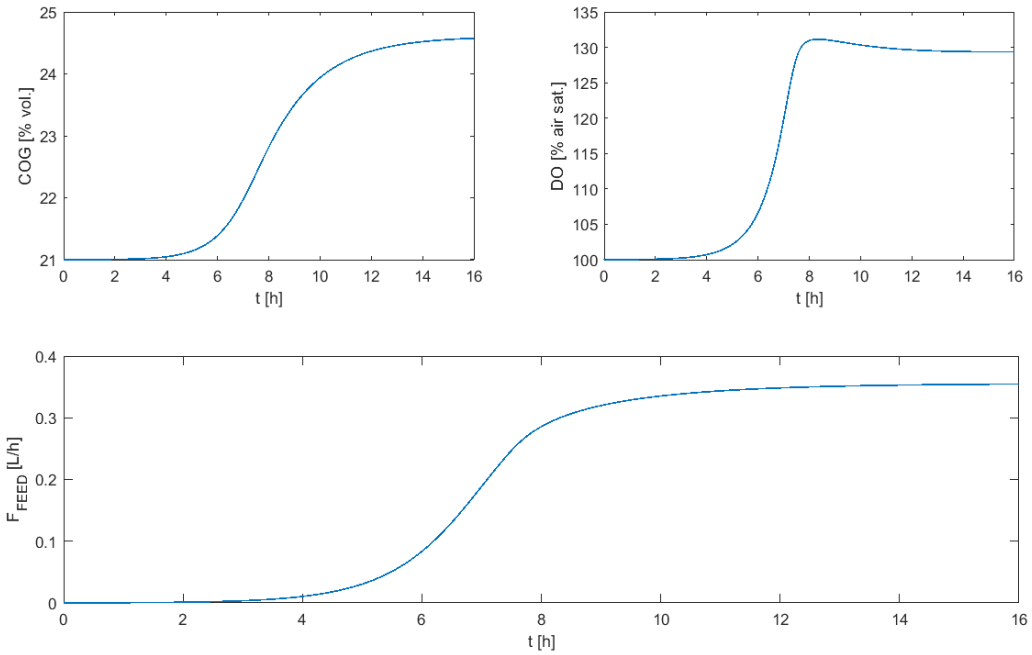

Figure 4.17: Dynamic evolution of the process with the continuous control system.

4.2.4 Clear sky and real light conditions on a cloudy day

The scenario in which the reactor is in constant light conditions, and therefore with a constant autotrophic oxygen production rate ($q_{O2,auto}$), is helpful to understand the system better, but it is not realistic in practice. The autotrophic oxygen production rate will change during the day. As an example of real light input, the daylight conditions implemented in the model refer to the irradiance profiles presented in Section 1.2.2 for the day of 15/08/2019 in Bennekom, The Netherlands. In this section, only the amount of daylight hours on that date is simulated (14.5 h). Photosynthetic active irradiance retrieved from the NSRDB is fitted with a linear interpolant function using Curve Fitting Toolbox (MATLAB R2020a).

Considering that the model does not include equations to relate $q_{O2,auto}$ to PFD during the day, an empirical approach is adopted to calculate $q_{O2,auto}$ in different light conditions. With this approach, the average $q_{O2,auto}$ during the day in clear sky conditions (with sinusoidal light input) is assumed constant and equal to the one in constant light conditions. This is done by converting the photosynthetically active irradiance curve to a $q_{O2,auto}$ curve, multiplying it by a constant conversion factor. In this way, the results of the simulations with constant and sinusoidal light are comparable. For the simulations with actual atmospheric conditions, $q_{O2,auto}$ is proportional to the one in sinusoidal light conditions the same way as clear sky irradiance is proportional to the true irradiance during the day, as a linear dependence between photosynthetically active irradiance and oxygen production is assumed (Figure 4.18).

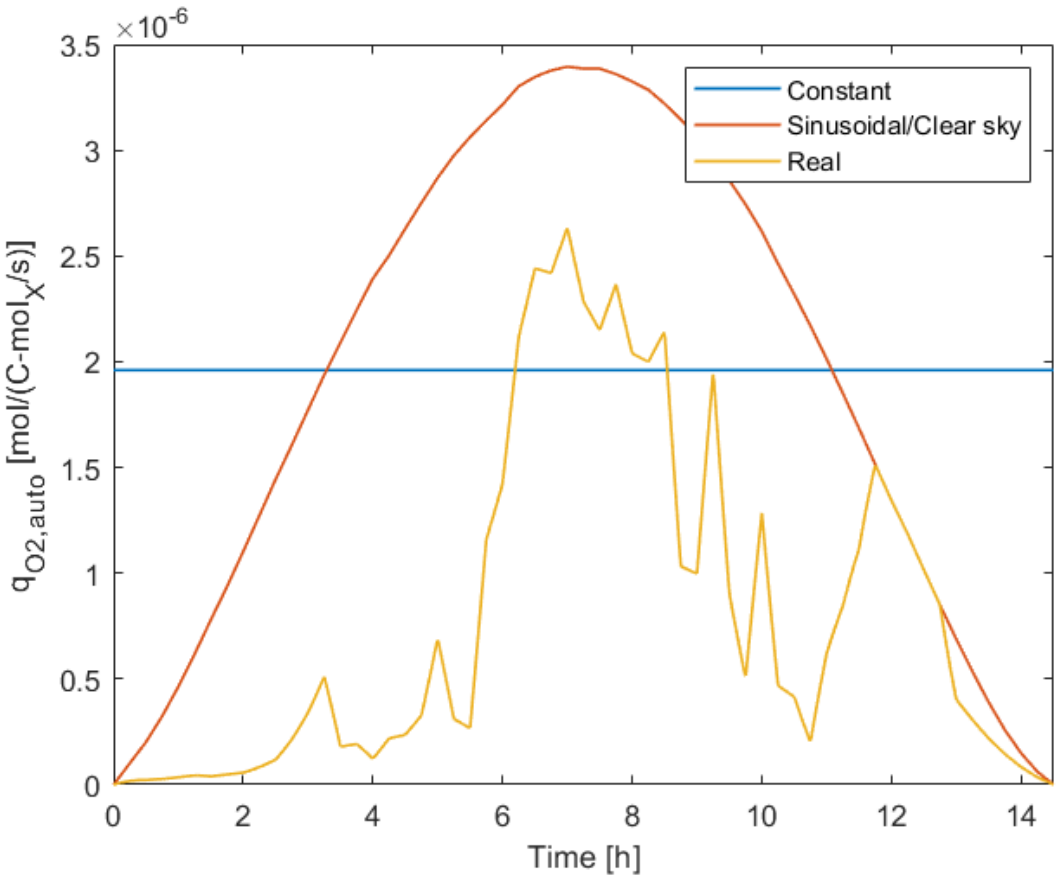

Figure 4.18: $q_{O2,auto}$ in constant, sinusoidal and real light conditions.

First, a simulation with constant stoichiometric substrate input is run, and the surface plots are shown in Figure 4.19. Because of the irradiance curve during the day, oxygen production is not constant. Thus, achieving oxygen balance with a constant substrate input in the system is impossible as heterotrophic oxygen consumption is dominant at the beginning and end of the day. In contrast, autotrophic oxygen production prevails during midday (Figure 4.20). Furthermore, anoxic conditions are reached twice a day when autotrophic oxygen production is too low to balance the heterotrophic oxygen consumption. A lower constant substrate flowrate may be a solution to avoid anoxia. With a flowrate of 10% of the stoichiometric value, photosynthesis is limited by the carbon dioxide in the liquid (Figure 4.21), and the same productivity values as in the previous simulation are not reached (Table 4.5).

A control system is indispensable for process optimization. Therefore, the control strategies based on COG as a control variable are implemented. Because of the assumed low carbon dioxide concentration at the start of the simulation (air equilibrium), a substrate flowrate equal to 10% of the stoichiometric substrate flowrate is provided for the first residence time to enhance carbon dioxide production. With the setpoint strategy, a PID control system is tuned, and the parameters are K_P = 4E-6, τ_I = 4.6E6, τ_D = 1E3 (surface plots in Figure 4.22). Even though the system cannot reach stability because of the light conditions defined for the simulation, dissolved oxygen fluctuates in a safe range. The control system must be precisely tuned, as wrong values of the design parameters could lead to a response in which much substrate is fed in the first few hours of the process. This great substrate accumulation would result in a quick drop in DO in the last daylight hours, when autotrophic oxygen production decreases as light irradiance is low. However, if substrate input to the process is low, the process could be limited by carbon dioxide (simulation with 10% stoichiometric flowrate).

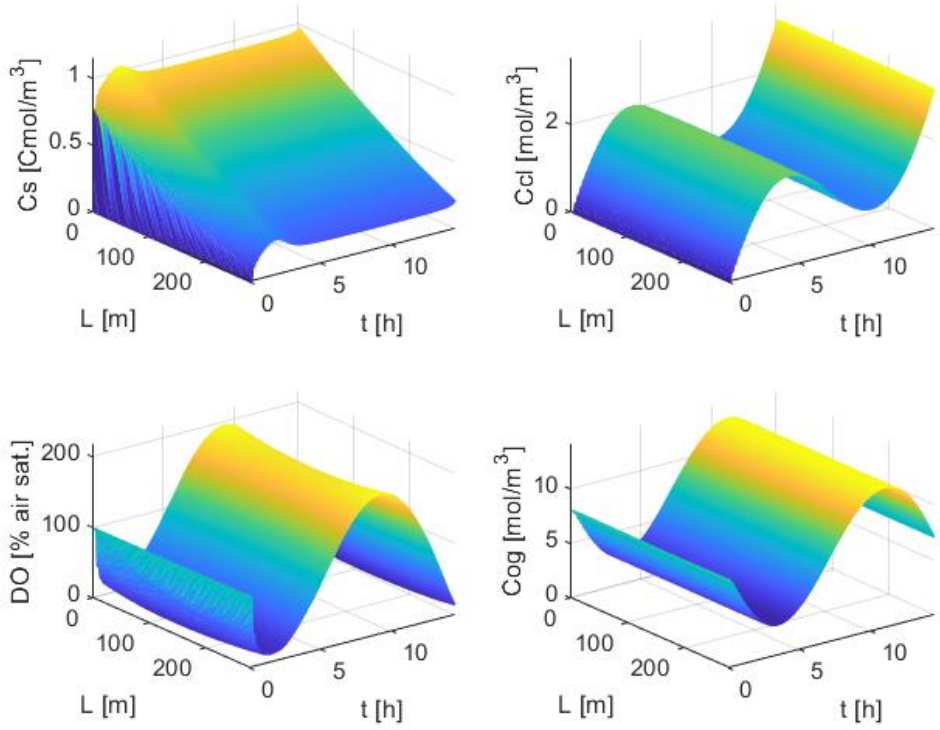

Figure 4.19: Surface plot of substrate concentration (C_S), carbon dioxide concentration in liquid phase ($C_{CO2,L}$), dissolved oxygen in liquid phase (DO), oxygen concentration in gas phase ($C_{O2,G}$). Clear sky light conditions and stoichiometric flowrate.

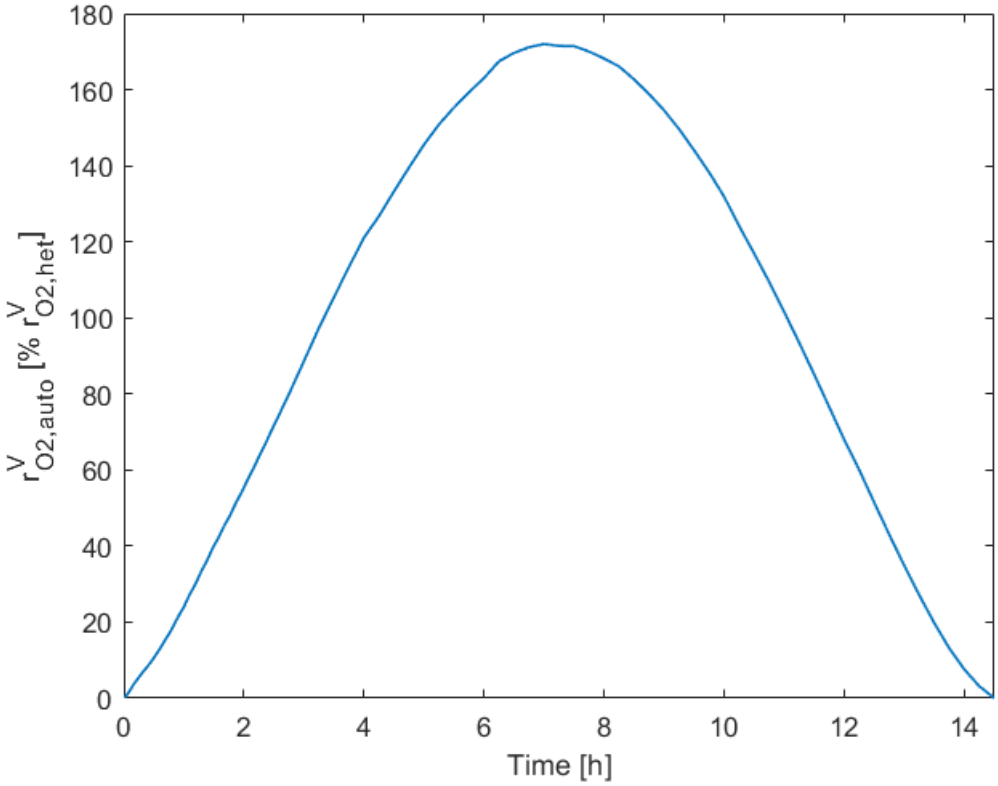

Figure 4.20: Autotrophic average oxygen production in the reactor as a percentage of the heterotrophic oxygen consumption. Clear sky light conditions and stoichiometric flowrate.

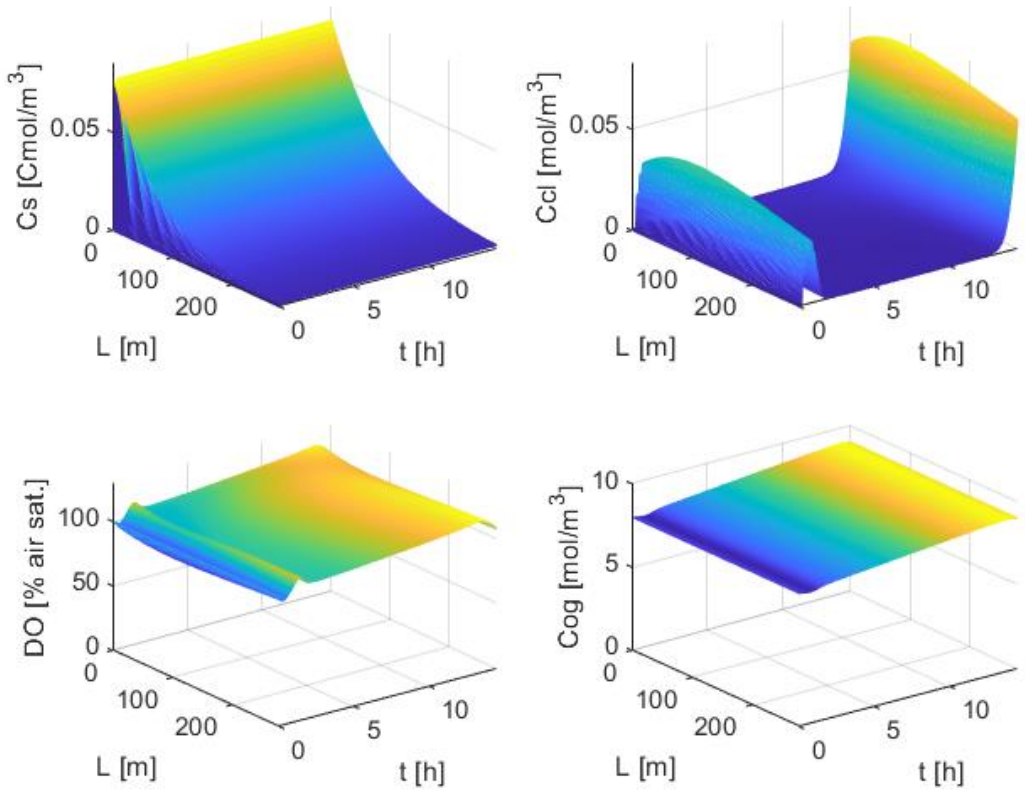

Figure 4.21: Surface plot of substrate concentration (C_S), carbon dioxide concentration in liquid phase ($C_{CO2,L}$), dissolved oxygen in liquid phase (DO), oxygen concentration in gas phase ($C_{O2,G}$). Clear sky light conditions and 10% of stoichiometric flowrate.

The control system that is designed to deal with clear sky irradiance also offers good results when real daylight data including atmospheric conditions is implemented in the simulation. The surface plots are shown in Figure 4.23.

In both these two simulations, the reactor is in mixotrophic conditions for most of the time. However, aiming for oxygen balance with a standard discontinuous PID control system is not trivial, and an optimization of the process with real light conditions might require more advanced control strategies. Some additional measures to save the culture for unexpected drops in DO during the day due to disturbances can be developed. For example, the reactor could be aerated with fresh air, or substrate supply can be immediately stopped when the absolute value of DO is low, or its decreasing rate is high. In this way, anoxia in the system might be prevented.

Finally, the surface plots with the continuous control system for sinusoidal and real light conditions are presented in Figure 4.24 and Figure 4.25. The PID control system that had been designed in constant light conditions can also manage this situation with good results, and the performances are similar to the discontinuous control system.

The substrate input, productivities, and DO range obtained from the simulations run in this section and some of the previous ones are reported in Table 4.4. In these simulations, a day is referred to the 14.5 hours. Both the control systems achieve a similar productivity in sinusoidal and real light conditions, with the continuous one being slightly better and with a lower range of DO oscillations. In real light conditions, productivity is around the half of the value in sinusoidal light conditions, because of the lower oxygen production in the system. The productivity obtained in real light conditions is comparable with the productivity obtained in pilot-scale experiments of 0.71 ± 0.43 $g_x/(L\ day)$ (de Winter, 2022). However, a true comparison could be only done if the same light conditions are simulated. Only a small reduction in productivity is expected in clear sky conditions with respect to constant light. This is true when the average autotrophic oxygen production in the system is not changing. Furthermore, the value of this parameter was obtained in the lab-scale photobioreactor in constant light conditions. Reaching this average autotrophic oxygen production in a day with clear sky is a significant challenge to be addressed for the process scale-up, as the model shows promising results in these conditions.

Table 4.5: Simulation results with control systems. Substrate input, productivity and DO.

Light conditions	Substrate feeding strategy	$m_{S,tot}$ [kg/day]	r_X [g_x/(L day)]	Minimum DO - Maximum DO
Sinusoidal	Constant, stoichiometric	1.08	1.19	4% - 198%
Sinusoidal	Constant, 10% stoichiometric	0.108	0.119	91% - 118%
Constant	COG control, discontinuous	1.06	1.17	52% - 129%
Constant	COG control, continuous	0.915	1.01	99% -129%
Sinusoidal	COG control, discontinuous	0.97	0.97	41% - 145%
Sinusoidal	COG control, continuous	0.98	1.09	81% - 143%
Real	COG control, discontinuous	0.38	0.425	58% - 145%
Real	COG control, continuous	0.40	0.446	74% - 154%

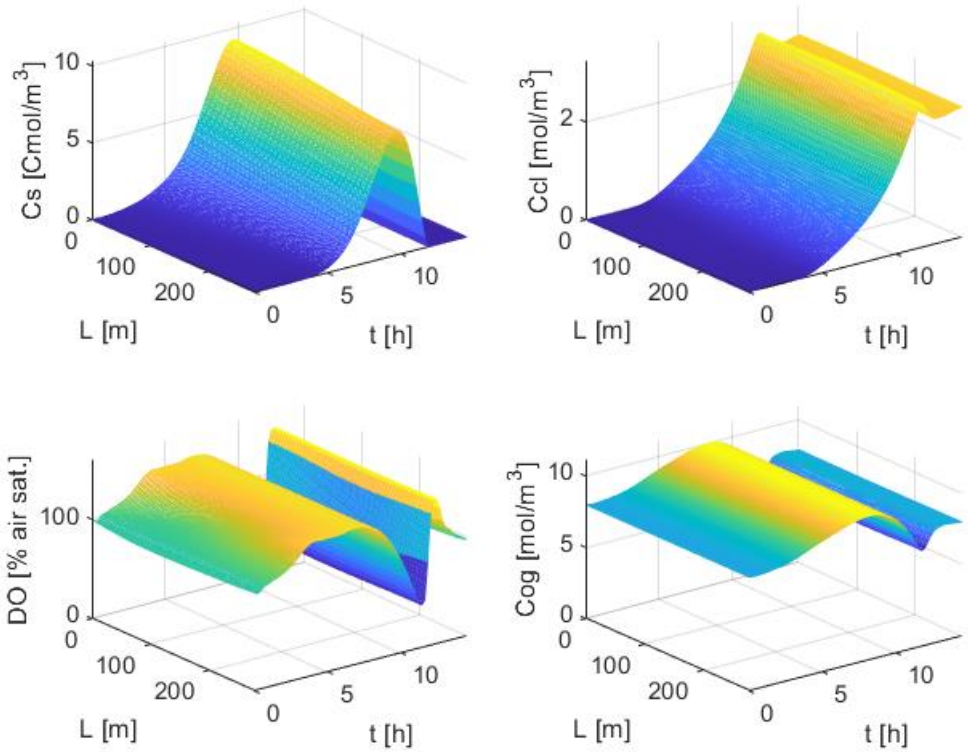

Figure 4.22: Surface plot of substrate concentration (C_S), carbon dioxide concentration in liquid phase ($C_{CO2,L}$), dissolved oxygen in liquid phase (DO), oxygen concentration in gas phase ($C_{O2,G}$). Sinusoidal light irradiance including atmospheric conditions, discontinuous control system with COG setpoint value.

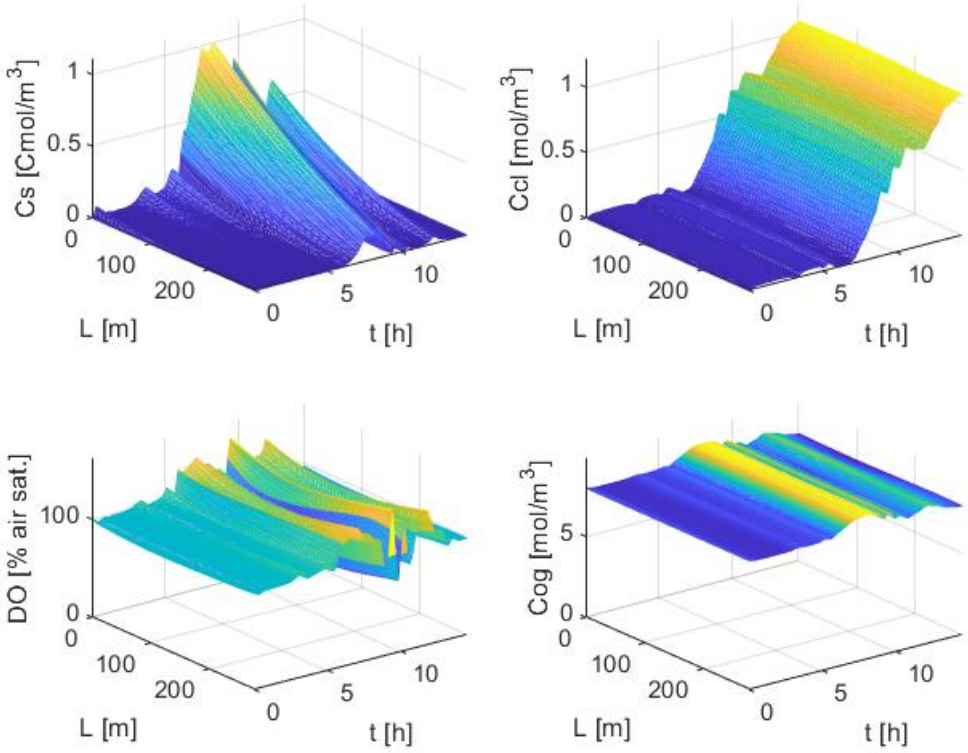

Figure 4.23: Surface plot of substrate concentration (C_S), carbon dioxide concentration in liquid phase ($C_{CO2,L}$), dissolved oxygen in liquid phase (DO), oxygen concentration in gas phase ($C_{O2,G}$). Real light irradiance including atmospheric conditions, discontinuous control system with COG setpoint value.

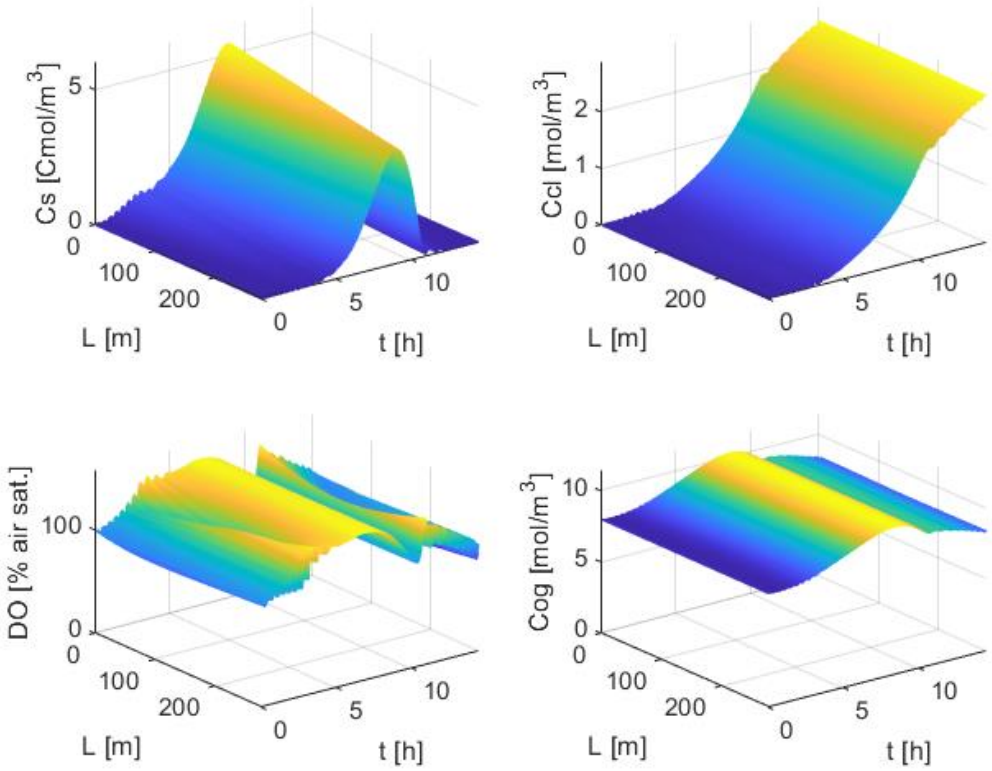

Figure 4.24: Surface plot of substrate concentration (C_S), carbon dioxide concentration in liquid phase ($C_{CO2,L}$), dissolved oxygen in liquid phase (DO), oxygen concentration in gas phase ($C_{O2,G}$). Sinusoidal light irradiance including atmospheric conditions, continuous control system with COG.

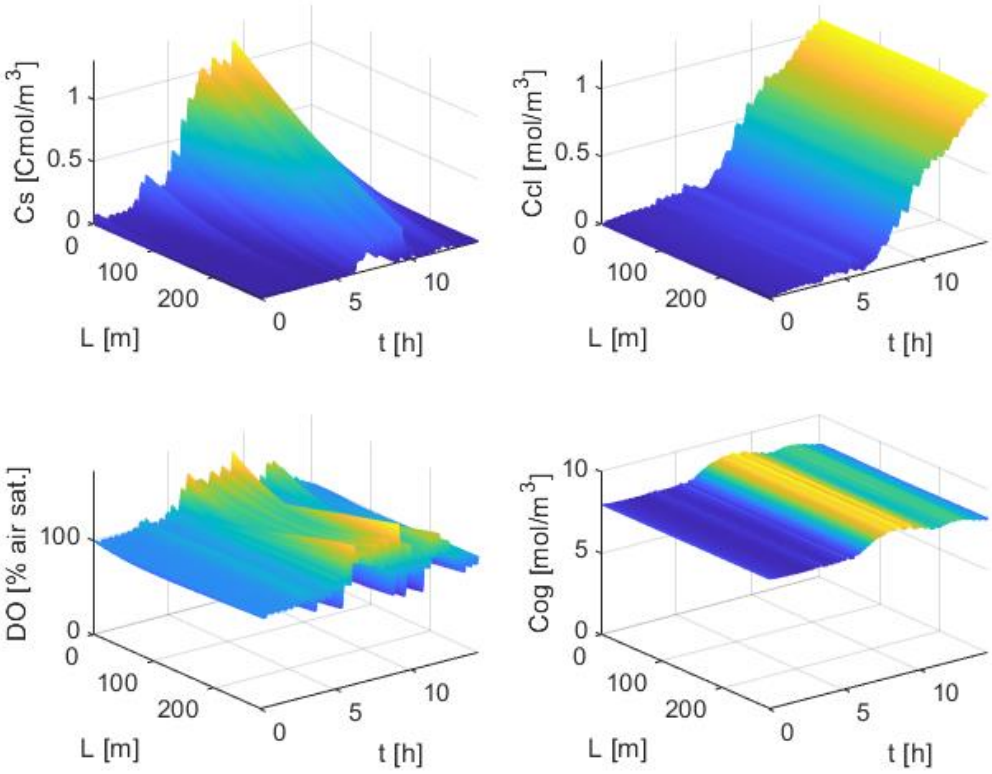

Figure 4.25: Surface plot of substrate concentration (C_S), carbon dioxide concentration in liquid phase ($C_{CO2,L}$), dissolved oxygen in liquid phase (DO), oxygen concentration in gas phase ($C_{O2,G}$). Real light irradiance including atmospheric conditions, continuous control system with COG.

4.3 Experimental results and model validation

In this section, only the main results of the validation experiments and the comparison with the model will be presented. The results of the batch preparation phase and the chemostat cultivation, are shown in Appendix C.

4.3.1 Oxygen concentration in gas phase and dissolved oxygen

All the validation experiments resulted in a stable COG between two to four hours. During the first experiment, dissolved oxygen decreased to a minimum value of 12%. Lower values were never registered during the other experiments. This is a proof that the control system that is designed from the model is working in keeping DO stable in the lab-scale reactor, where a plug flow reactor was experimentally simulated.

The variables DO, and COG obtained in the lab-scale photobioreactors are compared with the model results (Figures 4.26 to 4.28). The simulations are set with the same starting conditions of the experiments, which are slightly different from each other. In all three experiments, the profile of COG reasonably agrees with the model prediction.

At the beginning of the simulation, the COG shows an inverse response as the system's initial response is opposite to the direction of the final steady state. This response seems to be due to the imbalance between oxygen consumption and production rates when the microalgae have been growing without substrate for some time. This response is not present in the first experiment, because a manual action on the control system increased the pump flowrate to the maximum value for the first few pulses.

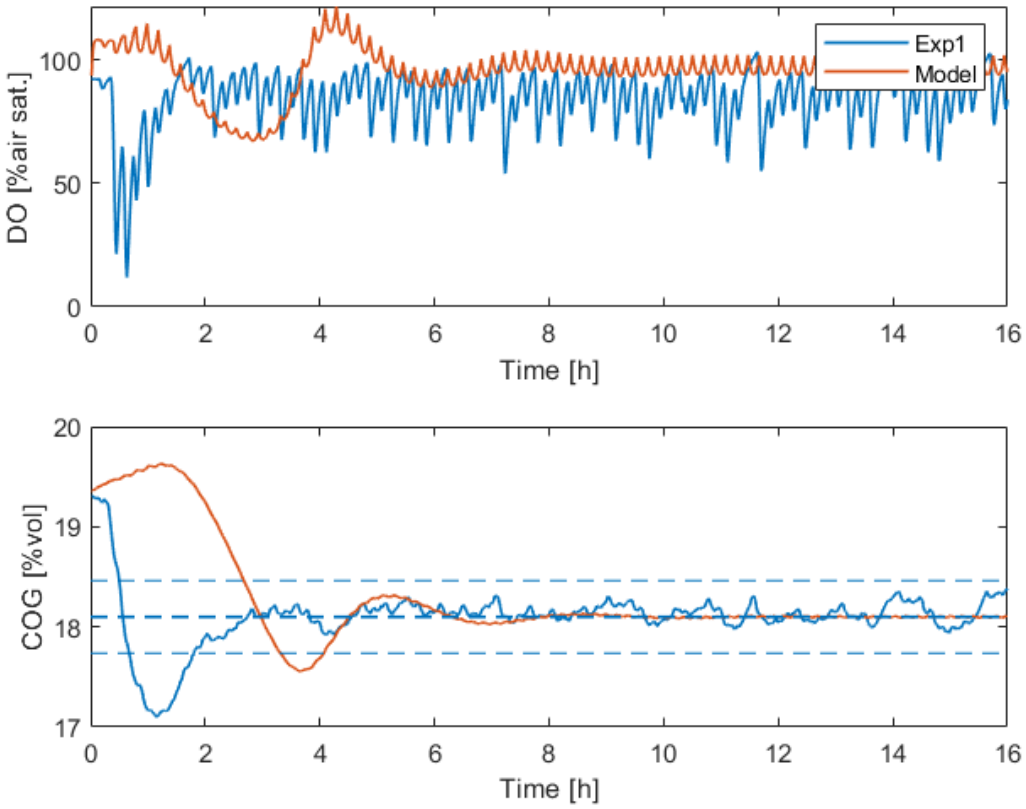

Figure 4.26: COG and DO profiles obtained in the first experiment, compared with the model predictions when the starting point is the same.

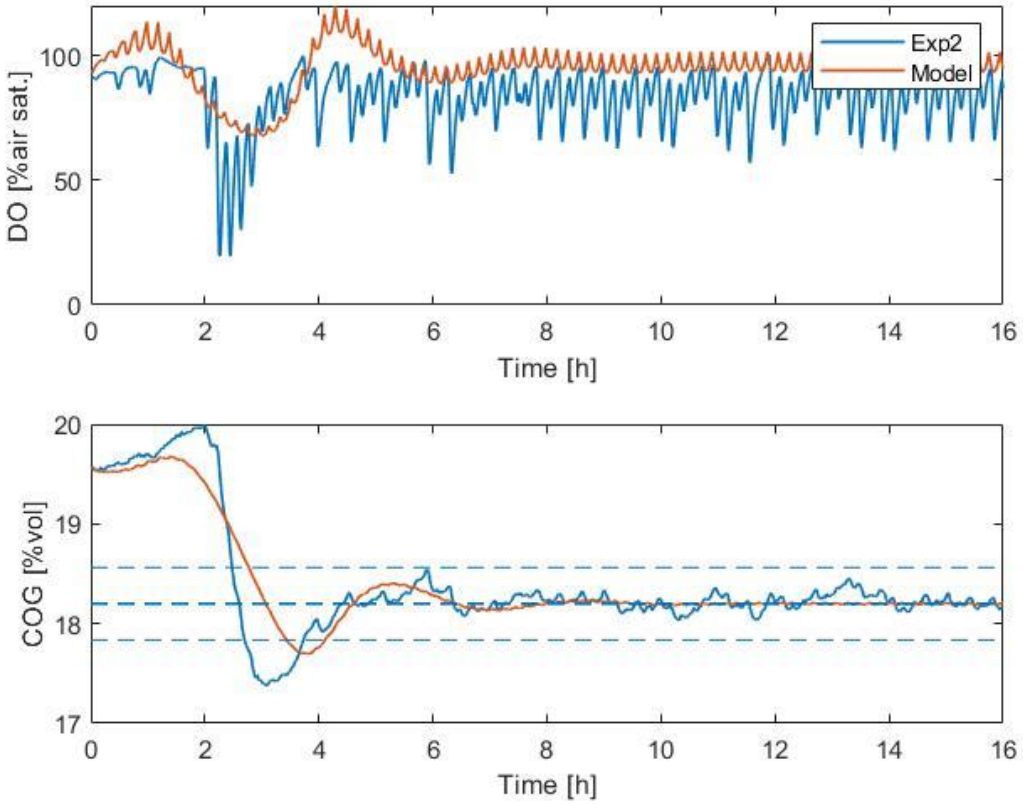

Figure 4.27: COG and DO profiles obtained in the second experiment, compared with the model predictions when the starting point is the same.

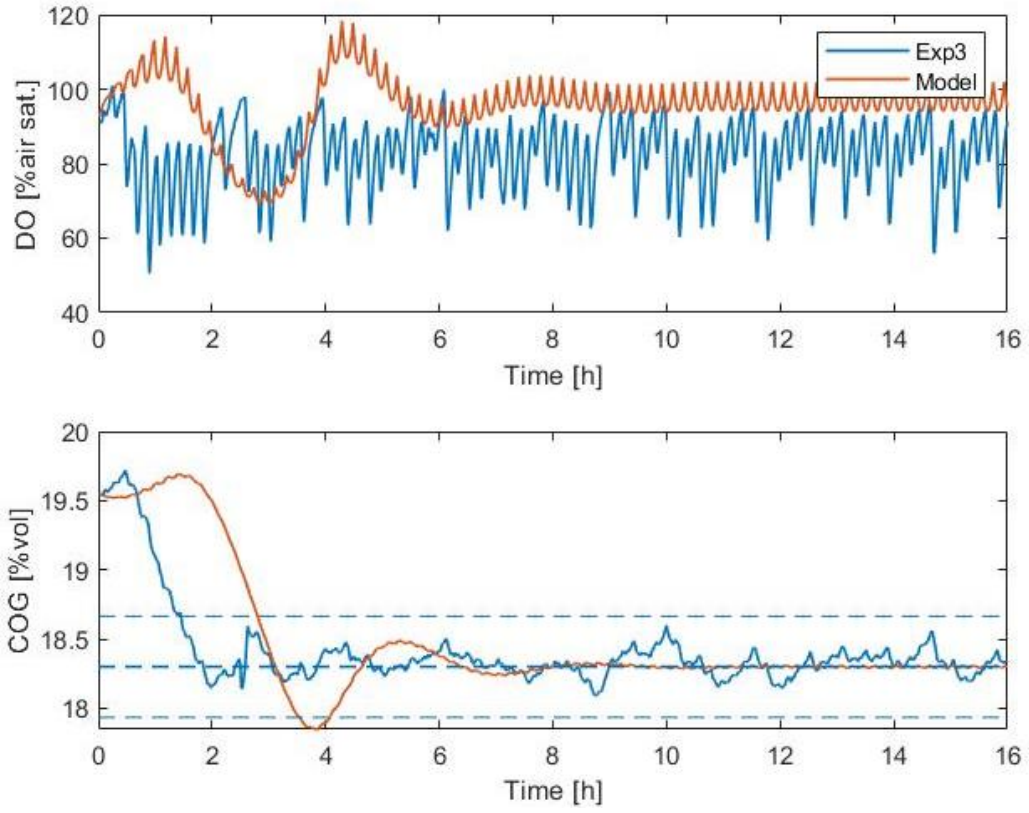

Figure 4.28: COG and DO profiles obtained in the third experiment, compared with the model predictions when the starting point is the same.

The stable state is reached when the response oscillates around ±2% of the COG setpoint value. The time point after which the oscillation is staying within this range is 1.8 h, 3.71 h, and 2h, respectively for the first, second and third experiments, while it is 4.15 h for the model. In all the experiments, the control system resulted in a faster response than expected in reaching stability. Dissolved oxygen profiles obtained in the experiments were less regular than the one simulated. Moreover, values of DO are usually lower in the experiment than in the model, even when the system reaches stability.

The profiles obtained from all three experiments and a simulation with a setpoint value of 18.2% are compared in Figure 4.29. The experiments were conducted at a different pressure, because the change in atmospheric pressure was not compensated by a change in the water height in the waterlock. This means that the same setpoint value in input to the program, which also depends on pressure, is a different value of COG for each experiment (respectively, 18.1%, 18.2%, and 18.3%) and this is the reason why the stable value of the three experiments is slightly different. However, this slight variation does not affect the whole process. The first experiment started with a lower COG because air enriched with carbon dioxide was provided before the beginning of the experiment.

4.3.2 Substrate concentration

The measurement of glucose concentration in each sample always resulted in a low value, below the detection limit of the YSI glucose analyzer. This means that the results are not accurate, and only offer information about the presence of traces of glucose. This is expected, and shows that glucose did not accumulate in the reactor. The fluctuating trend shown in Figure 4.30 is similar to the one of the model, although substrate concentration in the simulation is lower than experimentally observed.

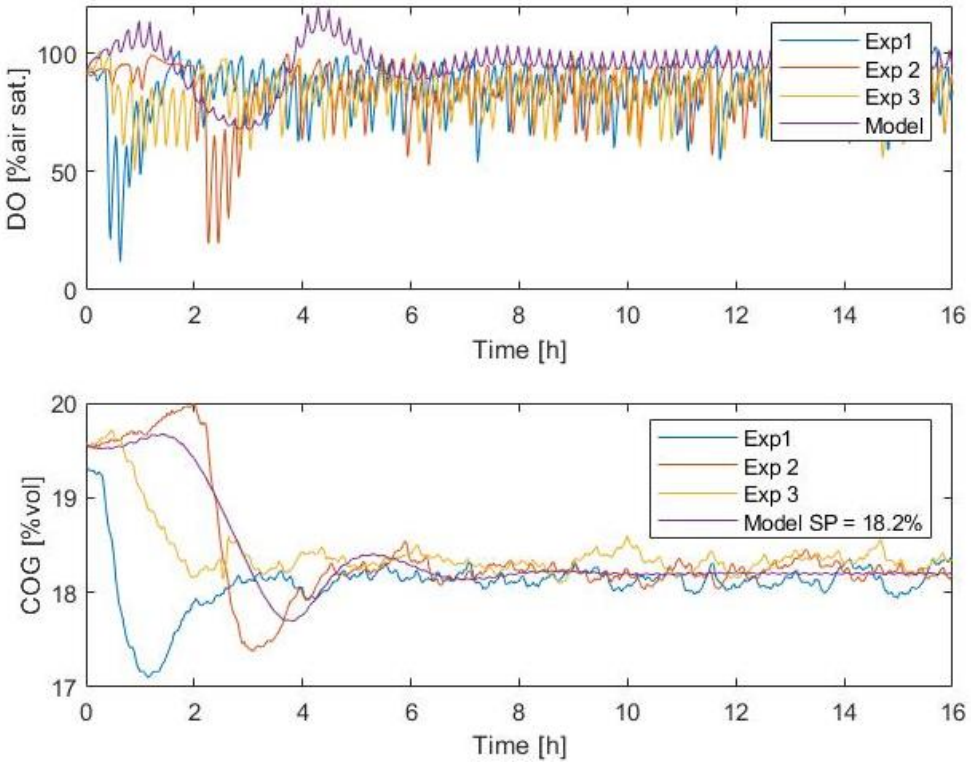

Figure 4.29: COG and DO profiles obtained in all the experiment, compared with the model predictions when the setpoint COG value is 18.2%.

Furthermore, the amount of glucose fed into the system can be obtained from the substrate balance (Figure 4.31). A different amount of substrate is fed in the beginning of the experiments, but when stable COG is reached and no other disturbances are present, the curves are linear and with a similar slope. This means that at the end of all the experiments, the same substrate flowrate is fed into the reactor to keep the system stable. Lastly, the amount of glucose fed to the reactor during the experiments is 3.4±0.5 g_{glu}, a value near 3.7 g_{glu} which is the model's prediction.

4.3.3 Dark-adapted photosystem II quantum yield, pigment profile

The dark-adapted efficiency of photosystem II can be quantified using the QY. High values of this parameter indicate that a large fraction of light absorbed by photosystem II is used for photosynthesis, while the rest is emitted as heat or fluorescence. Low QY values indicate photoinhibition, nutrient or substrate limitation, and also anoxic conditions. The range of QY values depends on the microalga, and for *Galdieria sulphuraria,* maximum values around 0.5 are measured when the culture is not photoinhibited (Abiusi et al., 2022). In all the validation experiments performed in this study, the culture expressed high QY, and the quantum efficiency of photosystem II even increased during the experiment (Table 4.4). This trend could be explained by the increase in biomass concentration, which goes along with a decrease in light exposure of individual cells and the potential reduction of photoinhibition.

Absorption cross-section spectra represent the quantity and type of pigments that absorb light in the range of 300 nm – 750 nm. The shape of the spectra is typical of the microalgal strain and the growth conditions. In Figure 4.32, the spectra for the three experiments are shown before and after the experiments, and no significative differences can be seen. This means that the oxygen and substrate gradients in time did not affect the pigment composition of *Galdieria*.

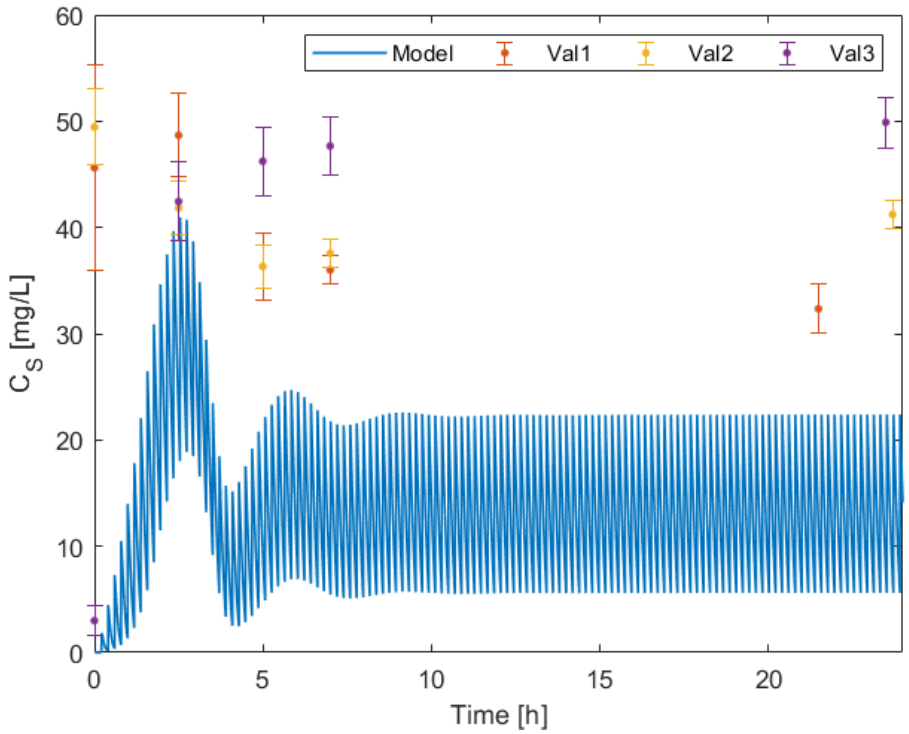

Figure 4.30: Substrate concentration measured from the samples collected during the experiments and comparison with the model.

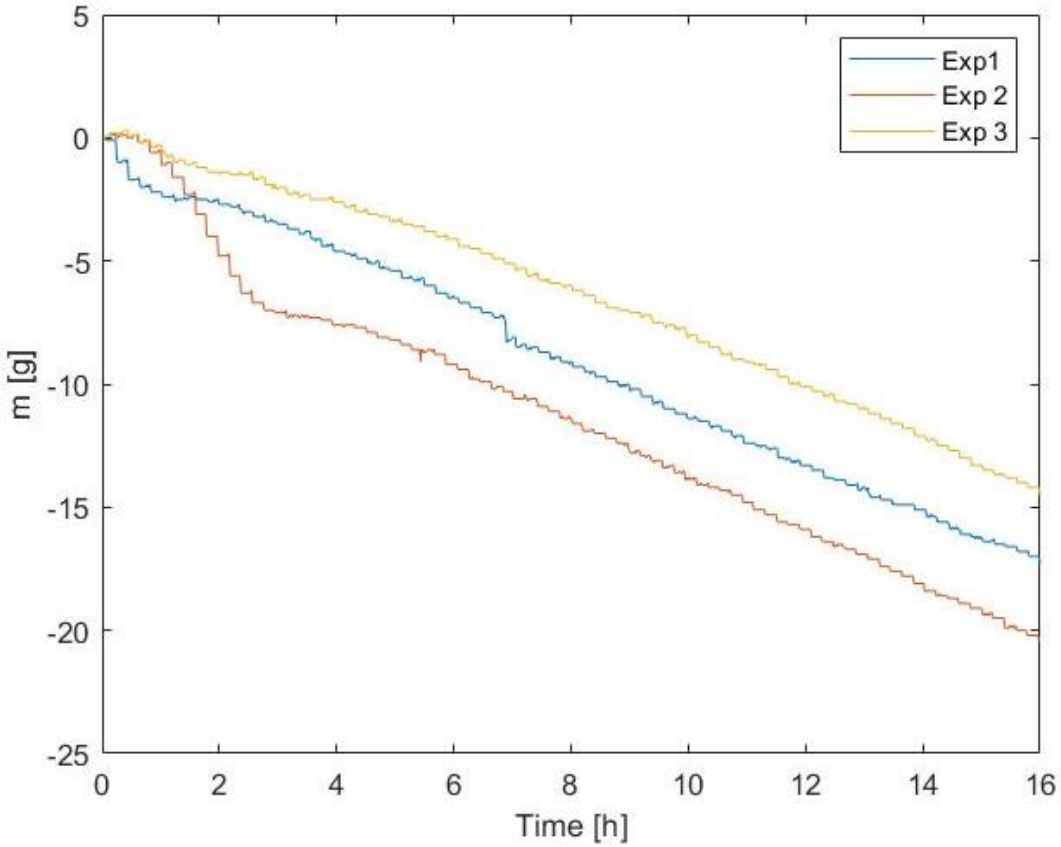

Figure 4.31: Mass decrease on the substrate balance in time.

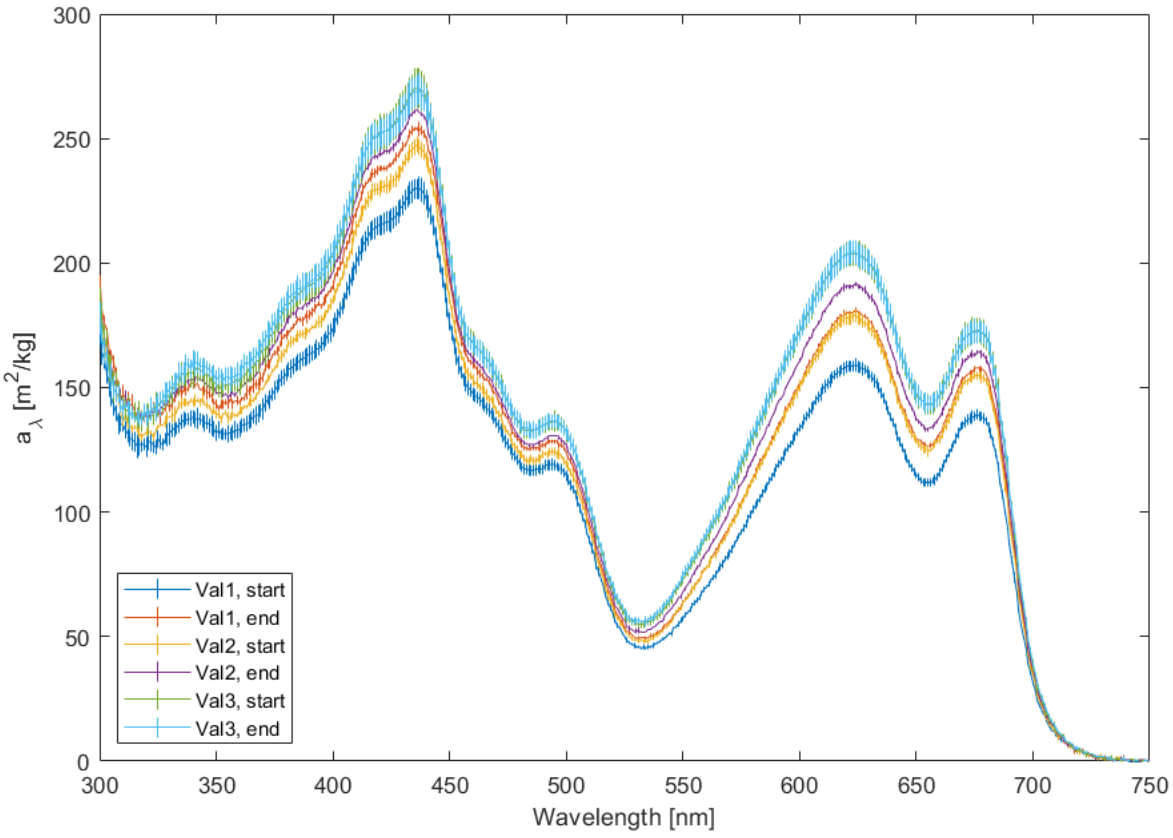

Figure 4.32: Absorption cross section spectrum before and after each validation experiment.

Also, the average absorption cross section, which is the average of the wavelength dependent absorption cross section between 400 nm and 700 nm, is not much affected during the experiments. The slight increase after the experiment is probably only because of the increase in biomass concentration (Table 4.6). The values in this table are comparable with the results obtained in previous studies (125 m^2/kg - 138 m^2/kg) in mixotrophic batches (Abiusi et al., 2021).

4.3.4 Carbon dioxide concentration in the liquid phase

Unfortunately, the measurement of carbon dioxide concentration in the liquid phase did not result in the expected increasing trend (Figure 4.33). Possible reasons could be related to the sampling procedure employed, and the resolution of the TOC-L for these low values of inorganic carbon concentration. In addition, the carbon dioxide concentration at the initial conditions in the simulation was set to zero. This is not happening in the experiment, probably because of the carbon dioxide production for maintenance or for glucose consumption that is not included in the model.

4.3.5 Volumetric biomass productivity

Volumetric biomass productivity during the three experiments, calculated according to equation (3.5), is reported in Table 4.7 and compared with the one obtained from the models and previous studies. The value obtained from the experiment matches the model prediction. Furthermore, the productivity is also comparable to the one of the OBM batch conducted before the validation experiments, meaning that the substrate and oxygen gradients during the validation did not affect the growth of the culture. Previous studies (Abiusi et al., 2021) measured higher biomass productivity in batch experiments. Even though this value was not reached during the three experiments, an increasing trend in productivity has been registered (Table 4.6). The same trend has been reported by Abiusi et al., and it can be explained as progressive acclimatation and adaptation to mixotrophy over time.

Table 4.6: Biomass concentration, quantum yield, average absorption cross section before and after the experiments and biomass productivity.

Validation	C_X start [g_X/L]	C_X end [g_X/L]	a_X start [m^2/kg]	a_X end [m^2/kg]	QY start [-]	QY end [-]	r_X [$g_X/(L\ day)$]
Val1	6.35	6.96	125.8	139.7	0.46	0.51	1.04
Val2	7.82	8.75	136.5	143.3	0.52	0.55	1.26
Val3	8.25	9.27	152.9	153.3	0.52	0.54	1.43

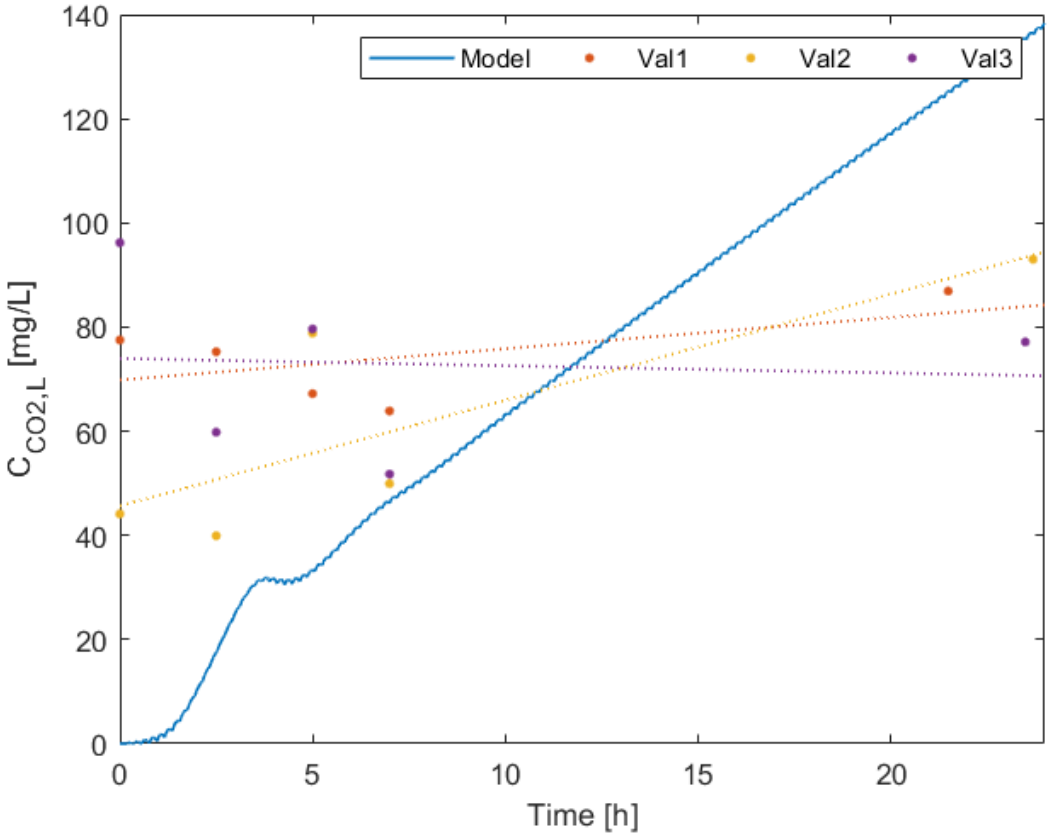

Figure 4.33: Carbon dioxide concentration in liquid phase, model, and experiments.

Table 4.7: Volumetric biomass productivity from the model, the experiments, and previous studies.

	rx **[g_x/(L day)]**	**Reference**
Model	1.22	This study
Validation experiment	1.24±0.15	This study
OBM preparation batch	1.21	This study
OBM VI batch experiment	1.72	(Abiusi et al., 2021)

5. Conclusions

In this Thesis, a model to predict substrate and oxygen gradients in a tubular photobioreactor was improved. It has been successfully used to simulate a mixotrophic outdoor cultivation of *Galdieria sulphuraria* in clear sky and real light conditions on a cloudy day.

The model was improved in the numerical methods adopted to solve the equations and in the input parameters, to give better results for the chosen culture conditions. A study of data from residence time distributions and a sensitivity on the model was conducted, and a number of stages of 100 has been defined.

When light input is constant, average autotrophic oxygen production and heterotrophic oxygen consumption are balanced only when dissolved oxygen decreases in time. It is possible to keep DO constant with a constant flowrate or a control system, resulting in unbalance with higher autotrophic oxygen production.

Three different control strategies have been designed and tested in the simulation. Controlling dissolved oxygen resulted in a faster response, as it is a more direct control approach to keep a constant DO. However, all three control strategies resulted in a stable system response.

In the clear sky and real light conditions, the continuous control of COG resulted in a better dynamic evolution of dissolved oxygen and slightly higher biomass productivity than the discontinuous control system. The productivity achieved in clear sky conditions is comparable to that obtained with constant light. When light intensity during the day is lower, lower oxygen production leads to low substrate input in the system and, thus, lower productivity.

A new lab-scale experimental setup was arranged to down-scale the gradients of a tubular photobioreactor in a stirred tank photobioreactor. A discontinuous setpoint control system designed from the model resulted in a stable COG response after some hours. Dissolved oxygen never reached values lower than 10%. Thus, anoxia was prevented during the experiments.

Glucose concentration in each sample was around the detection limit, thus, no substrate did accumulate in the reactor. Furthermore, the glucose input of 3.4 ± 0.5 g_{glu} is close to the one predicted by the model (3.7 g_{glu}). Absorption cross-section spectra, average absorption cross-section, and quantum yield did not show any changes that could be related to unfavorable conditions in the reactor. Volumetric biomass productivity of 1.24 ± 0.15 $g_x/(L\ d)$ was achieved during the experiments, a value that is close to 1.22 $g_x/(L\ d)$ predicted by the model.

The results obtained with the model and the experiment show that this process can be effectively up-scaled. Control system optimization is the key to achieving high biomass productivity and prevent anoxic conditions in outdoor light conditions.

6. Recommendations

Further study may be conducted to improve the model, the simulations, and the validation.

For the model, the maintenance term for oxygen consumption and carbon dioxide production may be included, as it appeared significant in the experiments conducted in this Thesis.

Additional simulations could be done to include different control strategies: for example, continuous setpoint control strategies need further attention. Furthermore, the control systems to control DO have yet to be studied in real light conditions, and the results obtained in constant light might also be generalized in that case.

As for the experimental validation, a different way to sample and measure carbon dioxide concentration in the liquid should be found. Additionally, carbon dioxide concentration could be measured in the gas phase using a carbon dioxide sensor. Lastly, further validation of control strategies could be conducted with a similar setup as the one described in this Thesis.

The model could also be adapted for additional studies related to the present topic. For example, it can be employed to simulate an autotrophic culture. However, in these cultures in tubular photobioreactors, carbon dioxide supply is commonly coupled with pH control, which needs to be implemented in the equations. In addition, it can be used to understand better whether the two-phase configuration, proper of the Lgem reactor, results in better performances than a homogeneous tubular photobioreactor. Lastly, other mixotrophic cultures could be simulated and compared with the *Galdieria* culture and the results of this Thesis. For instance, when employing *Chlorella sorokiniana*, all reaction rates are around double the values used in this Thesis. This means that a different amount of substrate should be fed to the reactor to achieve the oxygen balance. While the control strategies developed with *Galdieria* might also work with *Chlorella*, the control system would probably have to be tuned again on the specific process.

List of symbols

a	Gas-liquid transport area	m^2/m^3
a_x	Dry weight-specific absorption cross-section	m^2/kg
$Bias$	Control system bias	m^3/s
C_S	Substrate concentration	C-mol/m^3
C_X	Biomass concentration	C-mol/m^3
$C_{S,FEED}$	Substrate concentration in the feed solution	C-mol/m^3
$C_{O2,G}$	Oxygen concentration in the gas phase	mol/m^3
$C_{O2,L}$	Oxygen concentration in the liquid phase	mol/m^3
$C_{CO2,G}$	Carbon dioxide concentration in the gas phase	mol/m^3
$C_{CO2,L}$	Carbon dioxide concentration in the liquid phase	mol/m^3
C_I	Inert gas concentration	mol/m^3
C_{TG}	Total gas concentration	mol/m^3
C_{tracer}	Tracer concentration	mol/m^3
CFL	Courant-Friedrichs-Lewy condition	-
COG	Oxygen concentration in the gas phase	%
d_{Bubble}	Sauter-mean bubble diameter	m
D_{GL}	Gas-liquid diffusivity	m^2/s
DO	Dissolved oxygen	%
DW	Concentration obtained with dry weight measure	g_x/m^3
δ	Delta Dirac function	-
E	Residence time distribution function	1/s
ε_G	Gas holdup	-
F	Residence time cumulative function	-
F_{BLEED}	Bleed gas flowrate	m^3/s
F_{FEED}	Stoichiometric substrate feed flowrate	m^3/s
F_G	Gas flowrate	m^3/s
F_L	Liquid flowrate	m^3/s
H_{cp}	Henry solubility	mol/(m^3 Pa)
$\Delta_{sol}H$	Enthalpy of dissolution	J/(mol K)
$k_{O2,L}a$	Oxygen volumetric mass transfer coefficient	1/s
$k_{CO2,L}a$	Carbon dioxide volumetric mass transfer coefficient	1/s
K_p	Proportional control gain	-

K_S	Half saturation constant for substrate	C-mol$_S$/m^3
K_{O2}	Half saturation constant for oxygen	C-mol$_{O2}$/m^3
K_{CO2}	Half saturation constant for carbon dioxide	C-mol$_{CO2}$/m^3
L	Length of the tube	m
m_{CO2}	Carbon dioxide partition coefficient	-
m_{O2}	Oxygen partition coefficient	-
$m_{S,tot}$	Total substrate input during the day	kg/day
m_k	Moment of order k	min^k
μ	Viscosity	Pa s
N	Number of mixers/tanks/stages	-
OD	Optical density	-
P	Pressure	bar
P_u	Period of sustained oscillation	s
PFD	Photon flux density	$\mu mol_{ph}\ m^{-2}\ s^{-1}$
$q_{O2,auto}$	Specific autotrophic oxygen production rate	C-mol$_S$/(C-mol$_X$ s)
$q_{S,max}$	Maximum specific substrate consumption rate	C-mol$_S$/(C-mol$_X$ s)
QY	Photosystem II quantum yield	-
r_x	Biomass volumetric productivity	g$_x$/(m^3 day)
$r_{O2,auto}$	Autotrophic volumetric oxygen production rate	μmol$_{O2}$/(m^3 s)
$r_{O2,het}$	Heterotrophic volumetric oxygen consumption rate	μmol$_{O2}$/(m^3 s)
$r_{O2,net}$	Net volumetric oxygen production rate	μmol$_{O2}$/(m^3 s)
$r_{O2,transf}$	Volumetric oxygen transfer rate	μmol$_{O2}$/(m^3 s)
R	Gas constant	m^3 Pa/(K mol)
σ^2	Variance	min^2
t	Time	s or h
$t_{control}$	Control time	s
τ_C	Gas-liquid contact time	s
τ_D	Derivative time constant	s
τ_G	Residence time, gas	min
τ_I	Integral time constant	s
τ_L	Residence time, liquid	min
T	Temperature	K
TIC	Total inorganic carbon	mg/L
v_G	Velocity, gas	m/s

v_L	Velocity, liquid	m/s
V_G	Gas volume	m^3
V_L	Liquid volume	m^3
y	Controlled variable	-
y_{sp}	Set-point value of the controlled variable	-
$Y_{X/S}$	Stoichiometric biomass yield on substrate (het)	$C\text{-}mol_X/C\text{-}mol_S$
$Y_{X/ph}$	Stoichiometric biomass yield on photons (auto)	$C\text{-}mmol_X/mol_{ph}$
$Y_{C/S}$	Stoichiometric carbon dioxide yield on substrate (het)	$mol_{CO2}/C\text{-}mol_S$
$Y_{O/C}$	Stoichiometric oxygen yield on carbon dioxide (auto)	mol_{O2}/mol_{CO2}
$Y_{O/S}$	Stoichiometric oxygen yield on substrate (het)	$mol_{O2}/C\text{-}mol_S$

References

Abiusi, F., 2021. Oxygen balanced mixotrophy in microalgae. Wageningen University. https://doi.org/10.18174/542064

Abiusi, F., Moñino Fernández, P., Canziani, S., Janssen, M., Wijffels, R.H., Barbosa, M., 2022. Mixotrophic cultivation of Galdieria sulphuraria for C-phycocyanin and protein production. Algal Research 61. https://doi.org/10.1016/j.algal.2021.102603

Abiusi, F., Trompetter, E., Hoenink, H., Wijffels, R.H., Janssen, M., 2021. Autotrophic and mixotrophic biomass production of the acidophilic Galdieria sulphuraria ACUF 64. Algal Research 60. https://doi.org/10.1016/j.algal.2021.102513

Abiusi, F., Wijffels, R.H., Janssen, M., 2020a. Doubling of Microalgae Productivity by Oxygen Balanced Mixotrophy. ACS Sustainable Chemistry and Engineering 8, 6065–6074. https://doi.org/10.1021/acssuschemeng.0c00990

Abiusi, F., Wijffels, R.H., Janssen, M., 2020b. Oxygen Balanced Mixotrophy under Day–Night Cycles. ACS Sustainable Chem. Eng. 8, 11682–11691. https://doi.org/10.1021/acssuschemeng.0c03216

Acién, F.G., Fernández, J.M., Magán, J.J., Molina, E., 2012. Production cost of a real microalgae production plant and strategies to reduce it. Biotechnology Advances 30, 1344–1353. https://doi.org/10.1016/j.biotechadv.2012.02.005

Apel, A.C., Weuster-Botz, D., 2015. Engineering solutions for open microalgae mass cultivation and realistic indoor simulation of outdoor environments. Bioprocess Biosyst Eng 38, 995–1008. https://doi.org/10.1007/s00449-015-1363-1

Bhatt, A., Khanchandani, M., Rana, M.S., Prajapati, S.K., 2022. Techno-economic analysis of microalgae cultivation for commercial sustainability: A state-of-the-art review. Journal of Cleaner Production 370, 133456. https://doi.org/10.1016/j.jclepro.2022.133456

Caporgno, M.P., Mathys, A., 2018. Trends in Microalgae Incorporation Into Innovative Food Products With Potential Health Benefits. Front. Nutr. 5, 58. https://doi.org/10.3389/fnut.2018.00058

Čížková, M., Vítová, M., Zachleder, V., 2020. The Red Microalga *Galdieria* as a Promising Organism for Applications in Biotechnology, in: Vítová, M. (Ed.), Microalgae - From Physiology to Application. IntechOpen. https://doi.org/10.5772/intechopen.89810

de Mooij, T., 2016. Antenna size reduction in microalgae mass culture. Wageningen University. https://doi.org/10.18174/387545

de Winter, A., 2022. Upscaling oxygen balanced mixotrophic cultivation of Galdieria sulphuraria. Wageningen University and Research.

D'Imporzano, G., Veronesi, D., Salati, S., Adani, F., 2018. Carbon and nutrient recovery in the cultivation of Chlorella vulgaris: A life cycle assessment approach to comparing environmental performance. Journal of Cleaner Production 194, 685–694. https://doi.org/10.1016/j.jclepro.2018.05.174

Fernández, F.G.A., Camacho, F.G., Pérez, J.A.S., Sevilla, J.M.F., Grima, E.M., 1998. Modeling of biomass productivity in tubular photobioreactors for microalgal cultures: Effects of dilution rate, tube diameter, and solar irradiance. Biotechnol. Bioeng. 58, 605–616.

Fernández, I., Acién, F.G., Fernández, J.M., Guzmán, J.L., Magán, J.J., Berenguel, M., 2012. Dynamic model of microalgal production in tubular photobioreactors. Bioresource Technology 126, 172–181. http://dx.doi.org/10.1016/j.biortech.2012.08.087

Gross, W., Schnarrenberger, C., 1995. Heterotrophic Growth of Two Strains of the Acido-Thermophilic Red Alga Galdieria sulphuraria. Plant and Cell Physiology. https://doi.org/10.1093/oxfordjournals.pcp.a078803
Jordaan, D., 2022. Modelling dissolved oxygen levels in a two-phase tubular photobioreactor under mixotrophy. Wageningen University and Research.
Karanth, N.G., 1981. Some observations on the similarity of batch and plug-flow systems as applied to enzyme reactors. Biotechnol. Bioeng. 23, 225–230. https://doi.org/10.1002/bit.260230116
Kliphuis, A.M.J., Klok, A.J., Martens, D.E., Lamers, P.P., Janssen, M., Wijffels, R.H., 2012. Metabolic modeling of Chlamydomonas reinhardtii: energy requirements for photoautotrophic growth and maintenance. J Appl Phycol 24, 253–266. https://doi.org/10.1007/s10811-011-9674-3
Kumar, R., Hegde, A.S., Sharma, K., Parmar, P., Srivatsan, V., 2022. Microalgae as a sustainable source of edible proteins and bioactive peptides – Current trends and future prospects. Food Research International 157, 111338. https://doi.org/10.1016/j.foodres.2022.111338
Lau, R., Peng, W., Velazquez-Vargas, L.G., Yang, G.Q., Fan, L.-S., 2004. Gas−Liquid Mass Transfer in High-Pressure Bubble Columns. Ind. Eng. Chem. Res. 43, 1302–1311. https://doi.org/10.1021/ie030416w
Levenspiel, O., 1999. Chemical reaction engineering, 3rd ed. ed. Wiley, New York.
Masojídek, J., Kopecký, J., Giannelli, L., Torzillo, G., 2011. Productivity correlated to photobiochemical performance of Chlorella mass cultures grown outdoors in thin-layer cascades. J Ind Microbiol Biotechnol 38, 307–317. https://doi.org/10.1007/s10295-010-0774-x
Masojídek, J., Ranglová, K., Lakatos, G.E., Silva Benavides, A.M., Torzillo, G., 2021. Variables Governing Photosynthesis and Growth in Microalgae Mass Cultures. Processes 9, 820. https://doi.org/10.3390/pr9050820
Masojídek, J., Torzillo, G., Koblížek, M., 2013. Photosynthesis in Microalgae, in: Richmond, A., Hu, Q. (Eds.), Handbook of Microalgal Culture. John Wiley & Sons, Ltd, Oxford, UK, pp. 21–36. https://doi.org/10.1002/9781118567166.ch2
Merola, A., Castaldo, R., Luca, P.D., Gambardella, R., Musacchio, A., Taddei, R., 1981. Revision of Cyanidium caldarium. Three species of acidophilic algae. Giornale botanico italiano 115, 189–195. https://doi.org/10.1080/11263508109428026
Nedeltchev, S., 2022. Unified Approach for Prediction of the Volumetric Mass Transfer Coefficients in a Homogeneous and Heterogeneous Bubble Column Based on the Non-Corrected Penetration Theory: Case Studies. Processes 10, 1828. https://doi.org/10.3390/pr10091828
Nethravathy, M.U., Jitendra, G.M., Sandeep, N.M., Ajam, Y.S., 2019. Recent Advances in Microalgal Bioactives for Food, Feed, and Healthcare Products: Commercial Potential, Market Space, and Sustainability. Comprehensive Reviews in Food Science and Food Safety 18, 1882–1897. https://doi.org/10.1111/1541-4337.12500
Peter, A.P., Yew, G.Y., Tang, D.Y.Y., Koyande, A.K., Chew, K.W., Show, P.L., 2022. Microalgae's prospects in attaining sustainable economic and environmental development. Journal of Biotechnology 357, 18–27. https://doi.org/10.1016/j.jbiotec.2022.08.009
Rhie, M.N., Hong, K., Lee, T., 2022. Effects of the induction of anoxia in photobioreactor on effective cultivation of *Scenedesmus acuminatus* under mixotrophic cultivation mode. Environmental Technology 43, 2359–2379. https://doi.org/10.1080/09593330.2021.1880487

Rodrigues-Sousa, A.E., Nunes, I.V.O., Muniz-Junior, A.B., Carvalho, J.C.M., Mejia-da-Silva, L.C., Matsudo, M.C., 2021. Nitrogen supplementation for the production of Chlorella vulgaris biomass in secondary effluent from dairy industry. Biochemical Engineering Journal 165, 107818. https://doi.org/10.1016/j.bej.2020.107818

Sander, R., 2015. Compilation of Henry's law constants (version 4.0) for water as solvent. Atmos. Chem. Phys. 15, 4399–4981. https://doi.org/10.5194/acp-15-4399-2015

Sarian, F.D., Rahman, D.Y., Schepers, O., van der Maarel, M.J.E.C., 2016. Effects of Oxygen Limitation on the Biosynthesis of Photo Pigments in the Red Microalgae Galdieria sulphuraria Strain 074G. PLoS ONE 11, e0148358. https://doi.org/10.1371/journal.pone.0148358

Schmidt, R.A., Wiebe, M.G., Eriksen, N.T., 2005. Heterotrophic high cell-density fed-batch cultures of the phycocyanin-producing red algaGaldieria sulphuraria. Biotechnol. Bioeng. 90, 77–84. https://doi.org/10.1002/bit.20417

Sengupta, M., Weekley, A., Habte, A., Lopez, A., 2015. Validation of the National Solar Radiation Database (NSRDB) (2005–2012). Validation of the National Solar Radiation Database (NSRDB) (2005–2012).

Sforza, E., Pastore, M., Franke, S.M., Barbera, E., 2020. Modeling the oxygen inhibition in microalgae: An experimental approach based on photorespirometry. New Biotechnology 59, 26–32. https://doi.org/10.1016/j.nbt.2020.06.003

Sirohi, R., Kumar Pandey, A., Ranganathan, P., Singh, S., Udayan, A., Kumar Awasthi, M., Hoang, A.T., Chilakamarry, C.R., Kim, S.H., Sim, S.J., 2022. Design and applications of photobioreactors- a review. Bioresource Technology 349, 126858. https://doi.org/10.1016/j.biortech.2022.126858

Sloth, J.K., Wiebe, M.G., Eriksen, N.T., 2006. Accumulation of phycocyanin in heterotrophic and mixotrophic cultures of the acidophilic red alga Galdieria sulphuraria. Enzyme and Microbial Technology 38, 168–175. https://doi.org/10.1016/j.enzmictec.2005.05.010

Smetana, S., Sandmann, M., Rohn, S., Pleissner, D., Heinz, V., 2017. Autotrophic and heterotrophic microalgae and cyanobacteria cultivation for food and feed: life cycle assessment. Bioresource Technology 245, 162–170. https://doi.org/10.1016/j.biortech.2017.08.113

Somers, M.D., Chen, P., Clippinger, J., Cruce, J.R., Davis, R., Lammers, P.J., Quinn, J.C., 2021. Techno-economic and life-cycle assessment of fuel production from mixotrophic Galdieria sulphuraria microalgae on hydrolysate. Algal Research 59, 102419. https://doi.org/10.1016/j.algal.2021.102419

Toson, P., Doshi, P., Jajcevic, D., 2019. Explicit Residence Time Distribution of a Generalised Cascade of Continuous Stirred Tank Reactors for a Description of Short Recirculation Time (Bypassing). Processes 7, 615. https://doi.org/10.3390/pr7090615

Touloupakis, E., Faraloni, C., Carlozzi, P., 2022. An outline of photosynthetic microorganism growth inside closed photobioreactor designs. Bioresource Technology Reports 18, 101066. https://doi.org/10.1016/j.biteb.2022.101066

United Nations, 2022. World Population Prospects 2022: Summary of Results, Statistical Papers - United Nations (Ser. A), Population and Vital Statistics Report. United Nations. https://doi.org/10.18356/9789210014380

Wang, J., Liu, J., Liu, T., 2015. The difference in effective light penetration may explain the superiority in photosynthetic efficiency of attached cultivation over the conventional open pond for microalgae. Biotechnol Biofuels 8, 49. https://doi.org/10.1186/s13068-015-0240-0

Wijffels, R.H., Barbosa, M.J., 2010. An Outlook on Microalgal Biofuels. Science 329, 796–799. https://doi.org/10.1126/science.1189003

Zetrialdi, F., 2020. Modelling of a Two-phase Tubular Photobioreactor: Effects of Operating Parameters on Dissolved Gas Concentration and pH Gradient. Wageningen University and Research.
Zhang, D., An, S., Yao, R., Fu, W., Han, Y., Du, M., Chen, Z., Lei, A., Wang, J., 2022. Life cycle assessment of auto-tropically cultivated economic microalgae for final products such as food, total fatty acids, and bio-oil. Front. Mar. Sci. 9, 990635. https://doi.org/10.3389/fmars.2022.990635
Zhu, B., Wei, D., Pohnert, G., 2022. The thermoacidophilic red alga Galdieria sulphuraria is a highly efficient cell factory for ammonium recovery from ultrahigh-NH4+ industrial effluent with co-production of high-protein biomass by photo-fermentation. Chemical Engineering Journal 438, 135598. https://doi.org/10.1016/j.cej.2022.135598

Appendix

Appendix A: Input parameters list

Input parameters list			
Name	Symbol	Value	Reference
Heterotrophic carbon dioxide yield on substrate	$Y_{C/S}$	4.10E-1 mol_{CO2}/C-mol_S	Section 2.3
Autotrophic oxygen yield on carbon dioxide	$Y_{O/C}$	1.11E0 mol_{O2}/mol_{CO2}	Section 2.3
Heterotrophic oxygen yield on substrate	$Y_{O/S}$	3.46E-1 mol_{O2}/C-mol_S	Section 2.3
Maximum heterotrophic oxygen production rate	$q_{O2het,max}$	-3.26E-6 mol_{O2}/(C-mol_X s)	(Jordaan, 2022)
Substrate saturation constant	K_S	3.04E-1 C-mol_S/m^3	(Jordaan, 2022)
Oxygen saturation constant	K_O	1.30E-3 mol_{O2}/m^3	(Jordaan, 2022)
Carbon dioxide saturation constant	K_{CO2}	1.00E-2 mol_{CO2}/m^3	(Jordaan, 2022)
Maximum autotrophic oxygen production rate at constant light conditions	$q_{O2,auto}$	1.96E-6 mol_{O2}/(C-mol_X s)	Section 2.3
Oxygen mass transport coefficient	$k_{O2,L}a$	2.42E-3 1/s	Section 2.2
Carbon dioxide mass transport coefficient	$k_{CO2,L}a$	2.21E-3 1/s	Section 2.2
Tube diameter	d_t	6.20E-2 m	Lgem design
Tubelength	L_t	2.80E+2 m	Lgem design
Pressure	P	1 atm	Atmospheric conditions
Temperature	T	310 K	Section 2.2
Oxygen partition coefficient	m_{O2}	4.44E+1	Section 2.2
Carbon dioxide partition coefficient	m_{CO2}	1.84E0	Section 2.2
Gas flowrate	F_G	3.33E-04 m^3/s	(Zetrialdi, 2020)
Gas holdup	ε_G	2.8E-1	(Zetrialdi, 2020)
Liquid flowrate	F_L	8.78E-4 m^3/s	(Zetrialdi, 2020)
Calculated substrate feed flowrate	F_{FEED}	0.371 L/h	Section 2.3

Substate solution concentration	$C_{S,FEED}$	6.7E3 C-mol$_S$/m^3	Section 2.3
Biomass concentration	C_X	2.0E+2 C-mol$_X$/ m^3	Section 2.3
Residence time / Control time	-	7.15E+2 s	(Zetrialdi, 2020)
Number of mixers	N	1.00E+2	Section 4.1

Appendix B: Gas volume measurement

B.1 Reactor setup and methods

The reactor is run with 2 L of water and an inlet flowrate of air of 0.05 NL/min, with internal gas recycle switched on until a steady state is reached (gas composition value shown by the oxygen sensor inside the reactor is constant).

At time t = 0, a step change on inlet gas composition is implemented by closing the air valve and opening the nitrogen valve, so that inlet gas oxygen content goes from the oxygen content of air to zero. This step change is happening at a constant pressure, because the flowrate of inlet gas is constant, and the valve switch is performed in a short time. The change of gas composition inside the reactor is monitored using the oxygen probe, and data is collected until oxygen concentration in gas phase is around 0.5% for further analysis (this is done using the MATLAB Curve Fitting toolbox 3.5.11, non-linear least squares method).

B.2 Theoretical model

The gas volume of the system can be derived from the material balance of a component in gas phase. Considering an oxygen molar balance in gas phase, equation (B.1) can be written.

$$\frac{dn_{O2}}{dt} = \dot{n}_{O2,in} - \dot{n}_{O2,out} \qquad (B.1)$$

Where n_{O2} are the mols of oxygen in the system (mol) and $\dot{n}_{O2}$ is a oxygen flowrate (mol/min). Equation (B.2) can be obtained with the following assumptions:

- The gas phase behaves as an ideal gas.
- The gas phase is ideally mixed.
- Pressure and temperature are constant.
- Considering total molar balance, the system is at steady state ($F_{G,in} = F_{G,out} = F_G$).

$$\frac{dx_{O2}}{dt} = \frac{F_G}{V_G} \quad (x_{O2,in} - x_{O2}) \qquad (B.2)$$

Where x_{O2} is the molar fraction of oxygen in the reactor (-), F_G the total gas flowrate (L/min) and V_G the gas volume in the system. A balance with the same assumptions but at steady state can be written as shown in equation (B.3).

$$0 = \frac{F_G}{V_G} \quad (x_{O2,in,ss} - x_{O2,ss}) \qquad (B.3)$$

Subtracting equation (B.3) to equation (B.2) leads to the mathematical model with deviation variables in equation (B.4), where y is the output variable ($y = x_{O2} - x_{O2,ss}$) and u the input variable ($u = x_{O2,in} - x_{O2,in,ss}$).

$$\frac{dy(t)}{dt} = \frac{F_G}{V_G} \quad (u(t) - y(t)) \qquad (B.4)$$

This differential equation can be easily solved for any input signal by using Laplace transforms, and it is representative of a first order system with unit gain and characteristic time $\tau = V_G/F_G$ [Equation (B.5)].

$$y(s) = \frac{1}{\tau\, s + 1}\, u(s) \qquad (B.5)$$

The input function is a step function, defined in time-domain as shown in equation (B.6), where A is the amplitude of the step change in the oxygen composition of the inlet gas (-).

$$u(t) = \begin{cases} 0, & t = 0 \\ -A, & x > 0 \end{cases} \quad (B.6)$$

Therefore, the transfer function for this process in Laplace-domain can be written [Equation (B.7)], and the solution in equation (B.8) can be derived.

$$y(s) = \frac{1}{\tau s + 1}\left(-\frac{A}{s}\right) \quad (B.7)$$

$$y(t) = -A\left(1 - \exp\left(-\frac{t}{\tau}\right)\right) \quad (B.8)$$

This equation can be further elaborated, and equation (B.9) can be finally obtained.

$$x_{O2}(t) = A\ \exp\left(-\frac{t}{\tau}\right) \quad (B.9)$$

B.3 Data analysis, gas volume estimation

Equation (B.9) assumes that the oxygen fraction in the gas phase decreases exponentially, and it is assumed that it does not depend on the pressure of the system, given it is constant. However, the oxygen concentration measurements are dependent on pressure, so a correction on the measures performed at a pressure higher than atmospheric must be made. For this correction, it is considered that the measurements performed in the first ten minutes after the software is switched on are representative of oxygen percentage in the reactor at atmospheric pressure. So, calculating the mean value, the oxygen concentration in the reactor is 19.27%.

During the experiment, when the reactor is pressurized with inlet air, the measured oxygen percentage increases. Assuming that this change is only the effect of the increase in pressure, the pressure of the system can be calculated using equation (B.10).

$$P = \frac{x_{O2,measured}}{x_{O2,actual}}\ P_{atm} \quad (B.10)$$

Before switching the inlet gas to nitrogen, the pressure reaches the value of 1.126 atm (oxygen percentage in the reactor 21.7%). The valve switch is performed so that pressure is constant, but the inlet gas is nitrogen. Therefore, the oxygen concentration profile can be corrected.

The values for the model parameters are the following:

- A = 21%, which is the change of oxygen concentration when switching the gas stream from air to nitrogen.
- F_G = 0.0471 nL/min, which is the mean value of gas flowrate during the experiment. Considering the actual flowrate (at a pressure higher than atmospheric), the value is 0.0465 L/min.

Three replicates of the experiment were conducted. The experimental data is well fitted by the model (R^2 = 0.9985), showing that ideal model developed is suitable in describing the dynamic evolution of oxygen concentration in gas phase (Figure B.1). A mean residence time of 35.9 min can be estimated from the regression and, considering a gas flowrate of 0.0465L/min, the gas volume is 1.67 L. Even though some adjustments have been to the setup after this measurement, it is assumed that this volume did not change.

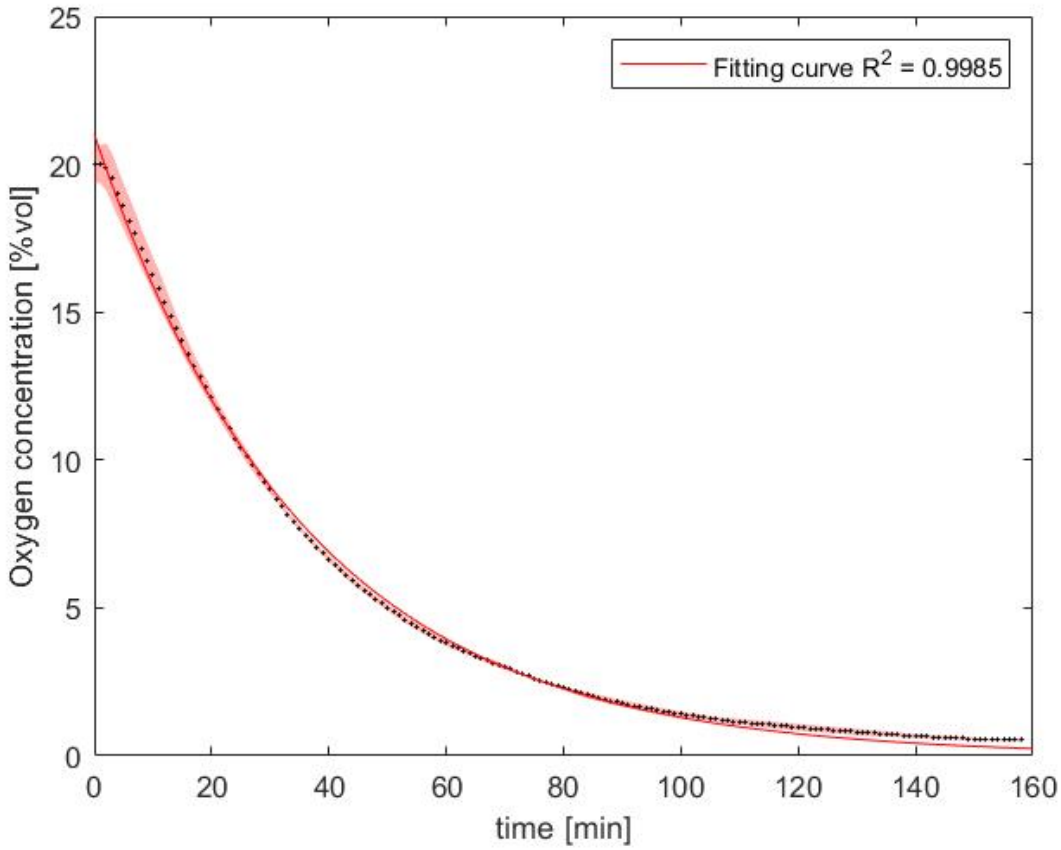

Figure B.1: Oxygen concentration evolution in time. Black dots are the mean of experimental values, the red area is the deviation of the experimental data, and the red curve is the model.

Appendix C: Experiment preparation

During the whole reactor run, some parameters of the culture were measured daily. These parameters include dry weight, quantum yield and average absorption cross section (Figure C.1).

During the first autotrophic batch, the microalgal culture was not dense enough, so it was stressed by the high light intensity (DW slowly increase and QY is decreasing the first days). During the first chemostat, a stable state was not reached, as DW was decreasing in time. This is probably due to a technical problem with the control system, that accumulated a delay during the previous days. Due to time limits, the following chemostats only lasted three days, but the system gave more stable results than in the first one.

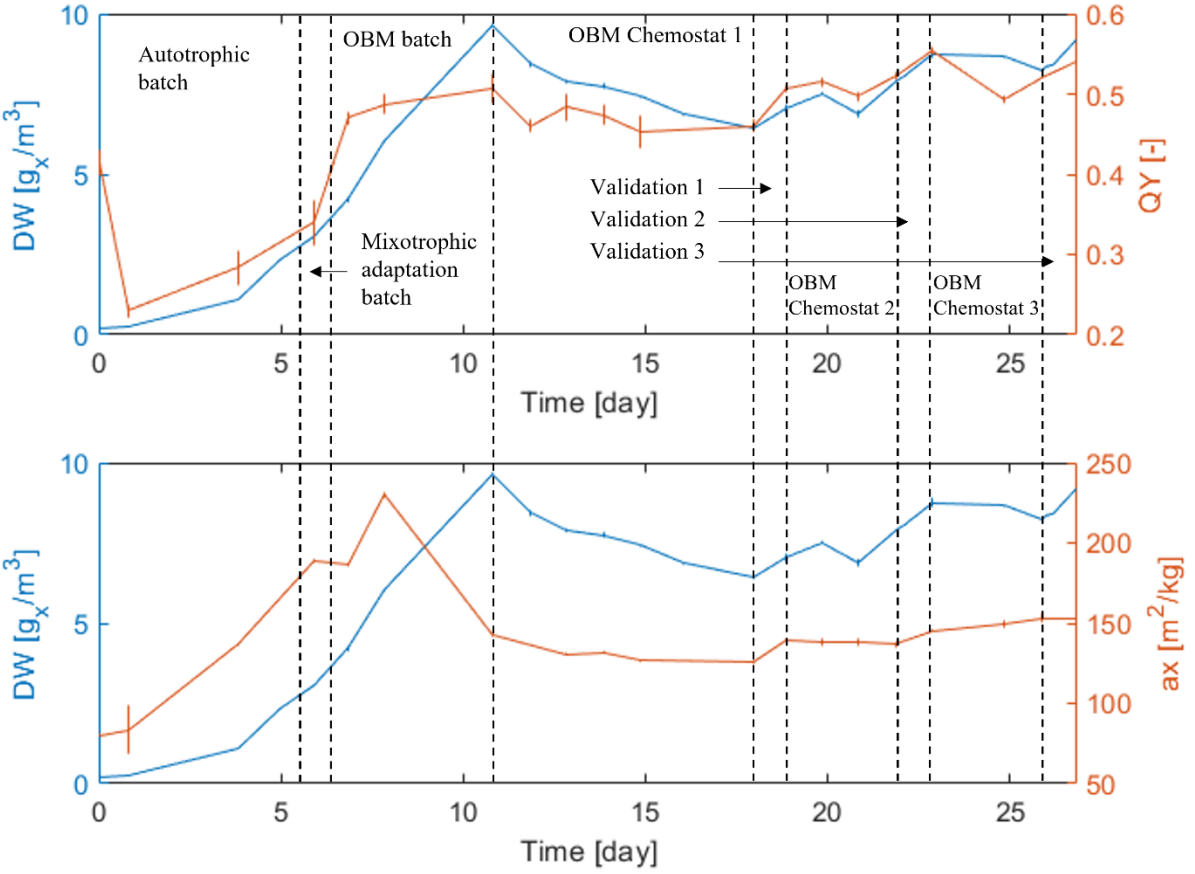

Figure C.1: Offline measurements during the whole reactor run.

Acknowledgments

It is relevant to me to say thank you to all the people who made this Thesis happen.

I would like to thank my supervisors Marcel and Pedro for allowing me to work on this wonderful topic. Thank you for giving me guidance and support through all the small problems encountered across the way. It has been a pleasure to work in BPE, with you all. Thank you to all the people that I met during these past months, it was an important experience of academic and personal growth.

Thank you to my family, to my parents and grandparents, who always had supportive words for me, even in the most difficult moments of this journey. You always encouraged me making my own choices, and I'm thankful for this.

Lastly, thank you to my friends who have been supporting me through the years and they still do it today. I'm grateful you're part of my life.

I wish this end will be the beginning of a new great journey.